Gaussian Description of Squeezed Light and Magnetometry

Vivi Petersen

QUANTOP
Department of Physics and Astronomy
University of Aarhus, Denmark

PhD Thesis
July 2006

This thesis is submitted to the Faculty of Science at the University of Aarhus, Denmark, in order to fulfill the requirements for obtaining the PhD degree in Physics.
The studies have been carried out at the Department of Physics and Astronomy under supervision of Professor Klaus Mølmer and Associate Research Professor Lars Bojer Madsen, from August 2002 to July 2006.

An electronic version of this thesis will be available at:
http://www.vivi.computing.dk/study/

Contents

Publications

[I] V. Petersen, L. B. Madsen, and K. Mølmer, *Minimizing the loss of entanglement under dimensional reduction*, Eur. Phys. J. D **29**, 293 (2004).

[II] V. Petersen, L. B. Madsen, and K. Mølmer, *Magnetometry with entangled atomic samples*, Phys. Rev. A **71**, 012312 (2005).

[III] V. Petersen, L. B. Madsen, and K. Mølmer, *Gaussian state description of squeezed light*, Phys. Rev. A **72**, 053812 (2005).

[IV] V. Petersen and K. Mølmer, *Estimation of fluctuating magnetic fields by an atomic magnetometer*, Phys. Rev. A **74**, 043802 (2006).

Preface

This thesis presents some of the work I have done during my PhD studies under the supervision of Klaus Mølmer and Lars Bojer Madsen.

The first one and a half years of my PhD I worked with entanglement transformation [I]. We investigated the possibility of transforming, under local operations and classical communication, a general bipartite quantum state on a $d_A \times d_B$ tensor-product space into a final state in 2×2 dimensions, while maintaining as much entanglement as possible.

This thesis presents the work I have done during the last two and a half years of my PhD, where I have worked on a Gaussian description of squeezing and magnetometry [II, III, IV].

Acknowledgments

First of all, I would like to thank my two supervisors, Lars Bojer Madsen and Klaus Mølmer for their never failing encouragement and support. It has been a pleasure working with you both, and certainly never boring.

I would also like to thank all my friends at the university for making the eight years I have spend here very enjoyable. In particular I want to thank my friends at TÅGEKAMMERET for keeping me company during my (much needed) breaks and for (almost) always having cold cokes in the refrigerator.

Finally I would like to thank my friends outside the university and my family. In particular I thank Henrik Kjær Andersen for his support and patience, and also for proofreading this thesis.

Vivi Petersen
July, 2006

Abstract

Dansk resumé. *I denne teoretiske afhandling beskrives det, hvordan man kan lave ekstremt præcise målinger af små magnetfelter. Til at lave målingerne bruger vi en gas af atomer. Atomerne kan ses som små magneter, og når disse små magneter placeres i et magnetfelt, vil de dreje ind efter feltet. Ved at måle på laserlys der har været sendt igennem atomerne kan vi bestemme, hvor meget atomerne har drejet og dermed hvor stort et magnetfelt de befinder sig i. I afhandlingen gennemgår vi bl.a. resultater for tidsafhængige magnetfelter, hvor vi viser, at det øjeblikkelige måleresultat ikke kun indeholder information om det nuværende magnetfelt, men også om magnetfeltet til tidligere tider. Det betyder, at en måling foretaget til et bestemt tidspunkt kan bruges til at forbedre resultatet af målinger foretaget tidligere.*

English abstract. This theoretical thesis describes how to make extremely precise measurements of small magnetic fields. To make the measurements we use a gas of atoms. The atoms can be thought of as small magnets and when they are placed in a magnetic field they will turn—how much depends on the size of the field. By sending a laser beam though the atoms we are able to measure how much they have turned and this gives us the size of the magnetic field. In this thesis we investigate, e.g., time-dependent magnetic fields and we show that if we make a measurement on the magnetic field, we get not only information about the present size of the field but also about the size of the field at earlier times. This information can be used to improve the results of the measurements back in time.

One

Introduction to the Thesis

Squeezed light is a quantum phenomenon which, e.g., can be used to improve precision measurements like magnetometry. In this very brief chapter an outline of the thesis will be given.

1.1 Introduction

Quantum variables must fulfill Heisenberg's uncertainty principle, which means that two non-commuting variables cannot both be determined with arbitrary good precision. It is however possible to determine one of the variables with arbitrary good precision if the other variable is correspondingly badly determined and in this case we have a squeezed state. Here we will investigate quantum mechanical squeezing of optical fields generated in an optical parametric oscillator (OPO). In the standard theory for describing squeezing (see, e.g., Ref. [1]) it is difficult to, e.g., include measurements on the output field from the cavity. As we will show, certain kinds of measurements made on the output field can be included when we use a Gaussian description. Squeezed light represents a means to improve precision measurements below the standard quantum noise limit for optical detection. An example is frequency-modulated (FM) saturation spectroscopy with squeezed light [2, 3]. Another example, which we will investigate in this thesis, is precision measurements of magnetic fields (magnetometry).

Precision atomic magnetometry relies on the measurement of the Larmor precession of a spin-polarized atomic sample in a magnetic field [4–7]. From standard counting statistics arguments, one might expect the uncertainty in such measurements to decrease with the interaction time t and with the number of atoms N_{at} as $1/\sqrt{N_{\mathrm{at}}t}$. It is however possible to surpass the above limit if the monitoring of the atomic sample, necessary for the read-out of the estimate of the magnetic field, squeezes the atomic spin. In a recent theoretical analysis a scalar B-field was estimated by a polarization rotation measurement of an off-resonant light beam passing through a trapped cloud of spin-1/2 atoms [8]. This interaction squeezes the spin of the atomic sample, and by quantum trajectory theory [9] combined with the classical theory of Kalman filters [10–12], the uncertainty in the field strength was found to decrease as $1/(N_{\mathrm{at}}t^{3/2})$ [10]. Very recently this proposal was implemented experimentally, and indeed sub-shotnoise sensitivity was found [13].

For decades superconducting quantum interference devices, SQUIDs, have been unrivaled as the most sensitive detectors of weak magnetic fields, and they have been applied in diverse scientific studies including NMR signal detection [14], visualization of human brain activity [15], and gravitational wave detection [16]. Optically pumped atomic gases offer an alternative means to detect weak magnetic fields via the induced Larmor precession of the polarized spin component of the atoms, and the possibility to avoid the need for cryogenic cooling and the relatively high price of the SQUID de-

vices, has spurred an interest in employing atomic magnetometers in medical diagnostics, see for example work on the mapping of human cardiomagnetic fields [17, 18]. Combined with the fact, that the atomic based magnetometers may now reach superior field sensitivity [4], we are now highly motivated to investigate and identify the optimal performance and fundamental limits of such devices.

Atoms constitute ideal probes for a number of physical phenomena, and since they are quantum systems, the statistical analysis of measurement results has to take into account the very special role of measurements in quantum theory. In high precision metrology the aim is to reduce error bars as much as possible, and there is an obvious interest in making the tightest possible conclusion from the measured data. How to optimally prepare and interact with a physical system to obtain maximum information, and even the simpler task of identifying precisely the information available from a specific (noisy) detection record, are not fully characterized at this moment. Large efforts are currently being made to combine techniques from classical control and parameter estimation theory with quantum filtering equations.

The precision measurements exercise a significant back-action on the probed system, and to assess the achievement of a detection scheme we need a formalism that can deal with light-matter interaction and measurement induced state reduction continuously in time. Now, a continuous wave beam of light is described by infinitely many modes, for example in time or frequency domain, and the quantum state of the light field and of the system interacting with the beam is in general too complicated to be fully accounted for in a Schrödinger picture representation. In many quantum optical problems with constant or periodic driving Hamiltonians, it has been possible, however, to provide solutions in the Heisenberg picture for the relationship between Fourier transformed frequency components of the field and system observables. Unfortunately this well-established technique does not apply in conjunction with measurements on the joint system acting locally in time and hence affecting all frequency components of the observables at each measurement event. This thesis does not provide a solution to this general problem. Instead, we shall demonstrate that for a specific dynamics restricted to a specific class of states, the so-called Gaussian states, a significant reduction in the number of parameters needed to fully characterize the system enables a complete description.

We describe the systems using Gaussian variables which have been studied widely in relation to entanglement [19]. A Gaussian state $\mathbf{y}$ is fully characterized by its mean value vector $\mathbf{m}$ and its covariance matrix γ where

$\gamma_{ij} = 2\mathrm{Re}\langle(y_i - \langle y_i\rangle)(y_j - \langle y_j\rangle)\rangle$[1]. As long as the Hamiltonian and the measurements all preserve the Gaussian state we do not need the density matrix, it is sufficient to look at the mean value vector and the covariance matrix. We can use the Gaussian approximation as long as the Hamiltonians are at most second order polynomials in the position and momentum operators. Physical operations which are implemented using linear optical elements and homodyne measurements all preserve a Gaussian state [20].

The interaction with an atomic system may destroy the Gaussian character, but we shall restrict our attention to optical interactions with a large collection of optically pumped atoms. Then the atoms can be described by an effective collective atomic observable, which may in turn be well described by a Gaussian quantum state. The Gaussian state formalism [20–22] was recently employed [8, 23, 24] for the off-resonant Faraday rotation-like interaction [25, 26] between a continuous beam of light and an atomic ensemble. To describe the interaction with a continuous wave of light, we will treat the beam as a sequence of short segments of light incident on the atoms. In the interaction, each light segment acquires some entanglement with the atomic sample and causes a modification of the atomic state when the light segment is probed after the interaction. The description of the incident optical beam is simple if the state of the field factorizes in components corresponding to each short segment of the beam. This is indeed the case for a coherent state of light, representing a normal laser beam.

The advantages obtained by introducing this description from the outset of the theoretical treatment are at least four-fold:

- The Gaussian description explicitly accounts for the dynamics of the system *and* its behavior under measurements through update formulas for the expectation values and the covariance matrix which together fully characterize the Gaussian state.
- The numerical treatment of the update formulas involves only the manipulation of low-dimensional matrices.
- In the limit of small time-steps the update formula for the covariance matrix translates into a matrix Ricatti differential equation which often lends itself to an analytical solution.
- Effects of noise introduced by, e.g., photon absorption and atomic decay are readily included.

[1] Compare with the classical Gauss distribution $F(\mathbf{x}) = \frac{1}{\sqrt{2\pi|\gamma|}} e^{-\frac{1}{2}(\mathbf{x}-\mathbf{m})\gamma^{-1}(\mathbf{x}-\mathbf{m})^T}$.

In the following chapters we will investigate generation of squeezed light in an OPO and estimation of magnetic fields, and the advantages of the Gaussian theory will then be appreciated.

1.2 Thesis Outline

Chapter 2. In this chapter we explain how to generate squeezed light in an (OPO). Moreover we introduce the concepts of squeezing, entanglement, and homodyne detection.

Chapter 3. Here, we describe the Gaussian theory and gives a recipe for how to use the theory on a given problem. We use the theory to describe the squeezing of the light both inside the cavity and of the output field. We also describe the squeezing of the output field when we make a homodyne detection of the output field. Moreover, we show that the light is only squeezed if we look for long enough time and we model a detector with finite bandwidth.

Chapter 4. Here, we explain how the magnetometer works: The B-field causes a rotation of an atomic spin, and the atomic spin causes a polarization rotation of a probe beam. We also show how to include noise in the Gaussian theory.

Chapter 5. In this chapter we will use the squeezed light that we generated in chapter 2 and 3 to improve our magnetometer from chapter 4.

Chapter 6. Here, we extend our previous analysis to explore the possibilities for estimating B-fields with not only one, but also two or three spatial components. In cases with more than one component, it is advantageous to use two or more polarized atomic samples. With such setups, we may identify sets of commuting observables which allow a simultaneous estimate of the B-field components. We also discuss how to gain precision and efficiency by entangling the atomic gases.

Chapter 7. So far we have only considered constant magnetic fields, but here we will extend our theory to include time-varying B-fields. We describe the B-field by an Ornstein-Uhlenbeck process and show by simulations that the estimator for the B-field systematically lags behind the actual value for the field, and we suggest a more complete theory, where measurement results at any time are used to update and improve both the estimator of the current value and the estimate of past values of the B-field.

Chapter 8. The results of the previous chapters are briefly summarized and discussed and possible future work is considered.

Two

Generation of Squeezing in a Cavity

Squeezed light can be generated in an optical parametric oscillator. A cavity is pumped by a classical pump laser, and a non-linear medium inside the cavity converts the pump photons into pairs of squeezed photons. In this chapter we will describe the conventional method to treat this problem. We will also introduce the concepts of squeezing, entanglement, and homodyne detection.

2.1 Introduction

In the following chapter we want to characterize the squeezing of light generated in an optical parametric oscillator (OPO), but first we will in this chapter describe how to generate the squeezed light. We use an OPO which is an optical cavity with a nonlinear medium placed inside. This is a well-known technique [27, 28] and in the standard treatment the squeezing is described by a Fourier transform into frequency space. This is fine in simple cases, but it is difficult to include, e.g., measurements on the output field into this theory, as a measurement occurs locally in time and therefore influences all the frequency components. In the next chapter we will use Gaussian theory such that we are able to include measurements etc.

In this chapter we will briefly introduce the concepts of squeezing and entanglement which are quantum mechanical properties that we will use throughout the thesis. This is done in Sec. 2.2 and 2.3. In Sec. 2.4, we explain how it is possible to generate squeezed light in an OPO by using the standard treatment involving Fourier transforms. In subsequent chapters we will perform measurements on light beams. Here we will use homodyne detection and we describe this method in Sec. 2.5.

2.2 Squeezing

Two quantum variables x and p must obey Heisenberg's uncertainty relation $\Delta x \Delta p \geq \frac{1}{2}|[x,p]|$. In our case the commutator is $[x,p] = i\hbar$ such that we get

$$\Delta x \Delta p \geq \tfrac{\hbar}{2}. \tag{2.1}$$

If there is equality $\Delta x \Delta p = \hbar/2$ we have a minimum uncertainty state. For a coherent state $\Delta x = \Delta p = \sqrt{\hbar/2}$, but it is possible to make, e.g., the uncertainty of x smaller than this but at the expense that then the uncertainty of p becomes larger. In this case we call x squeezed and p antisqueezed [29].

2.3 Entanglement

Entanglement is a unique quantum mechanical resource. A quantum state given by a wave function $|\Psi\rangle \in \mathcal{H}_A \otimes \mathcal{H}_B$ is entangled if it cannot be written on this form

$$|\Psi\rangle = |\Psi_A\rangle \otimes |\Psi_B\rangle. \tag{2.2}$$

The standard example of a two particle entangled state is the singlet state

$$|\psi\rangle = \frac{1}{\sqrt{2}}(|01\rangle - |10\rangle), \tag{2.3}$$

which, e.g., was used in the discussion of Einstein, Podolsky, and Rosen's criticism of the fundament of quantum mechanics [30]. That the state in Eq. (2.3) is entangled comes to expression in that even if the physical distance between the two particles is large, a measurement of an arbitrarily chosen property leads to the fact that it is possible to predict with certainty the result of a corresponding measurement on the other particle.

2.4 Standard Treatment of Squeezing in an Optical Parametric Oscillator

In this section, we present a simple model of squeezed light generation in a cavity as shown on Fig. 2.1. The cavity is pumped by a classical pump beam at frequency $2\omega_c$, twice the frequency of a cavity resonance frequency. Inside the cavity a nonlinear medium converts the pump photons into pairs of photons with frequency ω_c. This gives rise to creation and annihilation of pairs of photons described by the Hamiltonian [1]

$$\mathcal{H}_{\text{int}} = i\hbar g(a_c^{\dagger 2} - a_c^2), \tag{2.4}$$

where g is the coupling constant, and $a_c^\dagger$ and a_c are the creation and annihilation operators for the light inside the cavity. Their commutator are $[a_c, a_c^\dagger] = 1$.

We introduce the canonical conjugate variables

$$x_c = \frac{1}{\sqrt{2}}(a_c + a_c^\dagger), \tag{2.5a}$$

$$p_c = \frac{1}{i\sqrt{2}}(a_c - a_c^\dagger), \tag{2.5b}$$

which have commutator $[x_c, p_c] = i$ and use them to rewrite the Hamiltonian in Eq. (2.4)

$$\mathcal{H}_{\text{int}} = \hbar g(x_c p_c + p_c x_c). \tag{2.6}$$

We express the Hamiltonian in a frame rotating with the cavity frequency ω_c, and consider the dynamics in this rotating frame. In the absence of losses,

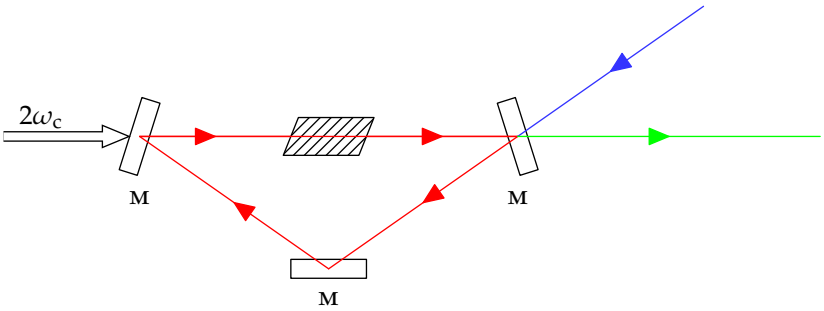

Figure 2.1: Generation of squeezed light by an optical parametric process pumped by a classical field at $2\omega_c$. We use a cavity with three mirrors (M) such that the light only propagates one way. The light inside the cavity (x_c, p_p) is shown in red, the input vacuum field $(x_{ph,in}, p_{ph,in})$ is shown in blue, and the output field $(x_{ph,out}, p_{ph,out})$ is shown in green.

the Heisenberg equations of motion ($\dot{A} = \frac{1}{i\hbar}[A, \mathcal{H}]$)

$$\dot{x}_c(t) = \quad 2g x_c(t), \tag{2.7a}$$
$$\dot{p}_c(t) = -2g p_c(t). \tag{2.7b}$$

can be solved straightforwardly, leading to an exponential squeezing of the p_c-variable and an accompanying antisqueezing of the x_c-variable, which maintains a constant value of the uncertainty product.

This model produces a squeezed state of a single light mode inside the cavity, and such states are subject to detailed analysis in most textbooks on quantum optics, e.g., [1]. Here, however, we aim at applications of squeezed light and hence we are interested in the squeezing properties of the light that leaks out of the cavity. This light propagates out of the cavity into a continuous beam, which corresponds to a continuum of modes in frequency space. We thus replace one of the perfectly reflecting cavity mirrors with a mirror with a small transmittance, which will lead to a loss of the cavity field with a rate Γ. The resulting intracavity field state can be found in many different ways, but for our purpose it is sufficient to note that the cavity mirror acts as a beamsplitter for the intracavity field (x_c, p_c) and for the vacuum field $(x_{ph,in}, p_{ph,in})$ incident on the cavity, see Fig. 2.1. At the partly transmitting mirror the incident vacuum field is reflected into the output field

$(x_{\mathrm{ph,out}}, p_{\mathrm{ph,out}})$, so the output field is a linear combination of the reflected incident field and the transmitted intracavity field. Imagine an incident beam segment of duration τ, short enough that the intensity transmitted at the mirror and the field amplitude built up by the Hamiltonian (2.6) can be treated to lowest order in τ. We can then iterate the Heisenberg equations of motion for the intracavity field and the output field from the cavity and we obtain

$$x_{\mathrm{c}}(t+\tau) = (\xi + 2g\tau)x_{\mathrm{c}}(t) + \sqrt{\Gamma\tau}\,x_{\mathrm{ph,in}}(t), \tag{2.8a}$$

$$p_{\mathrm{c}}(t+\tau) = (\xi - 2g\tau)p_{\mathrm{c}}(t) + \sqrt{\Gamma\tau}\,p_{\mathrm{ph,in}}(t), \tag{2.8b}$$

$$x_{\mathrm{ph,out}}(t+\tau) = -\sqrt{\Gamma\tau}\,x_{\mathrm{c}}(t) + \xi x_{\mathrm{ph,in}}(t), \tag{2.8c}$$

$$p_{\mathrm{ph,out}}(t+\tau) = -\sqrt{\Gamma\tau}\,p_{\mathrm{c}}(t) + \xi p_{\mathrm{ph,in}}(t), \tag{2.8d}$$

where $\xi^2 = 1 - \Gamma\tau$ denotes the probability for the segment to be reflected by the mirror. This quantity is very close to unity, and consequently $\xi \approx 1 - \Gamma\tau/2$. The expressions (2.8) are of course equivalent to the ones obtained by the conventional input-output formalism [27, 31], with the last terms in Eqs. (2.8a) and (2.8b) having the characteristic properties of Wiener noise increments in the limit of small τ. Since we assume that the input field is in the vacuum state, Eqs (2.8a) and (2.8b) can be solved directly for the variances of the intracavity field quadratures, starting from the vacuum state at $t = 0$, and taking the limit $\tau \to 0$

$$\mathrm{Var}(x_{\mathrm{c}}) = \frac{1}{2}\frac{\Gamma - 4ge^{-(\Gamma-4g)t}}{\Gamma - 4g}, \tag{2.9a}$$

$$\mathrm{Var}(p_{\mathrm{c}}) = \frac{1}{2}\frac{\Gamma + 4ge^{-(\Gamma+4g)t}}{\Gamma + 4g}. \tag{2.9b}$$

If $4g < \Gamma$, we see that these equations approach steady state for large times t. Since we are interested in operating the OPO in a regime where steady state can be obtained, we assume from now on that $4g < \Gamma$. The light inside the cavity is still squeezed as expected since $\mathrm{Var}(p_{\mathrm{c}}) < 1/2$, but it is entangled with the emitted light, and hence it is not in a pure state and also not in a minimum uncertainty state.

In the conventional input-output description we Fourier transform the equations (2.8) into frequency space, and they then become algebraic equations. The output field operators in frequency space are expressed as linear combinations of the input field operators at the same frequencies but with

frequency dependent coefficients [32]. All moments of the field annihilation and creation operators have trivial expectation values in the vacuum state. If ω denotes the difference between the optical frequency and the cavity resonance frequency ω_c, we have, for example, the following expression for the normal ordered expectation value[1] of the output field when the system has reached steady state (remembering $4g < \Gamma$)

$$\langle : x(\omega), x(\omega') : \rangle = \frac{2\Gamma g}{(\frac{\Gamma}{2} - 2g)^2 + \omega^2}\delta(\omega + \omega'). \tag{2.10}$$

The Lorentzian frequency dependence implies a temporal correlation between the light emitted at different times, which is due to the common origin in the intracavity field. The field at a single instance of time is obtained by a Fourier transformation of the expressions in frequency space. This will involve all frequencies, also the ones far from the cavity resonance and hence outside the bandwidth of squeezing. Consequently, one will not observe squeezing properties if one observes a light field in a time interval shorter than $\sim 1/\Gamma$. Integrating the signal over a finite time interval T, corresponding to detection of the variable

$$x_T = \frac{1}{\sqrt{T}}\int_t^{t+T} x(t')dt', \tag{2.11}$$

yields a quantity with normal ordered expectation value

$$\begin{aligned}\langle : x_T^2 : \rangle &= \frac{1}{2T}\int_0^T\int_0^T : x(t)x(t') : dtdt' \\ &= \frac{1}{4\pi T}\int_0^T\int_0^T\int_{-\infty}^{\infty}\int_{-\infty}^{\infty} : x(\omega)x(\omega') : e^{-i\omega t}e^{-i\omega' t'}d\omega d\omega' dtdt' \\ &= \frac{8g\Gamma}{T(\Gamma - 4g)^3}[(\Gamma - 4g) - 2 + 2e^{(-\Gamma/2+2g)T}].\end{aligned} \tag{2.12}$$

If we use that $\langle x_T^2 \rangle = \langle : x_T^2 : \rangle + 1/2$ we see that for short times $\big((\Gamma - 4g)T \ll 1\big)$, the output field has the standard noise of vacuum, whereas integration over a long time interval yields

$$\mathrm{Var}(x_T) \to \frac{1}{2}\frac{(\Gamma + 4g)^2}{(\Gamma - 4g)^2}. \tag{2.13}$$

[1] In a normal ordered expectation value all creation operators stand to the left and all annihilation operators to the right. The normal ordered expectation value is denoted by $\langle : \cdots : \rangle$.

The corresponding variance for the p_T component is obtained by replacing g by $-g$ in the above expressions, i.e., in the long-time limit the emitted field is described by a minimum uncertainty state, $\mathrm{Var}(x_T) \times \mathrm{Var}(p_T) = 1/4$.

The prediction of the noise properties of x_T and p_T should of course be in agreement with the ones observed if one carries out a homodyne measurement to detect these quantities, but it is important to remember that during such detection, the dynamics of the system will be different, and it is not clear how to modify the relations in frequency space between the intracavity field and the output field as the detection takes place in real time. However, in the next chapter, we will introduce the Gaussian state formalism which in fact allows an effective real-time treatment of the production *and* probing of squeezed light.

2.5 Homodyne Detection

Many measurements on quantum systems introduce noise in the system, such that successive measurements of the same observable yield different results. This is, e.g., the case for detections done by photocounting techniques. We want to avoid this back-action of the measurement on the detected observable due to the measuring process. This is exactly the case for a quantum non-demolition (QND) measurement, which is a measurement where one monitors an observable that can be measured repeatedly with the result of each measurement being completely determined by the result of an initial, precise measurement [1].

To detect a squeezed state, we need a phase-sensitive scheme that measures the variance of a quadrature (x_{ph} or p_{ph}) of the field. This can be done with homodyne detection which is a QND measurement [33–35]. The setup for homodyne detection is shown in Fig. 2.2. The input field, which we want to measure, is superimposed on the field from a local oscillator at a symmetric lossless beamsplitter. All the fields are described by the creation and annihilation operators. The modes which we detect are

$$a_1 = \tfrac{1}{\sqrt{2}}(A - a_{\mathrm{ph}}), \tag{2.14a}$$

$$a_2 = \tfrac{1}{\sqrt{2}}(A + a_{\mathrm{ph}}) \tag{2.14b}$$

as there is a $\pi/2$ phase shift between the reflected and transmitted beams for a symmetric beamsplitter. If we take A real, then the currents which we

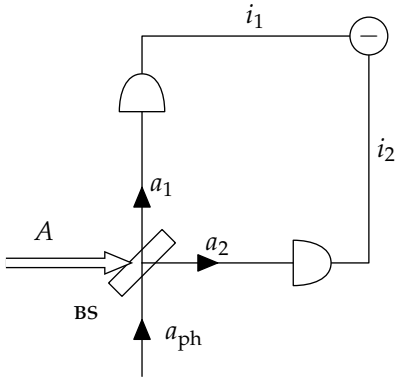

Figure 2.2: Setup for homodyne detection. The field we want to detect, a_{ph}, is mixed with a field from a local oscillator, A, on a beamsplitter (BS) which transmits 50% and reflects 50%. This gives two new fields, a_1 and a_2, which are detected. The currents from the detectors, i_1 and i_2 are then subtracted.

measure on the detectors are

$$\begin{aligned} i_1 \propto a_1^\dagger a_1 &= \tfrac{1}{2}(A - a_{\mathrm{ph}})^\dagger (A - a_{\mathrm{ph}}) \\ &= \tfrac{1}{2}A^2 - \tfrac{1}{2}A(a_{\mathrm{ph}}^\dagger + a_{\mathrm{ph}}) + \tfrac{1}{2}a_{\mathrm{ph}}^\dagger a_{\mathrm{ph}}, \end{aligned} \tag{2.15a}$$

$$\begin{aligned} i_2 \propto a_2^\dagger a_2 &= \tfrac{1}{2}(A + a_{\mathrm{ph}})^\dagger (A + a_{\mathrm{ph}}) \\ &= \tfrac{1}{2}A^2 + \tfrac{1}{2}A(a_{\mathrm{ph}}^\dagger + a_{\mathrm{ph}}) + \tfrac{1}{2}a_{\mathrm{ph}}^\dagger a_{\mathrm{ph}}. \end{aligned} \tag{2.15b}$$

The currents are then subtracted such that we can measure x_{ph}

$$i_2 - i_1 \propto A(a_{\mathrm{ph}}^\dagger + a_{\mathrm{ph}}) \propto x_{\mathrm{ph}}. \tag{2.16}$$

If we insert a phase shifter on the photon field $(x_{\mathrm{ph}}, p_{\mathrm{ph}})$ before it reaches the beamsplitter, then we can shift the phase of this field with $\pi/2$. By doing this we can measure p_{ph} instead of x_{ph}.

2.6 Conclusion

We have explained how to generate squeezed light in an OPO. We have done this by using the conventional method where we made a Fourier transform

into frequency space. In this way we showed that the quadrature fields p_c and x_c were squeezed and antisqueezed, respectively. Furthermore, we have introduced the concepts of squeezing, entanglement, and homodyne detection which will be used throughout this thesis.

Three

Gaussian Description of Squeezed Light

We present a Gaussian description of squeezed light generated in an optical parametric oscillator. We describe the squeezing of the light both inside the cavity and of the output field and by using the Gaussian description we are able to describe what happens, when we make a homodyne detection of the output field. Our theory also shows that the light is only squeezed if we look for long enough time and we show how to model a realistic detector with finite bandwidth. This chapter is based on paper [III].

3.1 Introduction

In the previous chapter we introduced the standard treatment of generation of squeezed light and as we noted it is not obvious how to include, e.g., measurements in this theory. Instead we want to use that the squeezed light produced in an optical parametric oscillator (OPO) is in a Gaussian state, implying that the field is fully characterized by the first-order and second-order correlation functions of the field variables. By using the Gaussian description which we will introduce in this chapter we are able to describe the squeezing of the light inside the cavity both with and without homodyne measurements on the output field. We will also look at the squeezing of the output field and show how to model a finite bandwidth detector. We do this by adding a second cavity where the light segments enter and the intracavity field in the new cavity builds up. With the Gaussian theory we are able to reproduce the results in the last chapter and, e.g., show that the output field is only squeezed if we look for long enough times.

In Sec. 3.2 we introduce the Gaussian theory and explain how to use it to find the uncertainties of the variables. Then in Sec. 3.3 we use the Gaussian theory to describe the squeezing of the intracavity field. Finally in Sec. 3.4 we examine the output field by using two different methods and show how to model a detector with finite bandwidth.

3.2 Gaussian Theory

We look at the situation in the previous chapter again, but this time we will use Gaussian variables to describe the situation shown in Fig. 3.1. The light inside the cavity is described by the Gaussian variables (x_c, p_c) defined in Eq. (2.5). We want to consider the continuous emission of light by the cavity, so we imagine one segment of light after the other leaving the cavity. The segments have a time duration τ. The linear transformation between the states of the cavity field and a segment of light initially incident on the cavity, and eventually propagating away from the cavity (2.8) is easy to deal with, because a state which is initially Gaussian in the field variables will remain Gaussian at later times. So an initially empty cavity and the incident vacuum field will lead to Gaussian states at all later times. We want to consider the continuous emission of light by the cavity, and we hence imagine one segment of light after the other leaving the cavity, and all field quadratures being given by a multi-mode Gaussian distribution.

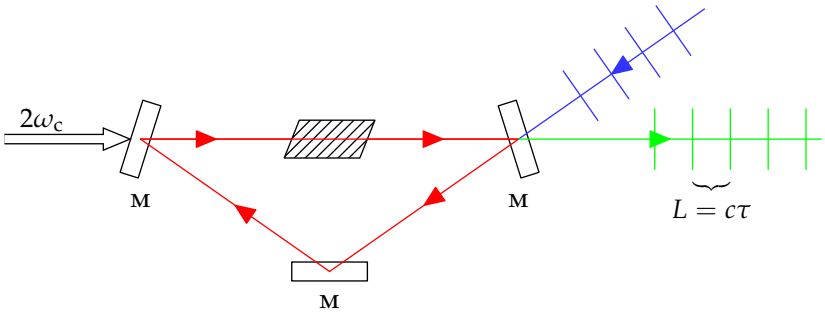

Figure 3.1: Generation of squeezed light by an optical parametric process pumped by a classical field at $2\omega_c$. As on Fig. 2.1 the light inside the cavity (x_c, p_p) is shown in red, the input vacuum field $(x_{ph,in}, p_{ph,in})$ is shown in blue, and the output field $(x_{ph,out}, p_{ph,out})$ is shown in green. We slice the continuous beam into field segments of duration τ and length $L = c\tau$. The figure shows three field segments in the vacuum state which enter the cavity, where a non-linear medium generates squeezing. Four segments of light are shown propagating away from the cavity.

As already mentioned, a Gaussian state is fully characterized by the mean value vector of all canonical variables, which we can arrange in a column vector $\mathbf{y}$, with $\mathbf{m} = \langle \mathbf{y} \rangle$ and the covariance matrix γ where $\gamma_{ij} = 2\mathrm{Re}\langle (y_i - \langle y_i \rangle)(y_j - \langle y_j \rangle) \rangle$. Accordingly, we only need update formulas for $\mathbf{m}$ and γ to account for the quantum state of the entire system. If the output field is discretized in N segments $\mathbf{m}$ has dimension $(2N + 2)$ with $2N$ effective variables $(x_{ph,i}, p_{ph,i})$ for the output field and 2 variables (x_c, p_c) for the cavity mode. The covariance matrix γ has dimension $(2N + 2) \times (2N + 2)$. These finite objects are of course far easier to deal with than the full $N + 1$ tensor products of infinite dimensional Hilbert spaces. In practice the formalism can be made even simpler if we assume that the output beam is detected right after it is emitted from the cavity, and hence the quantum state of each light beam segment is destroyed and only the classical output value is retained, while the next segment emerges from the cavity.

In the following we will explain the theory and in the next section we will show how to use this theory by using the squeezing inside the OPO as an example. We will explain how to include linear transformations and homodyne measurements in the theory. The equations can be solved numerically and

in some cases also analytically by deriving and solving a system of coupled differential equations. We will conclude this section by writing a recipe for how to obtain an analytical formula for the covariance matrix.

Linear Transformations

Let us consider the interaction between a single incident segment of light and the intracavity field, and let us write the linear transformation of the four field variables $\mathbf{y} = (x_c, p_c, x_{ph}, p_{ph})^T$ as follows

$$\mathbf{y} \mapsto \mathbf{S}\mathbf{y}, \tag{3.1}$$

where the elements of the 4×4 matrix $\mathbf{S}$ follow directly from the transformation (2.8). Under this transformation, the mean values $\mathbf{m}$ and the covariance matrix γ transform as

$$\mathbf{m}(t+\tau) = \mathbf{S}\mathbf{m}(t), \tag{3.2}$$

$$\gamma(t+\tau) = \mathbf{S}\gamma(t)\mathbf{S}^T. \tag{3.3}$$

Homodyne Measurements

If we want to perform a homodyne measurement on the output field, we write the mean value vector as

$$\mathbf{m} = \begin{pmatrix} \mathbf{m}_A \\ \mathbf{m}_B \end{pmatrix}, \tag{3.4}$$

where $\mathbf{m}_A$ is the mean value vector for the intracavity field variables $\mathbf{y}_1 = (x_c, p_c)^T$ and $\mathbf{m}_B$ is the mean value vector for the continuous beam $\mathbf{y}_2 = (x_{ph}, p_{ph})^T$. We white the 4×4 covariance matrix as

$$\gamma = \begin{pmatrix} \mathbf{A}_\gamma & \mathbf{C}_\gamma \\ \mathbf{C}_\gamma^T & \mathbf{B}_{\gamma,} \end{pmatrix}, \tag{3.5}$$

where $\mathbf{A}_\gamma$ is the covariance matrix for $\mathbf{y}_1$, $\mathbf{B}_\gamma$ is the covariance matrix for $\mathbf{y}_2$, and $\mathbf{C}_\gamma$ represents their mutual correlations. An advantage of the Gaussian description is that the back action on the residual system due to measurement may be accounted for explicitly. If we measure the variable x_{ph}, due to their mutual correlation, we learn something about the intracavity x_c variable, i.e., its variance decreases, and simultaneously, to fulfill Heisenberg's uncertainty

relation, $\mathrm{Var}(p_c)$ increases. From Refs. [21, 22], we have the explicit update formula for the intracavity field covariance matrix after homodyne detection on the beam segment

$$\mathbf{A}_\gamma \mapsto \mathbf{A}_\gamma - \mathbf{C}_\gamma(\pi\mathbf{B}_\gamma\pi)^-\mathbf{C}_\gamma^T, \tag{3.6}$$

where $\pi = \mathrm{diag}(1,0)$, and $()^-$ denotes the Moore-Penrose pseudo-inverse, so $(\pi\mathbf{B}_\gamma\pi)^- = \mathrm{diag}(B_{\gamma_{11}}^{-1},0)$ with $B_{\gamma_{11}}$ twice the variance of x_{ph}. To understand this formula we can look at it classically, and this is done on page 21. First we note that this result does not depend on the actual outcome of the measurement. However the measurement affects the mean values of the intracavity field variables. We also see that the beam segment has disappeared from the treatment, but to treat the interaction with the next segment we build the covariance matrix (3.5) describing the intracavity field and this new segment with

$$\mathbf{B}_\gamma \mapsto \mathbb{1}, \tag{3.7}$$
$$\mathbf{C}_\gamma \mapsto 0, \tag{3.8}$$

corresponding to an incident vacuum state with no correlation with the cavity field yet. The time evolution of $\mathbf{m}$ depends on the actual measurements in the optical detection which is a random process. Therefore the time evolution of the mean value vector is a stochastic process, and it transforms as [8, 20, 21]

$$\mathbf{m}_A \mapsto \mathbf{m}_A + \mathbf{C}_\gamma(\pi\mathbf{B}_\gamma\pi)^-(\chi,\cdot)^T, \tag{3.9}$$
$$\mathbf{m}_B \mapsto 0, \tag{3.10}$$

where χ is the difference between the measurement outcome and the expectation value of x_{ph}, i.e., a Gaussian random variable with mean value zero and variance $1/2$. Since $(\pi\mathbf{B}_\gamma\pi)^- = \mathrm{diag}(B_{\gamma_{11}}^{-1},0)$, we do not need to specify the second entry in the vector $(\chi,\cdot)$. Eq. (3.10) describes a new vacuum segment entering the cavity field.

Classical Explanation of Formulas

To try to understand Eq. (3.6) and (3.9) we will as already promised look at it classically [36]. The distribution for the variable $\mathbf{y} = (\mathbf{y}_1, \mathbf{y}_2)$ is given by

$$P(\mathbf{y}) \propto \exp\left(-\tfrac{1}{2}(\mathbf{y}-\mathbf{m})\gamma^{-1}(\mathbf{y}-\mathbf{m})^T\right). \tag{3.11}$$

If we measure $\mathbf{y}_2$, we get a high uncertainty on $\mathbf{y}_1$ and a low uncertainty on $\mathbf{y}_2$. When we only keep terms quadratic and linear in $\mathbf{y}_1$ the distribution is

$$\begin{aligned} P(\mathbf{y}) \propto \exp\big(-\tfrac{1}{2}\big[&\mathbf{y}_1(\gamma^{-1})_{11}\mathbf{y}_1^T - \mathbf{y}_1(\gamma^{-1})_{11}\mathbf{m}_1^T - \mathbf{m}_1(\gamma^{-1})_{11}\mathbf{y}_1^T \\ &+ (\mathbf{y}_2-\mathbf{m}_2)(\gamma^{-1})_{21}\mathbf{y}_1^T + \mathbf{y}_1(\gamma^{-1})_{12}(\mathbf{y}_2-\mathbf{m}_2)^T\big]\big). \end{aligned} \tag{3.12}$$

We know that after the measurement the distribution is given by

$$P(\mathbf{y}) \propto \exp\big(-\tfrac{1}{2}\big[\mathbf{y}_1\gamma_{11}'^{-1}\mathbf{y}_1^T - \mathbf{y}_1\gamma_{11}'^{-1}\mathbf{m}_1'^T - \mathbf{m}_1'\gamma_{11}'^{-1}\mathbf{y}_1^T\big]\big), \tag{3.13}$$

so by comparing these distributions we are able to determine the new mean value vector $\mathbf{m}_1'$ and covariance matrix γ_{11}'. The transformation of γ_{11} is then

$$(\gamma_{11}')^{-1} = (\gamma^{-1})_{11} = \Big[(\gamma_{11})^{-1} - \gamma_{12}(\gamma_{22})^{-1}\gamma_{21}\Big]^{-1}, \tag{3.14}$$

where we have used a formula for the inverse of a matrix (see, e.g., Ref. [37]). This equation corresponds to Eq. (3.6). The transformation of the mean value vector requires more calculations but can be derived in a similar way and the result is

$$\begin{aligned} \mathbf{m}_1' &= \mathbf{m}_1 - \gamma_{11}(\gamma^{-1})_{12}(\mathbf{y}_2-\mathbf{m}_2) \\ &= \cdots = \mathbf{m}_1 + \gamma_{12}(\gamma_{11})^{-1}(\mathbf{y}_2-\mathbf{m}_2)^T, \end{aligned} \tag{3.15}$$

which corresponds to Eq. (3.9).

Finding and Solving the Differential Equation

For the present we are interested in the uncertainty of the states, so we only need the covariance matrix γ, but in chapter 7 we will return to the mean value vector. To find the time evolution of the covariance matrix, we propagate the system according to Eq. (3.3), and we implement the effect of the subsequent measurement by Eq. (3.6). The continuous production and probing of the beam is obtained by repetition of the above steps. This can be done numerically with τ sufficiently small, or we may, in the limit of small time increments $\tau \to 0$, derive a differential equation for the intracavity field $\mathbf{A}_\gamma$.

$$\frac{\mathrm{d}\mathbf{A}_\gamma}{\mathrm{d}t} = \lim_{\tau\to 0}\frac{\mathbf{A}_\gamma(t+\tau)-\mathbf{A}_\gamma(t)}{\tau}. \tag{3.16}$$

In the cases where we do homodyne measurements there will be quadratic terms in this differential equation. To get rid of these we use that the differential equation is of the general non-linear matrix Ricatti form [11]

$$\dot{\mathbf{A}}_\gamma(t) = \mathbf{C}_\mathrm{R} - \mathbf{D}_\mathrm{R}\mathbf{A}_\gamma(t) - \mathbf{A}_\gamma(t)\mathbf{E}_\mathrm{R} - \mathbf{A}_\gamma(t)\mathbf{B}_\mathrm{R}\mathbf{A}_\gamma(t), \tag{3.17}$$

where the matrices $\mathbf{C}_\mathrm{R}$, $\mathbf{D}_\mathrm{R}$, $\mathbf{E}_\mathrm{R}$, and $\mathbf{B}_\mathrm{R}$ are all derived from the expressions (3.16). As shown in Ref. [11] the solution for $\mathbf{A}_\gamma$ can be expressed in terms of the solutions of two coupled linear matrix equations

$$\mathbf{A}_\gamma = \mathbf{W}\mathbf{U}^{-1}, \tag{3.18}$$

where

$$\dot{\mathbf{W}} = -\mathbf{D}_\mathrm{R}\mathbf{W} + \mathbf{C}_\mathrm{R}\mathbf{U}, \tag{3.19}$$

$$\dot{\mathbf{U}} = \mathbf{B}_\mathrm{R}\mathbf{W} + \mathbf{E}_\mathrm{R}\mathbf{U}. \tag{3.20}$$

We now have twice as many differential equations as before, but they only contain linear terms. Even though these are easier to solve than the original differential equation we have not been able to find an analytical solution in all cases. The length of one of our results (Eq. (A.1)) may indicate why this is the case.

Recipe for Determining the Covariance Matrix

As a summary of this section, here is a recipe for how we analytically determine the covariance matrix.

1. We write the Gaussian variables in the vector $\mathbf{y}$, for example $\mathbf{y} = (x_\mathrm{c}, p_\mathrm{c}, x_\mathrm{ph}, p_\mathrm{ph})^T$. x and p for the variable we measure must be last.

2. We then find the transformation matrix $\mathbf{S}$. Both here and in step 5 and 6 it is only necessary to keep terms at most first order in τ.

3. We now write down the initial value of the covariance matrix, for example it could be $\gamma_0 = \mathbb{1}$.

4. After n time-steps the value of the covariance matrix right after a homodyne detection is[1]

$$\gamma_n = \begin{pmatrix} \mathbf{A}_n & \mathbf{0} \\ \mathbf{0} & \mathbb{1}_{2\times 2} \end{pmatrix}, \quad \mathbf{A}_n = \begin{pmatrix} a_{11} & a_{12} \\ a_{12} & a_{22} \end{pmatrix}. \tag{3.21}$$

5. We find the covariance matrix after $n+1$ time-steps by applying the transformation matrix: $\widetilde{\gamma}_n = \mathbf{S}\gamma_n\mathbf{S}^T \ldots$

6. ... and by applying the homodyne detection:

$$\widetilde{\gamma}_n = \begin{pmatrix} \widetilde{\mathbf{A}}_n & \widetilde{\mathbf{C}}_n \\ \widetilde{\mathbf{C}}_n^T & \widetilde{\mathbf{B}}_n \end{pmatrix} \tag{3.22}$$

   and $\mathbf{A}_{n+1} = \widetilde{\mathbf{A}}_n - \widetilde{\mathbf{C}}_n(\pi\widetilde{\mathbf{B}}_n\pi)^-\widetilde{\mathbf{C}}_n^T$.

7. Now we rewrite it into a differential equation: $\dot{\mathbf{A}} = (\mathbf{A}_{n+1} - \mathbf{A}_n)/\tau$.

8. We find matrices $\mathbf{C}_\mathrm{R}$, $\mathbf{D}_\mathrm{R}$, $\mathbf{E}_\mathrm{R}$, and $\mathbf{B}_\mathrm{R}$ such that we can rewrite the differential equation on Ricatti form: $\dot{\mathbf{A}}(t) = \mathbf{C}_\mathrm{R} - \mathbf{D}_\mathrm{R}\mathbf{A}(t) - \mathbf{A}(t)\mathbf{E}_\mathrm{R} - \mathbf{A}(t)\mathbf{B}_\mathrm{R}\mathbf{A}(t)$.

9. We solve these differential equations: $\dot{\mathbf{W}} = -\mathbf{D}_\mathrm{R}\mathbf{W} + \mathbf{C}_\mathrm{R}\mathbf{U}$ and $\dot{\mathbf{U}} = \mathbf{B}_\mathrm{R}\mathbf{W} + \mathbf{E}_\mathrm{R}\mathbf{U}$ with boundary conditions that fulfill $\mathbf{A}_0 = \mathbf{W}_0\mathbf{U}_0^{-1}$, for example $\mathbf{W}_0 = \mathbf{A}_0$ and $\mathbf{U}_0 = \mathbb{1}$.

10. Finally we find the covariance matrix: $\mathbf{A} = \mathbf{W}\mathbf{U}^{-1}$.

3.3 Squeezing Properties of the Intracavity Field

We will now apply the above general formalism to the squeezed light problem. The field variables are $\mathbf{y} = (x_\mathrm{c}, p_\mathrm{c}, x_\mathrm{ph}, p_\mathrm{ph})^T$, and we want to find $\mathrm{Var}(x_\mathrm{c})$ and $\mathrm{Var}(p_\mathrm{c})$ so we look at the time evolution of the covariance matrix

[1] If there are more than 4 variables in $\mathbf{y}$ then the size of these matrices should be changed accordingly.

γ. The initial state is a vacuum state, so $\gamma(0) = \mathbb{1}_{4\times4}$. We find the transformation matrix $\mathbf{S}$ from the transformations (2.8)

$$\mathbf{S} = \begin{pmatrix} \xi + 2g\tau & 0 & \sqrt{\Gamma\tau} & 0 \\ 0 & \xi - 2g\tau & 0 & \sqrt{\Gamma\tau} \\ -\sqrt{\Gamma\tau} & 0 & \xi & 0 \\ 0 & -\sqrt{\Gamma\tau} & 0 & \xi \end{pmatrix}. \tag{3.23}$$

When we apply the update formulas for the linear transformation and for the homodyne detection, we find this differential equation

$$\begin{aligned} \dot{\mathbf{A}}_\gamma &= \frac{d}{dt}\begin{pmatrix} a_{11} & a_{12} \\ a_{12} & a_{22} \end{pmatrix} \\ &= \begin{pmatrix} (4g-\Gamma)a_{11} - \Gamma a_{11}^2 & -\Gamma a_{11}a_{12} \\ -\Gamma a_{11}a_{12} & (-4g-\Gamma)a_{22} + \Gamma - \Gamma a_{12}^2 \end{pmatrix}. \end{aligned} \tag{3.24}$$

To solve this differential equation we rewrite it on Ricatti form (3.17) and find the following matrices

$$\mathbf{C}_\mathrm{R} = \begin{pmatrix} 0 & 0 \\ 0 & \Gamma \end{pmatrix}, \tag{3.25a}$$

$$\mathbf{B}_\mathrm{R} = \begin{pmatrix} \Gamma & 0 \\ 0 & 0 \end{pmatrix}, \tag{3.25b}$$

$$\mathbf{D}_\mathrm{R} = \begin{pmatrix} -2g - \Gamma/2 & 0 \\ 0 & 2g + \Gamma/2 \end{pmatrix}, \tag{3.25c}$$

$$\mathbf{E}_\mathrm{R} = \mathbf{D}_\mathrm{R}. \tag{3.25d}$$

This gives us a new set of *linear* first-order differential equations which we can solve using Eq. (3.18)–(3.20). The solution for the variance of p_c is

$$\mathrm{Var}(p_\mathrm{c}) = \frac{1}{2}\frac{\Gamma - 4g}{\Gamma - 4ge^{-(\Gamma-4g)t}}, \tag{3.26}$$

while the variance of x_c is the same as when we did not measure on the output field (2.9a). In this case $\mathrm{Var}(x_\mathrm{c}) \times \mathrm{Var}(p_\mathrm{c}) = 1/4$ and we have a minimum uncertainty state of the intracavity field at all times. If $4g < \Gamma$ we reach steady state for large times, and the variances then read

$$\mathrm{Var}(x_\mathrm{c}) = \frac{1}{2}\frac{\Gamma}{\Gamma - 4g}, \tag{3.27a}$$

$$\mathrm{Var}(p_\mathrm{c}) = \frac{1}{2}\frac{\Gamma - 4g}{\Gamma}. \tag{3.27b}$$

In Fig. 3.2, we have plotted the equations (2.9a), (2.9b), and (3.26), which show how the variance of the Gaussian variables inside the cavity depends on time both with and without measurements on the output beam. The figure shows how p_c becomes squeezed as a function of time, and x_c becomes antisqueezed.

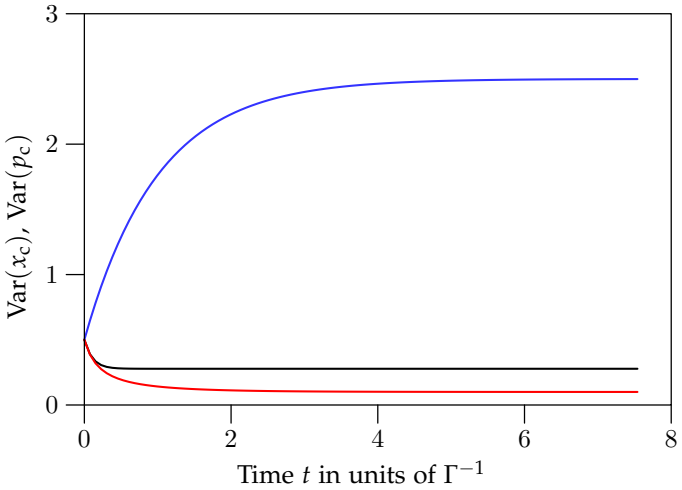

Figure 3.2: Variances of the cavity variables x_c and p_c as a function of time. We use $\Gamma = 2\pi \times 6 \times 10^6\,\mathrm{s}^{-1}$ and $g = 0.2\Gamma$ which are realistic experimental parameters for OPO's [38]. The variances of the antisqueezed variable x_c with and without homodyne detection of the x_{ph} variable of the output field are identical and shown by the upper blue curve. The black and the red curves show the variances of the squeezed variable p_c without and with homodyne detection of the output field, respectively.

3.4 Squeezing Properties of the Emitted Beam

In this section we will investigate the squeezing of the output beam using two different methods. First we will study the correlations between the segments in the emitted beam. Then we will describe how to model a detector with finite bandwidth.

3.4.1 Collective Observable for Many Light Segments

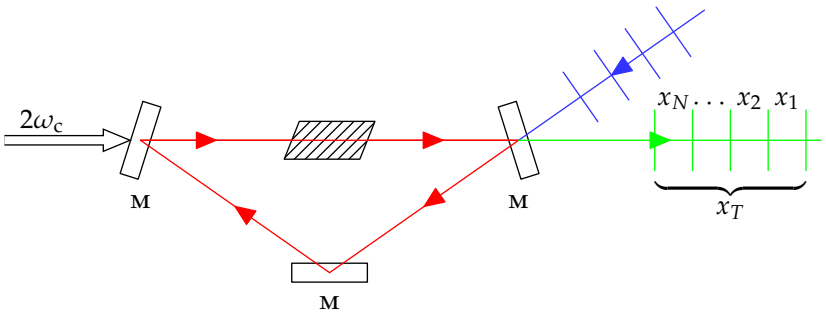

Figure 3.3: The figure shows how we label the beam segments of the output field which are accumulated in x_T and p_T given in Eq. (3.28). We only obtain squeezing if we observe many beam segments, not if we only observe one segment.

We now turn to the squeezing of the output beam. To study the correlations between different individual segments we define the following operators shown on Fig. 3.3

$$x_T = \frac{1}{\sqrt{N}} \sum_{i=1}^{N} x_{\mathrm{ph}_i}, \tag{3.28a}$$

$$p_T = \frac{1}{\sqrt{N}} \sum_{i=1}^{N} p_{\mathrm{ph}_i}, \tag{3.28b}$$

where $T = \tau N$ is the accumulated time in N segments each of duration τ and where the field variables of the i^{th} segment are retained in the formalism. As the calculations are a bit complicated, we will discuss the result first and in a moment we will show how to calculate the variances of these quantities. The result is given in Eq. (3.43)

$$\begin{aligned} \mathrm{Var}(x_T) = \frac{1}{2T(\Gamma-4g)^3}\Big[&(\Gamma-4g)(\Gamma+4g)^2 T \\ &-32\Gamma g + 32\Gamma g e^{(-\Gamma/2+2g)T}\Big]. \end{aligned} \tag{3.29}$$

The result for $\mathrm{Var}(p_T)$ is obtained by replacing g with $-g$. If we let $T \to 0$ corresponding to only a few segments, we obtain $\mathrm{Var}(p_T) = 1/2$ showing

that there is no squeezing if we only consider short times. If, on the other hand, we let $T \to \infty$ corresponding to many segments, we obtain

$$\mathrm{Var}(x_T) \to \frac{1}{2}\frac{(\Gamma+4g)^2}{(\Gamma-4g)^2}. \tag{3.30}$$

These results are in full agreement with the ones obtained by the usual quantum optics treatment, discussed in Sec. 2.4 (see Eq. (2.13)).

Calculations

To calculate the variance of x_T and p_T defined in Eq. (3.28) we use the Gaussian description which were introduced in Sec. 3.2. This time we get more and more light segments so our variable vectors and matrices grow as a function of time. This section describes how we handle this situation.

The initial variables are $\mathbf{y}_1 = (x_c, p_c, x_{\mathrm{ph}_1}, p_{\mathrm{ph}_1})$ and the initial intracavity field and incident vacuum segment covariance matrix is

$$\gamma_1 = \begin{pmatrix} a_{11} & a_{12} & 0 & 0 \\ a_{12} & a_{22} & 0 & 0 \\ 0 & 0 & 1 & 0 \\ 0 & 0 & 0 & 1 \end{pmatrix}. \tag{3.31}$$

The associated transformation matrix is given by Eq. (2.8)

$$\mathbf{S}_1 = \begin{pmatrix} \xi + 2g\tau & 0 & \sqrt{\Gamma\tau} & 0 \\ 0 & \xi - 2g\tau & 0 & \sqrt{\Gamma\tau} \\ -\sqrt{\Gamma\tau} & 0 & \xi & 0 \\ 0 & -\sqrt{\Gamma\tau} & 0 & \xi \end{pmatrix}. \tag{3.32}$$

where $\xi = 1 - \Gamma\tau/2$ as introduced in Eq. (2.8). After the interaction $\widetilde{\gamma}_1 = \mathbf{S}_1\gamma_1\mathbf{S}_1^T$. We now build the dynamics recursively illustrated in Fig. 3.3 by inserting two rows and columns between the second and third row and column in $\widetilde{\gamma}$. In this way we represent the subsequent incident vacuum segments by

$$\gamma_{k+1} = \begin{pmatrix} \{\widetilde{\gamma}_k\}_{(1:2,1:2)} & 0 & \{\widetilde{\gamma}_k\}_{(1:2,3:2k+2)} \\ 0 & \mathbb{1}_{2\times 2} & 0 \\ \{\widetilde{\gamma}_k\}_{(3:2k+2,1:2)} & 0 & \{\widetilde{\gamma}_k\}_{(3:2k+2,3:2k+2)} \end{pmatrix}. \tag{3.33}$$

The transformation matrix is

$$\mathbf{S}_k = \begin{pmatrix} \mathbf{S}_1 & 0 \\ 0 & \mathbb{1}_{(2k-2)\times(2k-2)} \end{pmatrix}, \tag{3.34}$$

and $\widetilde{\gamma}_k = \mathbf{S}_k \gamma_k \mathbf{S}_k^T$. Eq. (3.34) and (3.33) are now inserted, and the number of variables grows with time as we get more and more light segments, $\mathbf{y}_N = (x_\mathrm{c}, p_\mathrm{c}, x_{\mathrm{ph}_N}, p_{\mathrm{ph}_N}, \ldots, x_{\mathrm{ph}_1}, p_{\mathrm{ph}_1})$.

If $a_{12} = 0$ then every second element in γ is zero and γ can be rewritten on block diagonal form with similar x_ph and p_ph blocks. The system of equations for the x_ph, $\mathbf{y}_N = (x_\mathrm{c}, x_{\mathrm{ph}_1}, \ldots, x_{\mathrm{ph}_N})$, variables can then be written as

$$\mathbf{S}_k = \begin{pmatrix} 1-\Gamma\tau/2+2g\tau & \sqrt{\Gamma\tau} & 0 \\ -\sqrt{\Gamma\tau} & 1-\Gamma\tau/2 & 0 \\ 0 & 0 & \mathbb{1}_{(k-1)\times(k-1)} \end{pmatrix}, \tag{3.35}$$

$$\gamma_1 = \begin{pmatrix} a_{11} & 0 \\ 0 & 1 \end{pmatrix}, \tag{3.36}$$

$$\gamma_k = \begin{pmatrix} A_k & 0 & \mathbf{C}_k \\ 0 & 1 & 0 \\ \mathbf{C}_k^T & 0 & \mathbf{B}_k \end{pmatrix}, \tag{3.37}$$

where A_k is a real number, $\mathbf{C}_k$ is a $1 \times (k-1)$ row vector, and $\mathbf{B}_k$ is a $(k-1)\times(k-1)$ matrix.

From this we find the recurrence equations

$$A_{k+1} = (1-\Gamma\tau/2+2g\tau)^2 A_k + \Gamma\tau, \tag{3.38}$$

$$\mathbf{C}_{k+1}^T = \begin{pmatrix} -\sqrt{\Gamma\tau}(1-\Gamma\tau/2+2g\tau)A_k + \sqrt{\Gamma\tau}(1-\Gamma\tau/2) \\ (1-\Gamma\tau/2+2g\tau)\mathbf{C}_k^T \end{pmatrix}, \tag{3.39}$$

$$\mathbf{B}_{k+1} = \begin{pmatrix} \Gamma\tau A_k + (1-\Gamma\tau/2)^2 & -\sqrt{\Gamma\tau}\mathbf{C}_k \\ -\sqrt{\Gamma\tau}\mathbf{C}_k^T & \mathbf{B}_k \end{pmatrix}, \tag{3.40}$$

which can be solved, and the variance of x_T is found to be

$$\begin{aligned}\mathrm{Var}(x_T) &= \frac{1}{N}\sum_{i=1}^{N}\sum_{j=1}^{N}\mathrm{Cov}(x_i,x_j)\\ &= a_{11}\left[\frac{\Gamma\tau}{2N}\frac{1-\alpha^{2N}}{1-\alpha^2}+\frac{\Gamma\tau\alpha^4}{N(1-\alpha)}\left(\frac{1-\alpha^N}{1-\alpha}-\frac{1-\alpha^{2N}}{1-\alpha^2}\right)\right]\\ &\quad+\frac{\Gamma\tau^2}{2(1-\alpha^N)}-\frac{\Gamma\tau^2}{2N}\frac{1-\alpha^{2N}}{(1-\alpha^2)^2}+\tfrac{1}{2}(1-\Gamma\tau/2)^2\\ &\quad-\Gamma\tau(1-\Gamma\tau/2)\frac{1}{1-\alpha}+\frac{\Gamma\tau(1-\Gamma\tau/2)}{N}\frac{1-\alpha^N}{(1-\alpha)^2}\\ &\quad+\frac{\Gamma\tau^2\alpha}{N(1-\alpha^2)(1-\alpha)}\left(N-\frac{1-\alpha^N}{1-\alpha}+\alpha^3\frac{1-\alpha^{2N}}{1-\alpha^2}-\alpha^3\frac{1-\alpha^N}{1-\alpha}\right),\end{aligned} \tag{3.41}$$

where $\alpha = 1-\Gamma\tau/2+2g\tau$. If we let $T = N\tau$ and then let $\tau\to 0$ then

$$\begin{aligned}\mathrm{Var}(x_T)\to\frac{1}{2T(\Gamma-4g)^3}\Big\{&(\Gamma-4g)(\Gamma+4g)^2T\\ &-4\Gamma(\Gamma+8g)+4a_{11}\Gamma(\Gamma-4g)\\ &-8\Gamma\big[a_{11}(\Gamma-4g)-(\Gamma+4g)\big]e^{(-\Gamma/2+2g)T}\\ &-4\Gamma\big[\Gamma-a_{11}(\Gamma-4g)\big]e^{(-\Gamma+4g)T}\Big\}.\end{aligned} \tag{3.42}$$

In the $T\to\infty$ limit, the first term dominates, and the expression for $\mathrm{Var}(x_T)$ does not depend upon a_{11}.

If we wait until the cavity is in steady state we can insert $a_{11} = \frac{\Gamma}{\Gamma-4g}$ in Eq. (3.42), and we obtain

$$\begin{aligned}\mathrm{Var}(x_T) = \frac{1}{2T(\Gamma-4g)^3}\Big[&(\Gamma-4g)(\Gamma+4g)^2T\\ &-32\Gamma g+32\Gamma g e^{(-\Gamma/2+2g)T}\Big],\end{aligned} \tag{3.43}$$

and

$$\begin{aligned}\mathrm{Var}(p_T) = \frac{1}{2T(\Gamma+4g)^3}\Big[&(\Gamma+4g)(\Gamma-4g)^2T\\ &-32\Gamma g-32g(\Gamma-4g)e^{-(\Gamma/2+2g)T}\\ &-64g^2e^{-(\Gamma+4g)T}\Big]\end{aligned} \tag{3.44}$$

for the variances of the quadrature components.

3.4.2 Finite Bandwidth Detection

An alternative way to extract the squeezed component of the emitted beam, is to use a frequency filter, that selects the frequency range of interest. The modelling of such a detector involves a second cavity, in which the light segments enter and the intracavity field in the second cavity builds up. The squeezed beam contains photons in the relevant frequency band, but not only the intensity builds up in the detecting cavity, we also expect the intracavity field in this cavity to show squeezing properties.

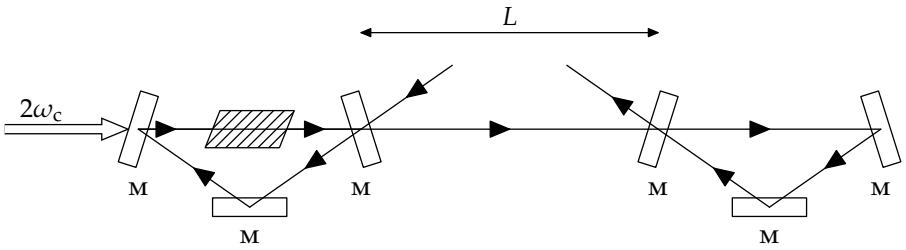

Figure 3.4: Proposed setup for the characterization of the spectrum of squeezed light from on OPO (to the left). The squeezing properties of the single-mode field accumulated in the frequency tunable cavity to the right are determined (see text).

The variables used in a Gaussian treatment of this problem, corresponding to the two cavity fields and the propagating beam segment, are $\mathbf{y} = (x_{c_1}, p_{c_1}, x_{c_2}, p_{c_2}, x_{\rm ph}, p_{\rm ph})$ and the Heisenberg equations of motion are obtained by a simple extension of the expressions (2.8) already used in the case of a single cavity, where we replace Γ with Γ_1. The second cavity has a decay constant Γ_2 and a cavity resonance frequency $\omega_c + \delta$. In our frame rotating at ω_c the field variables in the second cavity obey the equations

$$x_{c_2}(t+\tau) = (1-\Gamma_2\tau/2)x_{c_2}(t) + i\delta\tau p_{c_2}(t) + \sqrt{\Gamma_2\tau}x_{\rm ph,out}(t), \qquad (3.45a)$$

$$p_{c_2}(t+\tau) = (1-\Gamma_2\tau/2)p_{c_2}(t) - i\delta\tau x_{c_2}(t) + \sqrt{\Gamma_2\tau}p_{\rm ph,out}(t), \qquad (3.45b)$$

where $x_{\rm ph,out}$, $p_{\rm ph,out}$ are the quadrature variables for the field leaving the first cavity, cf., Eqs. (2.8c) and (2.8d). In Eq. (3.45) the field incident on the second cavity is the output field from the first cavity, cf. Fig. 3.4. Due to

the physical separation L of the two cavities and the finite speed of light the field variables in Eqs. (2.8c) and (2.8d) should in fact have been delayed by L/c, but since we are addressing the steady state properties of the system we can solve Eqs. (2.8c) and (2.8d) with the same time arguments. The output field from the second cavity is described by equations similar to Eqs. (2.8c) and (2.8d), but they will not be needed in the following. The detuning δ of the second cavity can be scanned, and the squeezing parameter of the intracavity variables x_{c_2}, p_{c_2} reflect the spectral properties of the output beam from the first cavity.

Figure 3.5 shows the eigenvalues $V_{\min}$ and $V_{\max}$ of the 2×2 covariance matrix for the probing cavity (x_{c_2}, p_{c_2}) as a function of the detuning with respect to ω_c. In Fig 3.5(a) the probing cavity has a damping rate Γ_2 comparable with the one of the OPO cavity, i.e., the intracavity field builds up with a memory time shorter than the time needed to see the full effect of squeezing. In Fig 3.5(b), we use a detector system with a narrow bandwidth, the cavity builds up light over a longer time interval, and the degree of squeezing is clearly larger than in 3.5(a). For $\delta = 0$, the Ricatti equation can be solved analytically, and we obtain

$$V_{\max} = \frac{8g\Gamma_2 - 2\Gamma_1\Gamma_2 - 16g^2 - \Gamma_1^2}{8g\Gamma_2 - 2\Gamma_1\Gamma_2 - 16g^2 - \Gamma_1^2 + 8g\Gamma_1}. \tag{3.46}$$

Here $V_{\min}$ is obtained from $V_{\max}$ by replacing g with $-g$. Figure 3.6 shows $V_{\min}$ and $V_{\max}$ as a function of Γ_2. For large Γ_2, the second cavity is equally fed by a wide range of frequency components, and the variance is dominated by vacuum uncertainty: $V_{\min} = V_{\max} = 1/2$. If $\Gamma_2 = 0$ we get

$$V_{\max} = \frac{16g^2 + \Gamma_1^2}{(\Gamma_1 - 4g)^2}, \tag{3.47a}$$

$$V_{\min} = \frac{16g^2 + \Gamma_1^2}{(\Gamma_1 + 4g)^2}. \tag{3.47b}$$

Which equals the long-time integrated amplitudes (3.30).

We note that the calculations here were significantly easier than in the case where we treated a large number of light segments simultaneously. This is because the mode of the second cavity in practice integrates the incident field over time and stores the contribution of many short beam segments in a single set of variables. We believe that this is a useful model of a realistic detector with finite bandwidth, and that the approach can be used quite

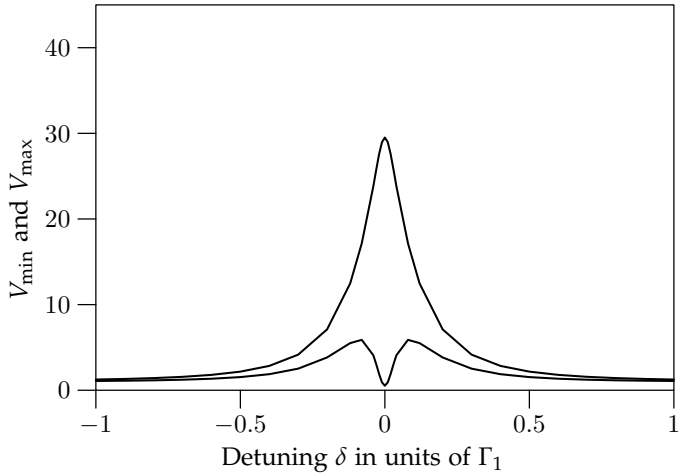

(a)

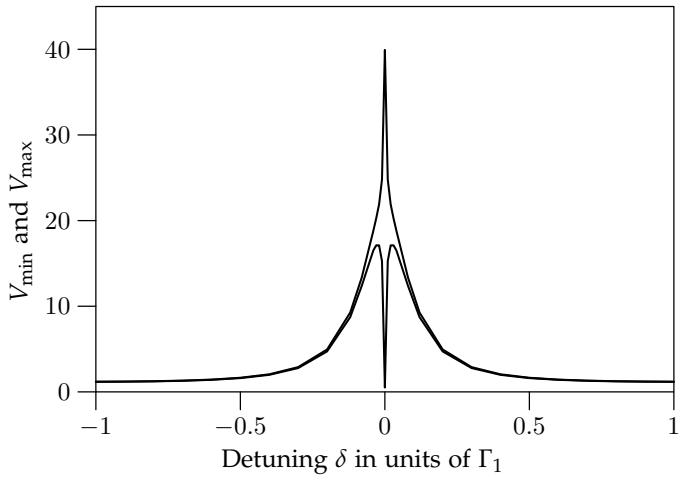

(b)

Figure 3.5: The variances V_{min} and V_{max} of the field inside the probing cavity as function of the detuning δ of this cavity with respect to ω_c in units of Γ_1. We have used $\Gamma_1 = 2\pi \times 6 \times 10^6\,\text{s}^{-1}$ and $g = 0.2\Gamma_1$ as in Fig. 3.2. In (a) we have used a damping rate comparable with the one of the OPO cavity, $\Gamma_2 = \Gamma_1/25$, so we do not see the full effect of squeezing. In (b) the damping rate is much smaller, $\Gamma_2 = \Gamma_1/400$, and consequently the degree of squeezing is much larger than in (a).

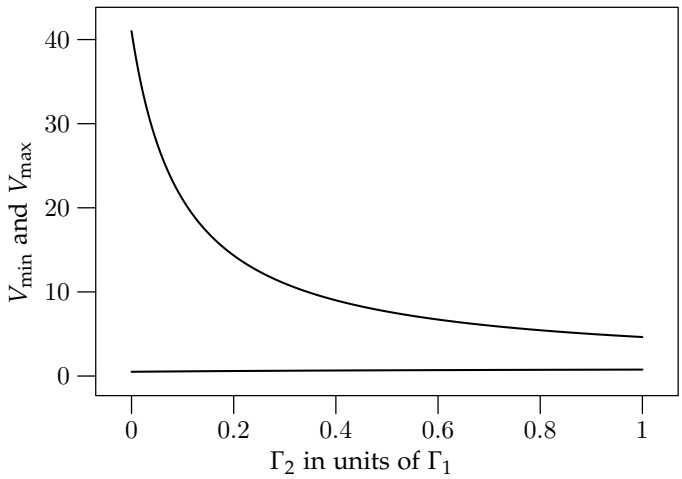

Figure 3.6: Shows the variances $V_{\min}$ and $V_{\max}$ of the field inside the probing cavity as a function of the decay width for $\delta = 0$. We have used $\Gamma_1 = 2\pi \times 6 \times 10^6\,\mathrm{s}^{-1}$ and $g = 0.2\Gamma_1$.

generally to investigate how finite optical bandwidth detection affects the sensitivity of metrology and the entanglement and spin squeezing of atomic samples.

3.5 Conclusion

In summary, we have presented a Gaussian state description of the light from an optical parametric oscillator and its interaction with large atomic samples. The treatment is very effective, because the state of the parts of the beam that have just left the OPO cavity can be treated as a single mode, corresponding to a short beam segment, and after the interaction, the segment can be eliminated from the formalism. In this chapter, we presented the dynamics when the field is probed by homodyne detection, and it is turned into classical information; if the beam propagates away without detection, it may be traced out of the formalism, which is an even simpler operation in the Gaussian formalism, since the corresponding rows and columns in the covariance matrix should just be removed. Finite bandwidth effects were included in the treatment by retaining the quantum state of the intracavity field, which is also a

single field mode, i.e., at the price of adding a single pair of canonically conjugate variables (x_c, p_c), which in the Gaussian formalism is done by adding two extra rows and columns to the covariance matrix.

The use of squeezed light holds the potential to, e.g., improve spin squeezing, entanglement, and precision probing, and in chapter 5 we will demonstrate such an improvement in the case of magnetometry compared with the infinite bandwidth case.

Four

Magnetometry

In this chapter we will use the Gaussian theory to describe how to estimate a magnetic field. When a magnetic field interacts with a trapped gas of spin polarized atoms, the magnetic field causes a rotation of the atomic spin. This rotation affects a probe beam propagating through the atomic gas and by measuring the probe beam we get an estimate of the magnetic field. In this chapter we will also discuss how to include noise in the Gaussian theory.

4.1 Introduction

We present a theory for the estimation of a scalar magnetic field by its influence on an ensemble of trapped spin polarized atoms which is continuously probed by a light beam like it is done in Refs. [8, 39–43]. The setup is shown in Fig. 4.1. The atoms interact off-resonantly with a continuous laser field, and the measurement of the polarization rotation of the probe light [44], induced by the dispersive atom-light coupling, leads to spin-squeezing of the atomic sample. This method enables an estimate of the magnetic field which is more precise than that expected from standard counting statistics. For polarized light and polarized atoms we can describe the non-classical components of the collective spin angular momentum for the atoms and the collective Stokes vectors of the light field by effective Gaussian position and momentum variables, and this description is practically exact.

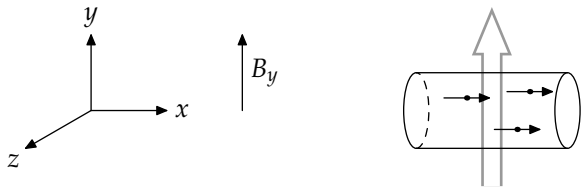

Figure 4.1: Setup for measuring the B-field component along the y-axis. In our method we use an atomic gas polarized along the x-axis and a photon probe beam propagating along the y-axis with a classical S_x. The B-field causes a rotation of the atomic spin J_z, and J_z causes a rotation of the Stokes parameter S_y, so by measuring S_y we obtain an estimate of the B-field.

The purpose of introducing the Gaussian state formalism is to provide a theoretical approach that allows a treatment of the interaction between light and an atomic sample in the regime where the quantum state of the atoms changes both because of the interaction itself and because the continuous measurements of the light field after the interaction teaches the observer about the state of the atoms. This measurement induced back-action on the quantum state of the atoms plays a role in atomic magnetometry. It has been used to spin squeeze atomic gases [43] and to entangle pairs of gases [24, 39, 45], and it recently played an important role in the realization of an atomic memory for light [45, 46]. Another advantage of the Gaussian formalism is that it is also possible to include noise. We will do this by in-

troducing stimulated emission of the atoms and photon absorption into our Gaussian description.

We have three kinds of variables (atoms, photons, and the B-field) and in Sec. 4.2 we will describe these variables and describe how to include them in the Gaussian theory. In Sec. 4.3 we will look at the interactions between these variables. It is due to these interactions that it is possible to estimate the B-field. Then in Sec. 4.4 we will use the Gaussian theory to estimate the B-field. Instead of estimating the B-field indirectly by measuring on the probe beam we could do a measurement directly on the atoms and this is discussed in Sec. 4.5. Finally in Sec. 4.6 we will include noise in the Gaussian theory and discuss how it affects the results.

4.2 Gaussian Variables

4.2.1 Atomic Variables

We consider a gas with a macroscopic number N_{at} of atoms with two degenerate Zeeman states. Initially, all the atoms are prepared by optical pumping in the same internal quantum state, and all interactions are assumed to be invariant under permutations of the atoms. The dynamics are conveniently described by the collective effective spin operator $\mathbf{J} = \frac{\hbar}{2}\sum_i \boldsymbol{\sigma}_i$ with $\boldsymbol{\sigma}_i$ being the Pauli matrices describing the individual two-level atoms. The atoms are initially prepared in such a way that their spin is polarized along the x-axis, and we assume only a small depolarization during the interaction, so that the operator J_x can be well approximated by a constant number $\langle J_x\rangle = \frac{\hbar N_{\text{at}}}{2}$. The other two projections of the collective spin, J_y and J_z, obey the commutation relation $[J_y, J_z] = i\hbar J_x$ and the resulting uncertainty relation on J_y and J_z, i.e., on the number of atoms populating the σ_y and σ_z atomic eigenstates, precisely reflects the binomial distribution of atoms on these states. The commutator may be rewritten as $[x_{\text{at}}, p_{\text{at}}] = i$ for the effective canonical position and momentum variables

$$x_{\text{at}} = \frac{J_y}{\sqrt{\hbar\langle J_x\rangle}}, \tag{4.1a}$$

$$p_{\text{at}} = \frac{J_z}{\sqrt{\hbar\langle J_x\rangle}}, \tag{4.1b}$$

and the binomial population statistics of the collective states nicely maps to the Gaussian probability distributions of x_{at} and p_{at}.

4.2.2 Stokes Parameters

The polarization of light can be described using the Stokes vector which describes the difference between the number of photons with different polarizations (see, e.g., [47])

$$S_x = \tfrac{1}{2}(n_x - n_y) = \tfrac{1}{2}(a^\dagger_{\sigma^+} a_{\sigma^-} + a^\dagger_{\sigma^-} a_{\sigma^+}), \tag{4.2a}$$
$$S_y = \tfrac{1}{2}(n_{+45^\circ} - n_{-45^\circ}) = \tfrac{i}{2}(a^\dagger_{\sigma^-} a_{\sigma^+} - a^\dagger_{\sigma^+} a_{\sigma^-}), \tag{4.2b}$$
$$S_z = \tfrac{1}{2}(n_{\sigma^+} - n_{\sigma^-}) = \tfrac{1}{2}(a^\dagger_{\sigma^+} a_{\sigma^+} - a^\dagger_{\sigma^-} a_{\sigma^-}). \tag{4.2c}$$

The light propagates in the z-direction, and x, y, and $\pm 45^\circ$ refer to linear polarized light in the xy-plane, whereas $\sigma^\pm$ refers to right and left circular polarized light. The Stokes vector satisfies angular momentum commutation relations

$$[S_y, S_z] = i\hbar S_x. \tag{4.3}$$

This can be shown by inserting the Stokes parameters from Eq. (4.2) into Eq. (4.3) and then use the commutation relations for a and $a^\dagger$. In this case the probe beam propagates along the y-axis and is linearly polarized such that its Stokes parameter S_x is classical, $\langle S_x \rangle = \frac{\hbar N_{\text{ph}}}{2}$, where N_{ph} is the number of photons.

From the Heisenberg uncertainty relation we obtain

$$\text{Var}(S_y) \times \text{Var}(S_z) \geq \frac{S_x^2}{4}. \tag{4.4}$$

If $\text{Var}(S_y) = \text{Var}(S_z) = S_x/2$ we say that the noise of S_y and S_z is at the shotnoise level.

We will also introduce dimensionless position and momentum operators for the non-classical components of the Stokes vector

$$x_{\text{ph}} = \frac{S_y}{\sqrt{\hbar \langle S_x \rangle}}, \tag{4.5a}$$
$$p_{\text{ph}} = \frac{S_z}{\sqrt{\hbar \langle S_x \rangle}}, \tag{4.5b}$$

as we did for the atomic variables in Sec. 4.2.1. The commutation relation is $[x_{\text{ph}}, p_{\text{ph}}] = i$.

4.2.3 The Magnetic Field

The B-field is a classical parameter, but we will here treat it as a quantum variable. The reason why we can do this is that a classical variable can be seen as a quantum variable for which a classical description is sufficient. We could also imagine a canonically conjugate variable to B having an uncertainty much larger than required by Heisenberg's uncertainty relation. However, we do not need this conjugate variable and will therefore not include it in our calculations.

In the following we will use quantum non-demolition (QND) measurements and this implies that the variance of the static B-field decreases monotonically and this is consistent with the classical parameter estimation (we will not forget what we have already learned about B so the variance of B cannot increase).

4.3 Interactions in the System

In the last section we have described the atoms, the photons, and the B-field separately, and thus our Gaussian variables are $\mathbf{y} = (B_y, x_{\text{at}}, p_{\text{at}}, x_{\text{ph}}, p_{\text{ph}})^T$. We will now look at the interactions between the B-field and the atoms, and between the atoms and the photons, which together makes it possible to estimate the B-field.

4.3.1 Larmor Precession of an Atomic Spin

When atoms are placed in an external magnetic field, the B-field causes a Larmor rotation of the atomic spin. The Hamiltonian for this interaction is (see e.g. [48])

$$\mathcal{H}_{\text{int}} = \frac{\beta}{\hbar}\mathbf{B}\cdot\mathbf{J} = \frac{\beta}{\hbar}B_y J_y, \tag{4.6}$$

where β is the atomic magnetic moment and where we have assumed that the B-field is oriented along the y-direction. As we can see from Heisenberg's equation of motion, the B-field causes a rotation of J_z

$$\dot{J}_z = -\frac{\beta}{\hbar}B_y J_x, \tag{4.7}$$

whereas J_y is unaffected by the interaction.

4.3.2 Faraday Rotation of the Polarization of Light

When the probe beam passes through the atoms, the polarization of the probe beam is changed. The Hamiltonian for this interaction is [49, 50]

$$\mathcal{H}_{\text{int}} = 2\frac{\tilde{g}^2}{\hbar\Delta} J_z S_z. \tag{4.8}$$

Here Δ is the detuning from resonance and $\tilde{g} = \sqrt{\frac{\hbar\omega}{Ac\tau\epsilon_0}}\frac{d}{\hbar}$ is the coupling constant, where $\hbar\omega$ is the photon energy, A is the intersection area, and d is the atomic dipole moment. From Heisenberg's equation of motion we can see that J_z causes a rotation of S_y

$$\dot{S}_y \propto J_z S_x, \tag{4.9}$$

and because the B-field causes a rotation of J_z, we are able to estimate the B-field by measuring how much S_y is rotated.

The complete derivation of Eq. (4.8) can be found in, e.g., [49]. Here we will show a qualitative derivation of the atom–light interaction [49]. When polarized light passes through an atomic sample the polarization of the light may change due to different effects. If different polarization components experience different absorption or different index of refraction, then the polarization will change. The absorption profile falls off as $1/\Delta^2$ whereas dispersion effects fall off as $1/\Delta$, so by choosing the detuning sufficiently large we can ignore absorption effects. Instead we will in the following consider different dispersion effects, i.e., situations where the index of refraction is different for two orthogonal polarization components.

In Fig. 4.2(a) we have a light beam propagating along the z-axis through an atomic sample which is polarized along the x-axis. If we look at it classically, then because of symmetry we may have $n_x \neq n_y$ (linear birefringence), while, e.g., $n_{+45^\circ} = n_{-45^\circ}$ and $n_{\sigma^+} = n_{\sigma^-}$. In this case x- and y-polarized light pass through the atoms without any change so S_x is unchanged. If we instead consider light polarized along the $+45^\circ$-direction then it has both an x-part and a y-part and they experience different phase shifts and thus the polarization of the light changes. This means that S_y and similarly S_z are changed when the light passes through the atoms.

In Fig. 4.2(b) we have a similar situation, but now the atoms are polarized along the z-axis instead of along the x-axis. Classically, a spin pointing along the z-axis is the same as a charged particle rotating in one direction around the z-axis, so we may have $n_{\sigma^+} \neq n_{\sigma^-}$ (circular birefringence), while $n_x = n_y$

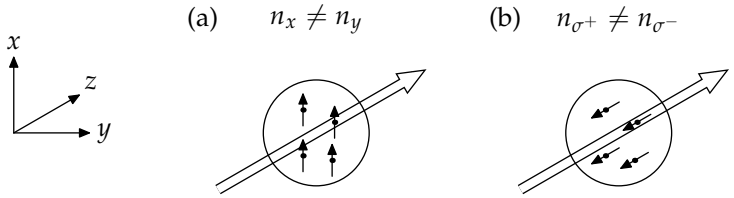

Figure 4.2: In (a) we have an atomic sample polarized along the x-axis, so we have $n_x \neq n_y$ (linear birefringence). This changes the polarization of a probe beam propagating along the z-axis such that S_y and S_z change and S_x is unchanged. In (b) the atomic sample is polarized along the z-axis, so we have $n_{\sigma^+} \neq n_{\sigma^-}$ (circular birefringence). This changes the polarization of the probe beam such that S_x and S_y change and S_z is unchanged.

and $n_{+45^\circ} = n_{-45^\circ}$. In this case σ^+- and σ^--polarized light is unchanged when it passes through the atoms, so S_z is unchanged. Linearly polarized light consists of both σ^+- and σ^--polarized light and as they experience different phase shifts the polarization of linear light changes and thus S_x and S_y change.

Linear birefringence is caused by alignment terms, e.g., $j_x^2 - j_y^2$ and for spin-1/2 atoms we have $j_x^2 = j_y^2 = 1/4$. If the detuning is much larger than the hyperfine splitting of the excited states, ω_{hfs}, then the probe laser only experiences the spin-1/2 properties of the electron. Linear birefringence is approximately proportional to $\omega_{\text{hfs}}/\Delta^2$, whereas circular birefringence is possible for spin-1/2 atoms and it is proportional to $1/\Delta$. We may therefore assume that the linear birefringence is zero.

We will now consider light propagating along the z-axis that is polarized along the x-axis and atoms polarized along the z-axis. We have a small spin component J_z[1] and due to circular birefringence this causes a rotation of S_y

$$S_{y,\text{out}}(t) = S_{y,\text{in}}(t) + \alpha S_x J_z(t), \tag{4.10}$$

where "in" and "out" refers to the light before and after the interaction with the atoms and where α is a constant that describes the strength of the interaction. This equation corresponds to Eq. (4.9). We neglected linear birefrin-

[1]For example due to the Larmor rotation caused by a B-field as shown in the previous section.

gence, and circular birefringence does not affect S_z, so S_z is unchanged by this interaction.

4.4 Estimation of the Magnetic Field

In this section we want to find the time-development of the uncertainty of the B-field so we use the theory described in Sec. 3.2. In this case our Gaussian variables are $\mathbf{y} = (B_y, x_{\text{at}}, p_{\text{at}}, x_{\text{ph}}, p_{\text{ph}})^T$. If there is more than one B-field, atomic gas, or probe beam then these should be included and the corresponding equations for the Gaussian theory should be modified according to this. This will be the case in chapter 6 where we will investigate how to estimate B-fields in 2 and 3 dimensions.

If we introduce the Gaussian variables in the Hamiltonians for the Larmor precession of the atoms (4.6) and the Faraday rotation of the light (4.8) then we obtain the following effective Hamiltonian in the little time step τ

$$\mathcal{H}_{\text{int}}\tau = \hbar(\kappa_\tau p_{\text{at}} p_{\text{ph}} + \mu_\tau B_y x_{\text{at}}). \tag{4.11}$$

The interaction constants are

$$\kappa_\tau = \kappa\sqrt{\tau} = \frac{\hbar\omega d^2}{\Delta A \hbar^2 c\epsilon_0}\sqrt{N_{\text{at}}\Phi}\sqrt{\tau}, \tag{4.12}$$

$$\mu_\tau = \mu\tau = \frac{\beta}{\hbar}\sqrt{\frac{N_{\text{at}}}{\hbar}}\tau, \tag{4.13}$$

where the different quantities are defined after Eq. (4.6) and (4.8). We derive the transformation matrix $\mathbf{S}$ using the Heisenberg equations of motion ($\dot{A} = \frac{1}{i\hbar}[A, \mathcal{H}]$)

$$\mathbf{S} = \begin{pmatrix} 1 & 0 & 0 & 0 & 0 \\ 0 & 1 & 0 & 0 & \kappa_\tau \\ -\mu_\tau & 0 & 1 & 0 & 0 \\ 0 & 0 & \kappa_\tau & 1 & 0 \\ 0 & 0 & 0 & 0 & 1 \end{pmatrix}. \tag{4.14}$$

We make a homodyne measurement on x_{ph} to estimate the B-field. When we use Eq. (3.5)–(3.8) we let $\mathbf{A}_\gamma$ be the covariance matrix for the B-field and the atoms, $\mathbf{y}_1 = (B_y, x_{\text{at}}, p_{\text{at}})^T$, and we let $\mathbf{B}_\gamma$ be the covariance matrix for the photons, $\mathbf{y}_2 = (x_{\text{ph}}, p_{\text{ph}})^T$, and $\mathbf{C}_\gamma$ is again the correlation matrix for $\mathbf{y}_1$ and $\mathbf{y}_2^T$.

Physical quantity	Value
Initial uncertainty	$\Delta B_0 = 1\,\mathrm{pT}$
Total number of atoms	$N_{\mathrm{at}} = 2 \times 10^{12}$
Total photon flux	$\Phi = 5 \times 10^{14}\,\mathrm{s}^{-1}$
Intersection area	$A = 2\,\mathrm{mm}^2$
Wavelength	$\lambda = 852\,\mathrm{nm}$
Detuning	$\frac{\Delta}{2\pi} = 10\,\mathrm{GHz}$
Atomic dipole moment	$d = 2.61 \times 10^{-29}\,\mathrm{Cm}$
Decay rate of atoms	$\Gamma = 3.1 \times 10^{7}\,\mathrm{s}^{-1}$
Small time step	$\tau = 1 \times 10^{-8}\,\mathrm{s}$
Coupling between atoms and B-fields	$\mu = 8.79 \times 10^{4}\,\mathrm{s}^{-1}$
Coupling between atoms and photons	$\kappa^2 = 1.83 \times 10^{6}\,\mathrm{s}^{-1}$
Noise due to atomic decay	$\eta = 1.76\,\mathrm{s}^{-1}$
Noise due to photon absorption	$\epsilon = 0.0281$

Table 4.1: Values of the physical quantities which we have used in the calculations. The noise terms will be discussed in Sec. 4.6.

It is possible to find the analytical expression for the covariance matrix as a function of time. When deriving the differential equation from the update formulas in Eq. (3.3) and Eq. (3.5)–(3.8), we keep only terms linear in τ, that is linear in κ_τ^2 or in μ_τ. As B_y only causes a rotation of $J_z \propto p_{\mathrm{at}}$, $x_{\mathrm{at}} \propto J_y$ does neither couple to B_y nor to p_{at} so we only have to solve a 2×2 system with $\mathbf{y} = (B_y, p_{\mathrm{at}})^T$. The differential equation can be solved by translating it into the matrix Ricatti form (3.17). In this case we have

$$\mathbf{C}_{\mathrm{R}} = 0, \tag{4.15}$$

$$\mathbf{D}_{\mathrm{R}} = \begin{pmatrix} 0 & 0 \\ \mu & 0 \end{pmatrix}, \tag{4.16}$$

$$\mathbf{E}_{\mathrm{R}} = \mathbf{D}_{\mathrm{R}}^T, \tag{4.17}$$

$$\mathbf{B}_{\mathrm{R}} = \begin{pmatrix} 0 & 0 \\ 0 & \kappa^2 \end{pmatrix}. \tag{4.18}$$

This gives us eight coupled differential equations which can be solved with

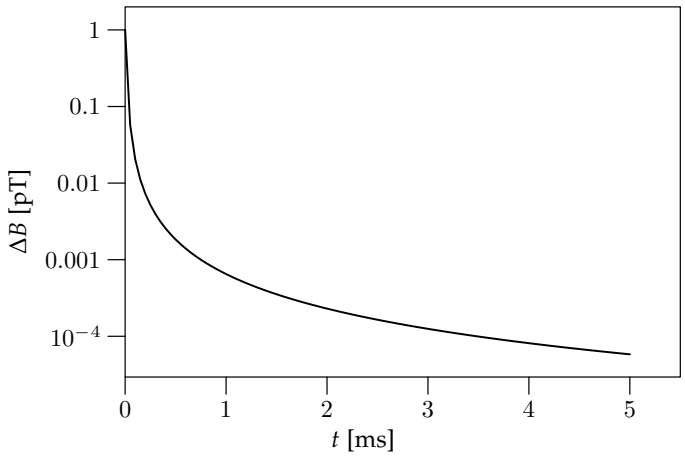

Figure 4.3: Uncertainty of B_y as a function of time. By using the setup in Fig. 4.1 the uncertainty decreases as $1/t^{3/2}$. The value at $t = 5\,\text{ms}$ is $\Delta B_y = 5.814 \times 10^{-5}\,\text{pT}$. We have used the values of Table 4.1 in our calculations.

this result for the variance of the B-field:

$$\begin{aligned} \text{Var}(B_y(t)) &= \frac{\text{Var}(B_{y_0})(\kappa^2 t + 1)}{\frac{1}{6}\kappa^4\mu^2\,\text{Var}(B_{y_0})t^4 + \frac{2}{3}\kappa^2\mu^2\,\text{Var}(B_{y_0})t^3 + \kappa^2 t + 1} \\ &\xrightarrow[t\to\infty]{} \frac{6}{\kappa^2\mu^2 t^3} \propto \frac{1}{N_{\text{at}}^2 \Phi t^3}. \end{aligned} \tag{4.19}$$

From standard counting statistics we would have expected the variance to decrease as $1/(N_{\text{at}}t)$. However, it is seen that we get a stronger decrease of $\text{Var}(B_y(t))$. Because our measurements squeeze the atoms, the variance on p_{at} decreases while the variance on x_{at} increases. We get a rapid reduction with time of the variance with the same $1/t^3$ scaling as predicted classically by the Cramer-Rao lower bound on frequency estimation. This bound is attained theoretically by maximum likelihood analyses and by linear regression on sequences of input data [51], and it was recently demonstrated experimentally with a data taking system for atomic magnetometry [52]. In Fig. 4.3 it is shown how the uncertainty of the B-field decrease as a function of the measuring time. The values we have used to generate the figure is shown in Table 4.1.

4.5 Stern-Gerlach Measurement on the Atoms

So far We have estimated the B-field indirectly by measuring the photons but we might imagine that we would obtain a better result if we measured directly on the atoms. However, there is a problem with this because when we measure directly on the atoms we also destroy the state such that we cannot measure again. It is therefore only possible to do this once, after we are finished with the measurements on the photons.

We want to take advantage of this possibility by once doing a destructive Stern-Gerlach measurement on the atoms. When we measure p_{at} we get directly information about the B-field. This measurement can be made in a similar way as the measurements on the photons, but now we only look at the system consisting of the magnetic fields and the atoms. We can use the transformations in Eq. (3.6)–(3.8) if we let $\mathbf{A}_\gamma$ be the covariance matrix for the B-field and $\mathbf{B}_\gamma$ the covariance matrix for the atoms and $\mathbf{C}_\gamma$ then contains the correlations between the B-field and the atoms.

If we perform this measurement at time t we get the following variance

$$\Delta B^2_{y_{\text{SG}}} = \frac{\Delta B^2_{y_0}}{\frac{2}{3}\kappa^2\mu^2\Delta B^2_{y_0}t^3 + 2\mu\Delta B^2_{y_0}t^2 + 1} \xrightarrow[t\to\infty]{} \frac{3}{2\kappa^2\mu^2t^3}, \tag{4.20}$$

which, for large t, is a factor of 4 smaller than the result in Eq. (4.19) where we did not perform a measurement directly on the atoms. So by doing a Stern-Gerlach measurement in the end we can improve the result with a factor of 4.

4.6 Magnetometry with Noise

So far we have ignored noise, but we will include that now. We look at two kinds of noise. Due to the photons there is a small probability for stimulated emission of the atoms which occurs at a rate [8, 53]

$$\eta = \Phi\frac{\sigma}{A}\frac{\frac{\Gamma^2}{4}}{\frac{\Gamma^2}{4} + \Delta^2}, \tag{4.21}$$

where Γ is the atomic decay rate and $\sigma = \frac{\lambda^2}{(2\pi)}$ is the resonant photon absorption cross-section. Another kind of noise is the probability for photon

absorption, which is given by [53]

$$\epsilon = N_{\text{at}} \frac{\sigma}{A} \frac{\frac{\Gamma^2}{4}}{\frac{\Gamma^2}{4} + \Delta^2}. \tag{4.22}$$

We need to modify the transformations in section 3.2 in order to include noise, and to do that we require that $\eta_\tau = \eta\tau \ll 1$ and $\epsilon \ll 1$.

When the atoms decay, the polarization of the atoms also decays and this introduce noise. One atom has a probability $\eta_\tau = \eta\tau$ to decay in time τ so in this time $\langle \mathbf{J} \rangle \mapsto (1 - \eta_\tau)\langle \mathbf{J} \rangle$. Thus the reduction of the coupling strengths in every time interval τ is

$$\kappa_\tau \mapsto \sqrt{1 - \eta_\tau}\kappa_\tau \tag{4.23}$$

and

$$\mu_\tau \mapsto \sqrt{1 - \eta_\tau}\mu_\tau. \tag{4.24}$$

Similarly the photon absorption reduces the polarization of the photons such that $\langle \mathbf{S} \rangle \mapsto (1 - \epsilon)\langle \mathbf{S} \rangle$ in a time step τ, but as we use a new pulse in every time step it does not reduce κ_τ and μ_τ correspondingly.

To determine the new transformation of the covariance matrix we derive how terms like $\langle J_z^2 \rangle$ and $\langle J_x \rangle$ transform. The total spin is a sum of the individual spins $\mathbf{J} = \frac{\hbar}{2} \sum_i \boldsymbol{\sigma}^{(i)}$ and similarly for the z-component. From this we get the following expression

$$\begin{aligned} \langle J_z^2 \rangle &= \frac{\hbar^2}{4} \sum_{i=1}^{N_{\text{at}}} \langle (\sigma_z^{(i)})^2 \rangle + \frac{\hbar^2}{4} \sum_{i \neq j} \langle \sigma_z^{(i)} \sigma_z^{(j)} \rangle \\ &= \frac{\hbar^2}{4} N_{\text{at}} \langle (\sigma_z^{(1)})^2 \rangle + \frac{\hbar^2}{4} N_{\text{at}}(N_{\text{at}} - 1) \langle \sigma_z^{(1)} \sigma_z^{(2)} \rangle, \end{aligned} \tag{4.25}$$

where we have used that there is symmetry under exchange of particles such that $\langle (\sigma_z^{(i)})^2 \rangle = \langle (\sigma_z^{(1)})^2 \rangle$ for all i and $\langle \sigma_z^{(i)} \sigma_z^{(j)} \rangle = \langle \sigma_z^{(1)} \sigma_z^{(2)} \rangle$ for all $i \neq j$. In a time τ, $\eta_\tau N_{\text{at}}$ atoms decay. This leads to a decrease in the collective spin squeezing so in the above expression each N_{at} should be multiplied with $(1 - \eta_\tau)$, but the atoms still provide a contribution of $\frac{\hbar^2}{4}$ per atom giving an

extra term

$$\begin{aligned}\langle J_z^2\rangle \mapsto\ & \tfrac{\hbar^2}{4}N_{\mathrm{at}}(1-\eta_\tau)\\ &+\tfrac{\hbar^2}{4}N_{\mathrm{at}}(1-\eta_\tau)(N_{\mathrm{at}}(1-\eta_\tau)-1)\langle\sigma_z^{(1)}\sigma_z^{(2)}\rangle\\ &+\tfrac{\hbar^2}{4}N_{\mathrm{at}}\eta_\tau.\end{aligned} \tag{4.26}$$

If we now isolate $\langle\sigma_z^{(1)}\sigma_z^{(2)}\rangle$ from Eq. (4.25) and insert it into Eq. (4.26) and if we use that the number of atoms is large, then we get this transformation

$$\langle J_z^2\rangle \mapsto (1-\eta_\tau)^2\langle J_z^2\rangle + \tfrac{\hbar^2}{4}N_{\mathrm{at}}\eta_\tau(2-\eta_\tau). \tag{4.27}$$

In a similar way we find the transformations for the other components

$$\langle J_i\rangle \mapsto \langle J_i\rangle(1-\eta_\tau), \qquad i=x,y,z. \tag{4.28}$$

We are now able to determine how one of the elements in the covariance matrix transforms by using the transformations in Eqs. (4.27) and (4.28) and by using that for small η_τ

$$\begin{aligned}2\,\mathrm{Var}(p_{\mathrm{at}}) &= 2(\langle P_{\mathrm{at}}^2\rangle - \langle p_{\mathrm{at}}\rangle^2)\\ &= 2\frac{\langle J_z^2\rangle - \langle J_z\rangle^2}{\hbar\langle J_x\rangle} \mapsto \frac{\hbar N_{\mathrm{at}}}{\langle J_x\rangle}\eta_\tau.\end{aligned} \tag{4.29}$$

The other elements in the covariance matrix involving the atoms can be derived in a similar way. The derivation for the photons is nearly identical except that we do not get the last term in Eq. (4.26) as we use new photons in each time step and this gives a factor of $\frac{1}{2}$ in Eq. (4.29).

To include noise in the transformation we therefore modify Eqs. (3.2) and (3.3) [53]

$$\mathbf{m}(t+\tau) = \mathbf{LS}\mathbf{m}(t), \tag{4.30}$$

$$\gamma(t+\tau) = \mathbf{LS}\gamma(t)\mathbf{S}^T\mathbf{L} + \frac{\hbar N_{\mathrm{at}}}{\langle J_x(t)\rangle}\mathbf{M} + \frac{\hbar N_{\mathrm{ph}}}{2\langle S_x(t)\rangle}\mathbf{N}, \tag{4.31}$$

where we have $\mathbf{L} = \mathrm{diag}(1, \sqrt{1-\eta_\tau}, \sqrt{1-\eta_\tau}, \sqrt{1-\epsilon}, \sqrt{1-\epsilon})$, $\mathbf{M} = \mathrm{diag}(0, \eta_\tau, \eta_\tau, 0, 0)$, and $\mathbf{N} = \mathrm{diag}(0,0,0,\epsilon,\epsilon)$. In each time step τ the factor in front of $\mathbf{M}$ is divided by $(1-\eta_\tau)$ due to the transformation of $\langle J_x\rangle$. We must also remember to update κ_τ and μ_τ due to Eq. (4.23) and (4.24). The update formulas due to homodyne detection are unchanged.

4.6.1 Analytical Solution

We will now try to solve the equations for estimating a B-field when we include noise as described above. As in Sec. 4.4 x_{at} does neither couple to B_y nor to p_{at} so we "only" have to solve the differential equation for $\mathbf{y} = (B_y, p_{\text{at}})^T$ which we can rewrite on Ricatti form with the following matrices

$$\mathbf{C}_{\text{R}} = \begin{pmatrix} 0 & 0 \\ 0 & \dfrac{N_{\text{at}}}{\langle J_x(t)\rangle}\eta \end{pmatrix}, \tag{4.32a}$$

$$\mathbf{D}_{\text{R}} = \begin{pmatrix} 0 & 0 \\ \mu & \eta/2 \end{pmatrix}, \tag{4.32b}$$

$$\mathbf{E}_{\text{R}} = \mathbf{D}_{\text{R}}^T, \tag{4.32c}$$

$$\mathbf{B}_{\text{R}} = \begin{pmatrix} 0 & 0 \\ 0 & \dfrac{(1-\epsilon)\kappa^2(t)}{1-\epsilon\left(1-\frac{N_{\text{ph}}}{2\langle S_x(t)\rangle}\right)} \end{pmatrix}. \tag{4.32d}$$

One can show that the noise terms in $\mathbf{D}_{\text{R}}$ and $\mathbf{E}_{\text{R}}$ will have vanishing effect, and if we restrict ourselves to times corresponding to $\eta t \ll 1$, we may neglect the time dependence of $\langle J_x\rangle$, $\langle S_x\rangle$, and κ such that $N_{\text{at}}/\langle J_x\rangle = 2$, $N_{\text{ph}}/\langle S_x\rangle = 2$, and $\kappa(t) = \kappa(0)$. With these approximations, the resulting linear equations for the matrices $\mathbf{U}$ and $\mathbf{W}$ can be solved analytically, leading to lengthy expressions with sums of products of exponential functions, constant terms, and terms linear in time t. In the limit $\sqrt{\eta\kappa^2}t \gg 1$, it is an accurate approximation to maintain only the leading exponential and we find

$$\text{Var}(B_y(t)) \to \frac{\eta}{\mu^2 t}. \tag{4.33}$$

Compared with the result for the noiseless case (4.19), we note that in the long time limit the uncertainty decreases as $1/(N_{\text{at}}t)$, and not as $1/(N_{\text{at}}^2t^3)$.

The black line in Fig 4.4 shows the time evolution of the uncertainty of the B-field from a numerical calculation with noise included. For short times the analytical expression disregarding the noise (red line) is a good approximation, and for long times the numerical result follows the expression (4.33), shown as a blue curve on the interval between 0.5 and 5 ms.

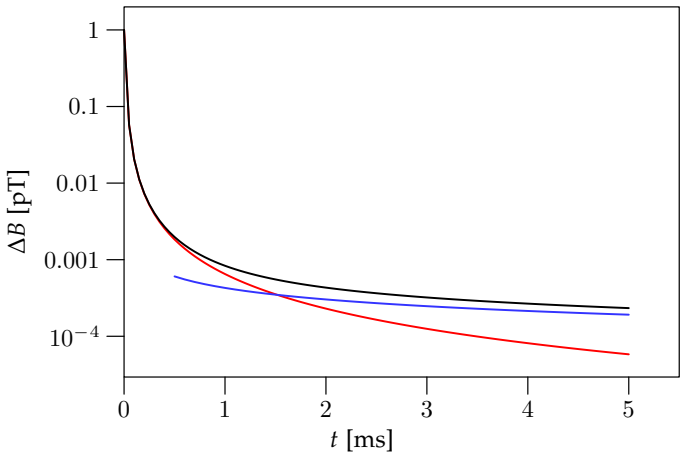

Figure 4.4: Uncertainty of the B-field as a function of time. The black line is the result of a full numerical calculation with noise included and the value at $t = 5\,\text{ms}$ is $\Delta B_y = 2.333 \times 10^{-4}\,\text{pT}$. The red line is without inclusion of noise and the value at $t = 5\,\text{ms}$ is $\Delta B_y = 5.814 \times 10^{-5}\,\text{pT}$. The blue curve shows the analytical result of Eq. (4.33) valid for $t \ll 1\,\text{s}$ and $\sqrt{\eta\kappa^2}t \gg 1$. The values which we have used can be found in Table 4.1.

4.7 Conclusion

In this chapter we have used the Gaussian theory from the previous chapter to estimate a magnetic field. We estimated the B-field by using that a B-field causes a rotation of an atomic spin of a gas of spin polarized atoms. Because the measurement squeezes the atoms the uncertainty of the B-field decreases as $1/(N_{\text{at}}t^{3/2})$ instead of $1/\sqrt{N_{\text{at}}t}$. When the photons propagates through the atoms there is a small probability for stimulated emission of the atoms, and there is a probability for photon absorption. One of the strengths of the Gaussian theory is that we can include these noise processes into the theory. When we did that we found that in the long time limit the uncertainty now only decreases as $1/\sqrt{N_{\text{at}}t}$. We also showed that by applying a destructive Stern-Gerlach measurement on the atoms in the end of the measurements the uncertainty of the B-field would be a factor of 4 smaller.

Five

Magnetometry with Squeezed Light

In the previous chapter we showed how to estimate a magnetic field. One way to improve this estimate would be to use a squeezed probe beam. In this short chapter we will use the squeezed light we generated in chapter 3 to refine the results of chapter 4. This chapter is based on the last part of paper [III]

5.1 Introduction

In the previous chapter we estimated a magnetic field by using the fact that a B-field causes a Larmor rotation of an atomic spin which again causes a polarization rotation of a probe beam. We would like to improve this estimate by using a squeezed probe beam. We will describe a simple model where we use a squeezed probe beam with infinite bandwidth. Realistic sources of squeezed light, on the other hand, have a finite bandwidth of squeezing which implies that correlations exist between the field observables at different times. This is for example the case for an optical parametric oscillator (OPO) as we showed in Sec. 3.4. We will therefore use the squeezed output light from the cavity as probe beam.

In Sec. 5.2 we will present a simple model of how to use a squeezed probe beam to estimate a B-field. In Sec. 5.3 we will describe a more realistic method, where we use the squeezed light generated in an OPO as probe beam.

5.2 Simple Model (Infinite Bandwidth)

A simple (but not correct) way to use squeezed light as probe beam is by introducing the squeezing parameter r such that Eq. (3.7) is replaced by

$$\mathbf{B}_\gamma \mapsto \begin{pmatrix} 1/r & 0 \\ 0 & r \end{pmatrix}, \tag{5.1}$$

i.e., every beam segment enters the interaction in a squeezed state. The calculations are very similar to those leading to Eq. (4.19) where we did not use squeezed light. Going though the calculations we find that κ^2 should be replaced with $\kappa^2 r$ in Eq. (4.19)

$$\begin{aligned} \mathrm{Var}(B_y(t)) &= \frac{\mathrm{Var}(B_{y_0})(\kappa^2 r t + 1)}{\frac{1}{6}\kappa^4 r^2 \mu^2 \,\mathrm{Var}(B_{y_0}) t^4 + \frac{2}{3}\kappa^2 r \mu^2 \,\mathrm{Var}(B_{y_0}) t^3 + \kappa^2 r t + 1} \\ &\xrightarrow[t\to\infty]{} \frac{6}{\kappa^2 r \mu^2 t^3} \propto \frac{1}{r N_{\mathrm{at}}^2 \Phi t^3}. \end{aligned} \tag{5.2}$$

So by using squeezed light the B-field estimate is improved with a factor $1/r$ compared with Eq. (4.19) where we did not use squeezed light as probe beam.

As noted in Ref. [8], this treatment of a squeezed beam, in the limit of small τ, is only valid if the squeezing bandwidth is infinite. The squeezing

properties of the beam from an OPO, however, only reveal themselves if a narrow frequency component is selected, or if the field is integrated over times longer than the inverse bandwidth of squeezing, which are certainly longer than the infinitesimal τ employed in the continuous limit, where the Ricatti equation is solved.

The full probing may well take longer than the inverse bandwidth, and one would hence expect that one still would benefit from the squeezing in this longer time limit. We shall verify this expected behavior by a calculation in which we treat the probing with the field coming out of our OPO cavity in the full Gaussian formalism.

5.3 Squeezed Light from an Optical Parametric Oscillator (Finite Bandwidth)

The example described in this section serves as a model for how to consider other atomic probing schemes with realistic squeezed light sources. We treat the B-field, the atomic variables, the intracavity field, and a single segment of light $\mathbf{y} = (B_y, x_{\rm at}, p_{\rm at}, x_{\rm c}, p_{\rm c}, x_{\rm ph}, p_{\rm ph})^T$ as Gaussian variables. As shown

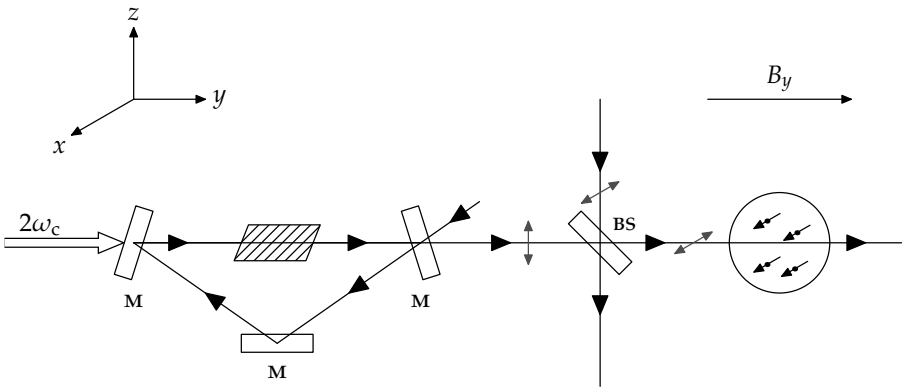

Figure 5.1: Setup for estimating a B-field using a squeezed probe beam. In the cavity, we generate squeezed light which is linearly polarized along the z-axis. We mix this field at an asymmetric beamsplitter (BS) with a strong x-polarized beam. The light then passes through a gas of x-polarized atoms, causing a rotation of the field polarization towards the z-axis (see the text for further comments).

in Fig. 5.1 the beam segment enters on the cavity mirror in the vacuum state and it is reflected off the mirror with some squeezing and some entanglement with the partly transmitted intracavity field. It then interacts with the atoms, and finally it is detected by homodyne detection, causing a moderate change of the joint covariance matrix for the B-field, the atoms, and the intracavity field.

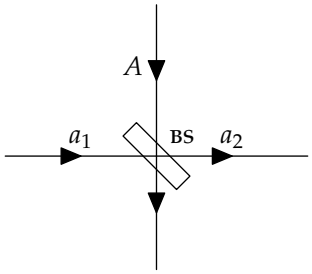

Figure 5.2: In Fig. 5.1 we showed a setup for estimating a B-field using squeezed light generated in an OPO. This figure shows the notation we use for the part where we mix the output from the cavity with a strong x-polarized beam on a beamsplitter (BS).

The OPO cavity produces a squeezed vacuum state which is not immediately in an appropriate state for polarization rotation measurements. As in the previous chapter we need a light beam that propagates along the y-axis and is linearly polarized along x such that its Stokes operator $\langle S_x \rangle = N_{\text{ph}}/2 = \Phi\tau/2$ is classical. To obtain a suitable state we therefore mix the field coming out of the cavity a_1 with a classical x-polarized field A on a beamsplitter as shown in Fig. 5.2. We denote the field propagating away from the beamsplitter and through the atoms with a_2. The reflectance and transmittance of the beamsplitter is $\rho_x = 1$ and $\tau_x = 0$ for x-polarized light and $\rho_y = 0$ and $\tau_y = 1$ for y-polarized light. The field propagating away from the beamsplitter is then

$$a_{2_x} = \rho_x A_x + \tau_x a_{1_x} = A_x, \tag{5.3a}$$
$$a_{2_y} = \rho_y A_y + \tau_y a_{1_y} = a_{1_y}. \tag{5.3b}$$

The Stokes operators for this field is then

$$S_x = \tfrac{1}{2}(a_{1_x}^\dagger a_{1_x} - a_{1_y}^\dagger a_{1_y}) = \tfrac{1}{2}A_x^2, \tag{5.4a}$$

$$S_y = \tfrac{1}{2}(a_{1_y}^\dagger a_{1_x} + a_{1_x}^\dagger a_{1_y}) = \tfrac{1}{\sqrt{2}}A_x x_{\mathrm{ph}_1}, \tag{5.4b}$$

$$S_z = \tfrac{i}{2}(a_{1_y}^\dagger a_{1_x} - a_{1_x}^\dagger a_{1_y}) = \tfrac{1}{\sqrt{2}}A_x p_{\mathrm{ph}_1}, \tag{5.4c}$$

where we have chosen the classical field A_x to be real. From Eq. (5.4a) we observe that S_x is given by the number of photons divided by 2 as requested ($A_x^2 = N_{\mathrm{ph}}$). If we use this in Eq. (5.4b) and (5.4c) we obtain the formulas for x_{ph_1} and p_{ph_2} in Eq. (4.5). We can therefore use the output field from the cavity, which is squeezed, directly in our formalism to probe the photons.

We will now use the Gaussian theory to calculate the variance of the B-field. The transformation matrix to lowest order in τ of the variables is now given by

$$\mathbf{S} = \begin{pmatrix} 1 & 0 & 0 & 0 & 0 & 0 & 0 \\ \mu\tau & 1 & 0 & 0 & 0 & 0 & 0 \\ 0 & 0 & 1 & \kappa\sqrt{\Gamma\tau} & 0 & -\kappa\sqrt{\tau} & 0 \\ 0 & 0 & 0 & \xi + 2g\tau & 0 & \sqrt{\Gamma\tau} & 0 \\ 0 & 0 & 0 & 0 & \xi - 2g\tau & 0 & \sqrt{\Gamma\tau} \\ 0 & 0 & 0 & -\sqrt{\Gamma\tau} & 0 & \xi & 0 \\ 0 & -\kappa\sqrt{\tau} & 0 & 0 & -\sqrt{\Gamma\tau} & 0 & \xi \end{pmatrix}, \tag{5.5}$$

with $\xi = 1 - \Gamma\tau/2$ as introduced in Eq. (2.8a). Note that this matrix combines the elements present in the transformation of the field components alone (3.23), used to generate squeezed light, and the B-field–atoms and light–atom interaction (4.14), used to estimate the B-field. Again the beam segment is inserted in its vacuum state (3.7), and it is probed by homodyne detection leading to the update formula (3.6). The bandwidth is taken care of by the intracavity field which establishes the necessary correlation between beam segments detected at different times. In the continuous limit we find the corresponding Ricatti equation, and its solution provides the variance of the B-field as a function of time The analytical result for $\mathrm{Var}(B)$ is very lengthy and given in appendix A. For small times t we get the result without squeezing as can be seen in Fig. 5.3, and for large t the result is exactly the same as in the infinite bandwidth case

$$\mathrm{Var}(B(t)) = \frac{6}{\mu^2 r\kappa^2 t^3} \tag{5.6}$$

if we identify the squeezing parameter by $r = \frac{(\Gamma+4g)^2}{(\Gamma-4g)^2}$. Fig. 5.3 shows the results of this calculation. The figure shows both the results without squeezing (4.19), with finite bandwidth squeezing (A.1), and the simple infinite bandwidth result (5.2) with a simple squeezing parameter r applied to each segment. We take the value $r = \frac{(\Gamma+4g)^2}{(\Gamma-4g)^2}$, corresponding to the long time limit of Eq. (3.30), and we see a good agreement for long times between the two curves for squeezed states. We also see, that the finite bandwidth curve is an improvement with respect to the case of non-squeezed light, but that we have to probe for a time on the order of the inverse squeezing bandwidth before we see the effect of squeezing. Indeed, the finite bandwidth curve is to a good approximation simply delayed by $16g\frac{3\Gamma+4g}{(\Gamma-4g)(\Gamma+4g)^2}$ compared with the infinite broad-band squeezed light curve.

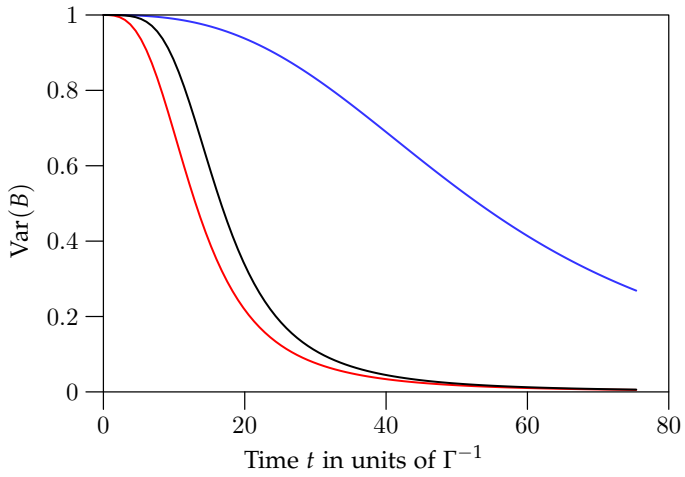

Figure 5.3: Variance of the B-field as a function of time. We use the same value of g and Γ as in Fig. 3.2 and $\kappa^2 = 1.83 \times 10^6\,\mathrm{s}^{-1}$ and $\mu = 8.79 \times 10^4\,(\mathrm{s\,pT})^{-1}$. The blue line is without squeezing, the black line is with squeezed light generated in a cavity (finite bandwidth), and the red line is with the squeezing parameter r (infinite bandwidth).

5.4 Conclusion

By using squeezed light as probe beam we demonstrated an improvement of the magnetometer described in chapter 4. We used the squeezed light generated in an OPO from chapter 3 which has a finite bandwidth of squeezing. For short probing times we obtained the same results as in the previous chapter where we did not use squeezed light. For long probing times the result agreed with a simple model where we used light with infinite bandwidth of squeezing. We also showed how the finite bandwidth of squeezing manifests itself as a time lag before the improvement is obtained in agreement with the earlier observation that squeezing is only present in a light beam, if one integrates a sufficiently long part of the beam.

Six

Magnetometry in Two and Three Dimensions

In this chapter, multi-component magnetic fields are estimated by the measurement of suitably chosen atomic observables. Precision and efficiency is gained by dividing the atomic gas into two or more samples which are entangled by the dispersive atom-light interaction. This chapter is based on paper [II].

6.1 Introduction

In chapter 4 we investigated how to obtain an estimate of one component of a magnetic field. If we want to estimate two or three B-field components we could use two or three setups like the one described in Fig. 4.1 suitably rotated, but it turns out that other setups are better. In order to make a fair comparison of different schemes, we shall assume that all measurements are carried out in a time interval of the same duration, e.g., 5 ms and that the total photon and atom number used are kept constant. In Eq. (4.19) we found this formula for the uncertainty of one B-field component for large t

$$\Delta B(t) \propto \frac{1}{N_{\mathrm{at}}\Phi^{1/2}t^{3/2}}. \tag{6.1}$$

From this formula we are able to predict the results for many of the different measurement schemes which we present in this chapter. If we, e.g., divides the atoms into two gases and such that we only use half of the atoms to estimate one B-field component we will expect that the uncertainty increases with a factor of two compared with the case where we only have one gas.

In Sec. 6.2 and Sec. 6.3 we describe how to estimate two and three B-field components respectively. In the optimal schemes we use entangled gases so therefore we quantify the amount of entanglement in Sec. 6.4.

6.2 Measuring Two Magnetic Field Components

In this section we describe how to estimate two B-field components (B_y and B_z). In the setup in Fig. 4.1 we could obtain a measurement of one component by using one atomic gas and one probe beam. If we add another probe beam we can obtain a measurement of the other B-field component as it will be described in section 6.2.1. The problem with this approach is that the two atomic components which we measure through the probe beams do not commute, so we cannot measure both at the same time with arbitrary precision. However, we can avoid this problem by using two atomic gases, which is done in section 6.2.3. In section 6.2.4 we show how to improve the measurements by entangling the two atomic gases.

6.2.1 Two Probe Beams and One Atomic Gas

Let us first consider how to measure B_y and B_z using two probe beams and one atomic gas. We are able to obtain measurements of B_y by using the setup

in Fig. 4.1. In order to obtain estimates of B_z we observe that B_z causes a rotation of $x_{\text{at}} \propto J_y$ so if we add a second optical probe beam propagating in the z-direction and with S_x classical then x_{at} will cause a rotation of the field variable $p_{\text{ph}} \propto S_z$ on the second beam which we can then measure. This gives us a symmetric setup with respect to y and z so we obtain the same uncertainty on both B_y and B_z. The problem with this approach is that unlike the unknown classical quantities B_y and B_z, the atomic observables x_{at} and p_{at} do not commute. While the first beam squeezes x_{at} and antisqueezes p_{at}, the second beam does the opposite. This means that effectively we have no squeezing of the atoms, leaving us with the $1/t$ decrease in the variance of the B-field components, which comes from classical counting statistics, as shown in Fig. 6.1.

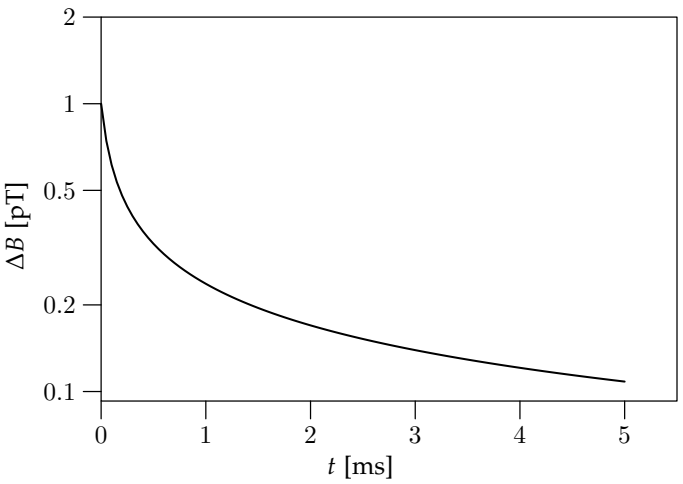

Figure 6.1: Uncertainty of two B-field components as a function of time. Here we have used a single atomic gas and two probe beams which are turned on simultaneously. The joint uncertainty of the two B-field components at $t = 5\,\text{ms}$ is $\Delta B_y = \Delta B_z = 0.1083\,\text{pT}$. We have used the numerical values of Table 4.1 in the calculations.

6.2.2 Sequential Measurements

To avoid the problem with the non-commuting variables we could either use two atomic gases as we do in the next section or we could restrict ourselves to

only using one probe beam at a time. If we turn the beams on alternately then every time we shift to the other probe beam the atoms are antisqueezed. For this reason it is best only to shift once as we have done in Fig. 6.2, where we obtain measurements of B_y in the first half and of B_z in the second half. When we switch probe beam the atoms have had some time to get rotated so they have rotated a greater angle, which would give a more precise measurement, but at the same time the relevant component of the atoms are antisqueezed, which give a less precise measurement. Which of the final uncertainties is lowest is thus an interplay between these two effects, and in this case the final uncertainty of B_z is a bit lower than the final uncertainty of B_y. The values at large t of both ΔB_y and ΔB_z is about a factor $2\sqrt{2}$ greater than if we had only estimated one component. This is because we use the same number of atoms and the same photon flux but we only measure half of the time.

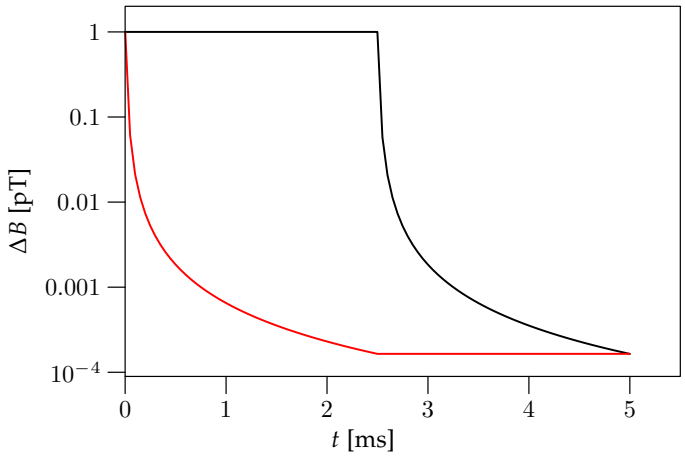

Figure 6.2: Uncertainty of two B-field components as a function of time using one atomic gas. B_y is estimated in the first half of the probing time and B_z in the second half. The red line is for B_y and the value at $t = 5\,\text{ms}$ is $\Delta B_y = 1.647 \times 10^{-4}\,\text{pT}$. The black line is for B_z and the value at $t = 5\,\text{ms}$ is $\Delta B_z = 1.645 \times 10^{-4}\,\text{pT}$. We have used the numerical values of Table 4.1 in the calculations.

6.2.3 Two Separate Gases and Two Probe Beams

In order to estimate two B-field components more precisely we need to measure on two commuting variables. We can do this by using two separate systems and estimate one B-field component on each system. So we divide our atomic gas into two separate gases and use two probe beams, one for each gas. The first system is identical to the setup in Fig. 4.1 and is used to measure B_y. The second system is nearly identical to the first system except that the probe beam propagates in the z-direction such that we estimate B_z by measuring p_{ph} on this beam.

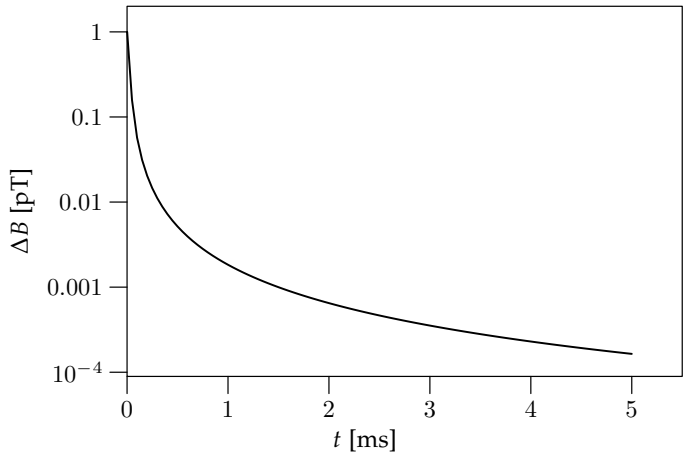

Figure 6.3: Uncertainty of two B-field components as a function of time using two separate atomic gases and two probe beams. The uncertainty at $t = 5\,\text{ms}$ is $\Delta B_y = \Delta B_z = 1.644 \times 10^{-4}\,\text{pT}$. We have used the numerical values of Table 4.1 in the calculations.

The uncertainty of the B-fields as a function of time for the situation just described is shown in Fig. 6.3 and the result is similar to the result in Fig. 4.3 except that the number of atoms and the photon flux are each divided by two as they are divided between the two systems. The uncertainty of the B-fields for large t is proportional to $1/(N_{\text{at}}\sqrt{\Phi})$ so the uncertainty for estimating two B-field components is $2\sqrt{2}$ as large as if we had only estimated one component. This is the same result as we obtained in the previous section. But actually the approach described in this section is slightly better, if we include

noise as described in Sec. 4.6. In this approach we use fewer atoms (and a smaller photon flux) and this reduces the noise giving a better estimate.

6.2.4 Two Entangled Gases and Two Probe Beams

If we entangle two gases we can obtain two commuting variables [39]. This can be done if we let one gas be polarized along x and the other along $-x$ such that $\langle J_{x_1}\rangle = -\langle J_{x_2}\rangle$. Then the two observables $(J_{y_1} - J_{y_2})$ and $(J_{z_1} - J_{z_2})$, and equivalently $(x_{\mathrm{at}_1} - x_{\mathrm{at}_2})$ and $(p_{\mathrm{at}_1} - p_{\mathrm{at}_2})$, commute. Therefore we want to couple these observables to the B-field components and the probe beams, so we use the setup shown in Fig. 6.4. Both optical probe beams have S_x classical, and one beam propagates along y, the other along z. Both beams pass through both gases and, opposite to the protocol in the previous section, we use all atoms to estimate both B-field components. The effective Hamiltonian for this setup is

$$\begin{aligned}\mathcal{H}_{\mathrm{int}}\tau = {} & \mu_\tau B_y(x_{\mathrm{at}_1} + x_{\mathrm{at}_2}) + \mu_\tau B_z(p_{\mathrm{at}_1} + p_{\mathrm{at}_2}) \\ & + \kappa_\tau(p_{\mathrm{at}_1} - p_{\mathrm{at}_2})p_{\mathrm{ph}_1} + \kappa_\tau(x_{\mathrm{at}_1} - x_{\mathrm{at}_2})x_{\mathrm{ph}_2},\end{aligned} \tag{6.2}$$

where the two minus signs can be implemented by changing the sign on κ_τ after the probe beams have passed through the first gas. In an experimen-

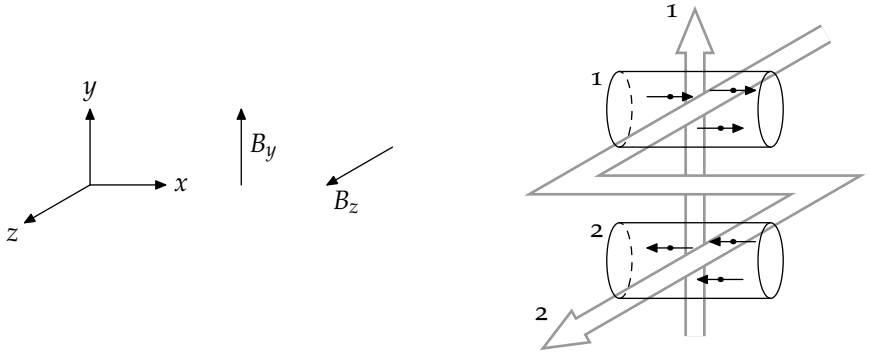

Figure 6.4: Setup for measuring two components of a B-field using two entangled gases and two probe beams. The spins of the atomic gases are polarized along x and $-x$ respectively. Both probe beams have S_x classical and both beams pass through both gases. One beam propagates along y the other along z.

tal setup the change in sign could be effectuated by changing the sign of the detuning or by interchanging σ^+ and σ^- polarizations which, e.g., can be done using a half-wave-plate [47]. In this case the Gaussian state vector is $\mathbf{y} = (B_z, B_y, x_{\mathrm{at}_1}, p_{\mathrm{at}_1}, x_{\mathrm{at}_2}, p_{\mathrm{at}_2}, x_{\mathrm{ph}_1}, p_{\mathrm{ph}_1}, x_{\mathrm{ph}_2}, p_{\mathrm{ph}_2})^T$ and from the Heisenberg equations of motion we get the following transformation matrix

$$\mathbf{S} = \begin{pmatrix} 1 & 0 & 0 & 0 & 0 & 0 & 0 & 0 & 0 & 0 \\ 0 & 1 & 0 & 0 & 0 & 0 & 0 & 0 & 0 & 0 \\ \mu_\tau & 0 & 1 & 0 & 0 & 0 & 0 & \kappa_\tau & 0 & 0 \\ 0 & -\mu_\tau & 0 & 1 & 0 & 0 & 0 & 0 & -\kappa_\tau & 0 \\ -\mu_\tau & 0 & 0 & 0 & 1 & 0 & 0 & \kappa_\tau & 0 & 0 \\ 0 & \mu_\tau & 0 & 0 & 0 & 1 & 0 & 0 & -\kappa_\tau & 0 \\ 0 & 0 & 0 & \kappa_\tau & 0 & -\kappa_\tau & 1 & 0 & 0 & 0 \\ 0 & 0 & 0 & 0 & 0 & 0 & 0 & 1 & 0 & 0 \\ 0 & 0 & 0 & 0 & 0 & 0 & 0 & 0 & 1 & 0 \\ 0 & 0 & -\kappa_\tau & 0 & \kappa_\tau & 0 & 0 & 0 & 0 & 1 \end{pmatrix}. \tag{6.3}$$

The time evolution of the uncertainty of the B-field components where we use two entangled gases is shown in Fig. 6.5. If we compare the final

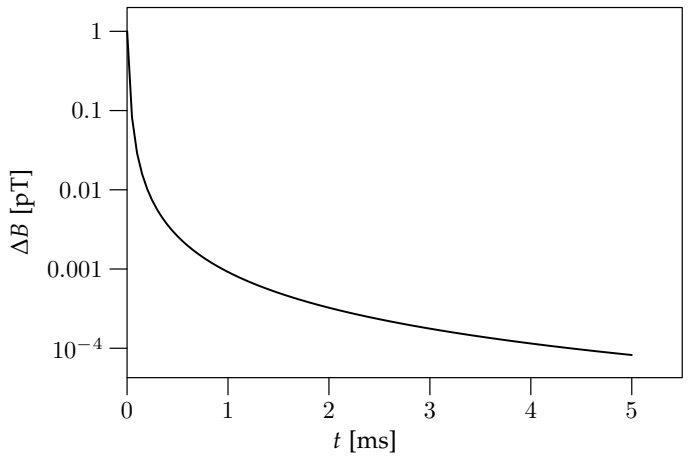

Figure 6.5: Uncertainty of two B-field components as a function of time using two atomic entangled gases and two probe beams. The uncertainty at $t = 5\,\mathrm{ms}$ is $\Delta B_y = \Delta B_z = 8.221 \times 10^{-5}\,\mathrm{pT}$. We have used the numerical values of Table 4.1 in our calculations.

uncertainty of the B-field components then it is a factor of two lower than in Fig. 6.3 where we did not entangle the atomic gases. That is what we would expect because of the $1/N_{\mathrm{at}}$ dependence. If we compare with Fig. 4.3 where we only estimated one B-field-component but used the same number of photons and atoms, then we get a $\sqrt{2}$ higher uncertainty when we estimate both B-field components. The $\sqrt{2}$ comes from the $1/\sqrt{\Phi}$ time dependence. By using entangled gases we use all the atoms to obtain measurements of both B-field components, but we only use half of the photon flux to estimate each B-field component.

6.3 Measuring All Three Components of a Magnetic Field

For the estimation of all three components of a magnetic field, the situation changes since a spin-polarized sample is not a probe for the field component parallel with the spin. For the sequential probing one would thus measure B_y and B_z as just described, but one would have to rotate the sample by 90° to determine the last component B_x, and the errors of such a rotation would limit the precision. As an alternative approach, we can divide our atomic gas and probe beam into three individual systems. This is done in section 6.3.1. This procedure is similar to our attempts of estimating two B-field components in section 6.2.3, and since this was not the most efficient way to estimate two B-field components we do not expect it to be the most efficient approach for three components either. In fact we know from the previous section that we can obtain more precise measurements if we use two entangled gases to estimate two of the components and a separate gas to estimate the third component. We discuss this scheme in section 6.3.2. In section 6.3.3 we will describe how we can obtain even more precise measurements by using six entangled gases and three probe beams.

6.3.1 Three Separate Gases and Three Probe Beams

With the setup in Fig. 4.1 we are able to estimate one B-field component. We now divide our atomic gas and probe beam into three separate systems such that we have three systems similar to the one in Fig. 4.1 but where the number of atoms and the photon flux is divided by three between the systems. With suitable rotations of two of these systems we are then able to obtain measurements of one B-field component on each system. We get a result similar to the result in section 6.2.3 where we estimated two B-field

components using two separate systems. The uncertainty of the B-fields at $t = 5\,\text{ms}$ are $\Delta B_x = \Delta B_y = \Delta B_z = 3.017 \times 10^{-4}\,\text{pT}$. We observe that this value is a factor of $3\sqrt{3}$ larger than in Fig. 4.3 where we only estimated one B-field component. This is as expected from the dependence of the number of atoms and the photon flux.

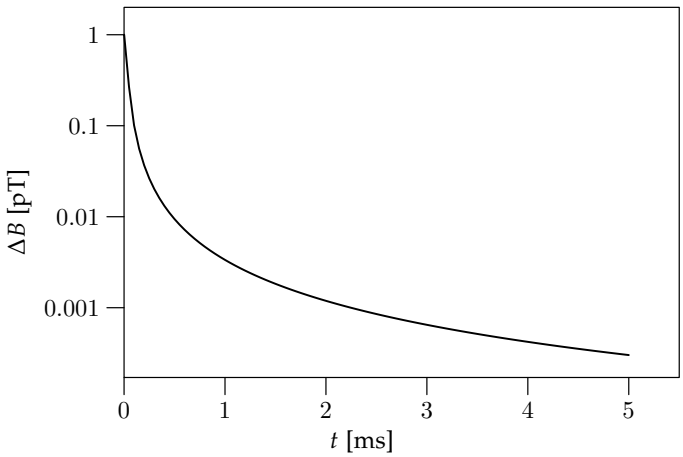

Figure 6.6: Uncertainty of three B-field components using three separate systems. The value at $t = 5\,\text{ms}$ is $\Delta B_x = \Delta B_y = \Delta B_z = 3.017 \times 10^{-4}\,\text{pT}$. We have used the numerical values of Table 4.1 in our calculations.

6.3.2 Two Entangled Gases and One Separate Gas

In the previous section we estimated all three components of a B-field using three separate systems. A better attempt would be to reuse the result from section 6.2.4, where we used two entangled gases to estimate two components and then use a separate system for the last B-field component. If we want equal variances on all B-field components then the three atomic gases and three probe beams should not be of the same size. However, if we let the three photon fluxes be equal and divide the atoms such that half of the atoms are used for the separate system and $1/4$ of the atoms is used for each of the entangled gases, then we would get the same final variance of all three B-field components. The uncertainty at $t = 5\,\text{ms}$ is $\Delta B_x = \Delta B_y = \Delta B_z =$

2.012×10^{-4} pT in this situation as shown on Fig. 6.7. The uncertainty at large t is thus a factor $2\sqrt{3}$ greater than if we had only estimated one component.

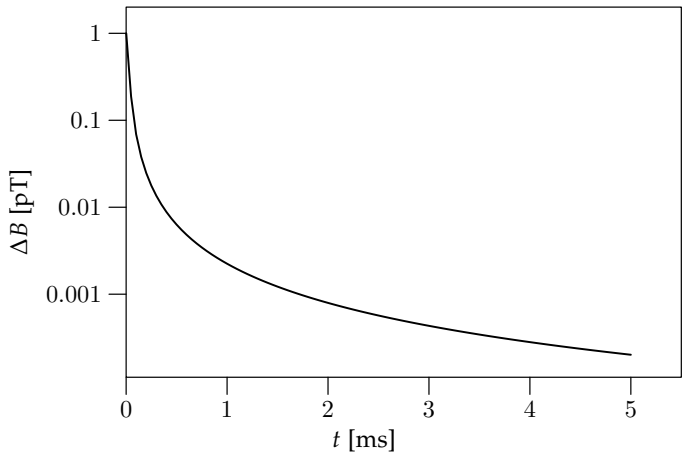

Figure 6.7: Uncertainty of three B-field components as a function of time using one separate gas and two entangled gases. The value at $t = 5\,\text{ms}$ is $\Delta B_x = \Delta B_y = \Delta B_z = 2.012 \times 10^{-4}\,\text{pT}$. We have used the numerical values of Table 4.1 in our calculations.

6.3.3 Six Entangled Gases and Three Probe Beams

In this section, we want to couple the B-field components to three *commuting* atomic operators, involving as many atoms as possible. We do this by using a better, but also more complicated, setup for estimating three B-field components as shown in Fig. 6.8. In this setup we use six entangled gases and we let three probe beams pass through four gases each. The gases are polarized such that the following components are classical: $\langle J_{x_1}\rangle = -\langle J_{x_4}\rangle$, $\langle J_{y_2}\rangle = -\langle J_{y_5}\rangle$, and $\langle J_{z_3}\rangle = -\langle J_{z_6}\rangle$. The optical fields are linearly polarized with macroscopic Stokes parameters $\langle S_{z_1}\rangle$, $\langle S_{y_2}\rangle$, and $\langle S_{x_3}\rangle$. The Hamiltonian for this system is given by

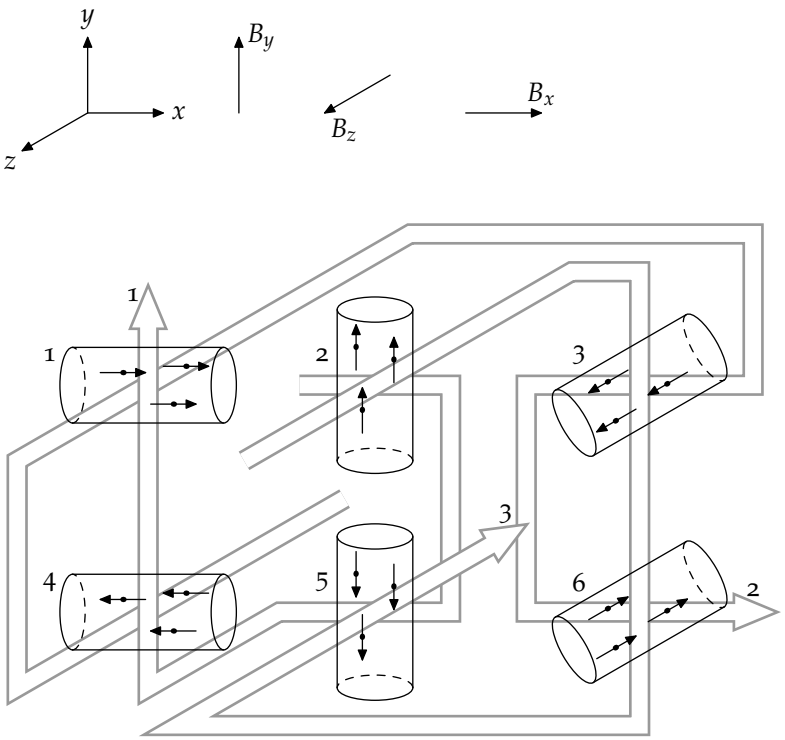

Figure 6.8: Setup to obtain measurements of all three components of a magnetic field. To do this we use six entangled atomic gases and three probe beams. Each probe beam passes through four atomic gases.

$$\begin{aligned}\mathcal{H}_{\text{int}}\tau\sqrt{\hbar\langle J_{x_1}\rangle} = {} & \mu_\tau(J_{x_2}+J_{x_3}+J_{x_5}+J_{x_6})B_x \\ & +\mu_\tau(J_{y_1}+J_{y_3}+J_{y_4}+J_{y_6})B_y \\ & +\mu_\tau(J_{z_1}+J_{z_2}+J_{z_4}+J_{z_5})B_z \\ & +\kappa_\tau(J_{z_2}-J_{y_3}-J_{z_5}+J_{y_6})S_3 \\ & +\kappa_\tau(J_{z_1}-J_{x_3}-J_{z_4}+J_{x_6})S_2 \\ & +\kappa_\tau(J_{y_1}-J_{x_2}-J_{y_4}+J_{x_5})S_1.\end{aligned} \tag{6.4}$$

The index on S depends on the propagation directions through the individual gases. Terms like $\mu_\tau J_{x_1} B_x$, which couple the classical components of

the atomic spins to the B-fields, are omitted from the interaction Hamiltonian as they do not contribute to the interactions to the same order, e.g., $[J_{y_1}, \mu_\tau J_{x_1} B_x] = -i\mu_\tau \hbar J_{z_1} B_x$, the product of two small quantities. By using this Hamiltonian we measure three commuting observables $(J_{z_2} - J_{y_3} - J_{z_5} + J_{y_6})$, $(J_{z_1} - J_{x_3} - J_{z_4} + J_{x_6})$, and $(J_{y_1} - J_{x_2} - J_{y_4} + J_{x_5})$ and from their commutators with the Larmor term in Eq. (6.4), we see that they evolve in direct proportion with the three B-field components.

The uncertainty of the B-field components is shown as a function of time in Fig. 6.9. As we use $4/6$ of the atoms and $1/3$ of the photon flux to estimate each B-field component, the value of the uncertainty at $t = 5\,\text{ms}$ is $3\sqrt{3}/2$ as big as if we only estimated one B-field component and a factor of two smaller than if we use three separate systems to estimate the three B-field components.

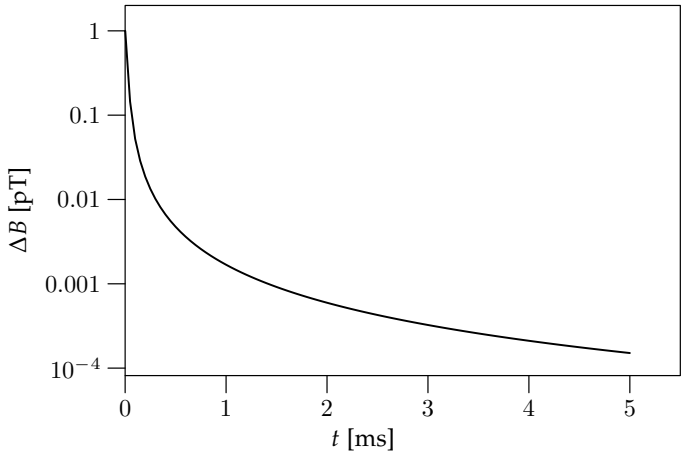

Figure 6.9: Uncertainty of three B-field components using six entangled gases and three probe beams. The value at $t = 5\,\text{ms}$ is $\Delta B_x = \Delta B_y = \Delta B_z = 1.510 \times 10^{-4}\,\text{pT}$. We have used the numerical values of Table 4.1 in our calculations.

6.4 Entanglement

To measure two or three B-field components most efficiently, we have shown that we should use entangled gases. There exist different entanglement mea-

sures which can be used to quantify the degree of entanglement. Here we will use the Gaussian entanglement of formation (GEOF) [54].

The GEOF is calculated from the covariance matrix of the atoms γ_{at}. Every time we apply the update formula, we may extract γ_{at} for a pair of gases from our numerical procedure and up to local unitary operations this matrix turns out to be of the form

$$\gamma_{\text{at}} = \begin{pmatrix} n & 0 & k_x & 0 \\ 0 & n & 0 & -k_p \\ k_x & 0 & n & 0 \\ 0 & -k_p & 0 & n \end{pmatrix}, \tag{6.5}$$

where $k_x \geq k_p \geq 0$ ($k_x = k_p$ in our case). n, k_x, and k_p are the quantities of interest for the evaluation of the GEOF. The EPR uncertainty is given by

$$\Delta = \min\left(1, \sqrt{(n - k_x)(n - k_p)}\right) \tag{6.6}$$

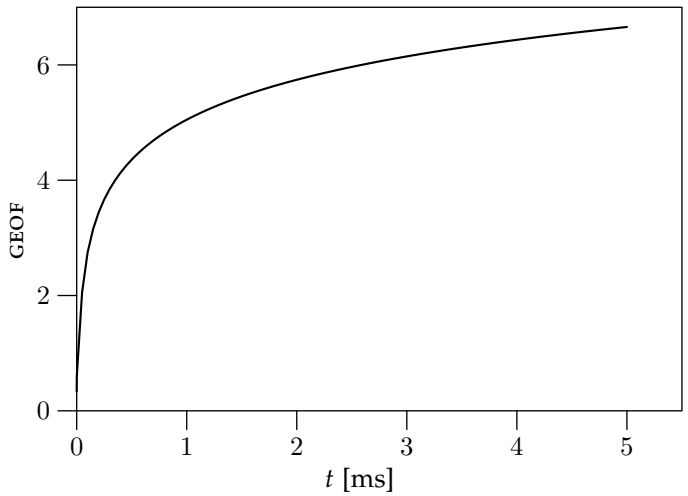

Figure 6.10: GEOF for two entangled gases corresponding to the case considered in Sec. 6.2.4 where we used two entangled gases to estimate two B-field components. We have used the numerical values of Table 4.1 in the calculations.

and the GEOF is

$$E = c_+(\Delta)\log[c_+(\Delta)] - c_-(\Delta)\log[c_-(\Delta)], \tag{6.7}$$

where $c_\pm(\Delta) \equiv \frac{1}{4}(\Delta^{-\frac{1}{2}} \pm \Delta^{\frac{1}{2}})^2$.

The GEOF for the two gases used to measure two B-field components is shown in Fig. 6.10.

For three B-field components we used six atomic gases, and we have calculated the GEOF between different pairs of the gases. Figure 6.11 shows the GEOF between two gases polarized in opposite directions, e.g., gas number 1 and 4. The GEOF between pairs like 1 and 2 is zero.

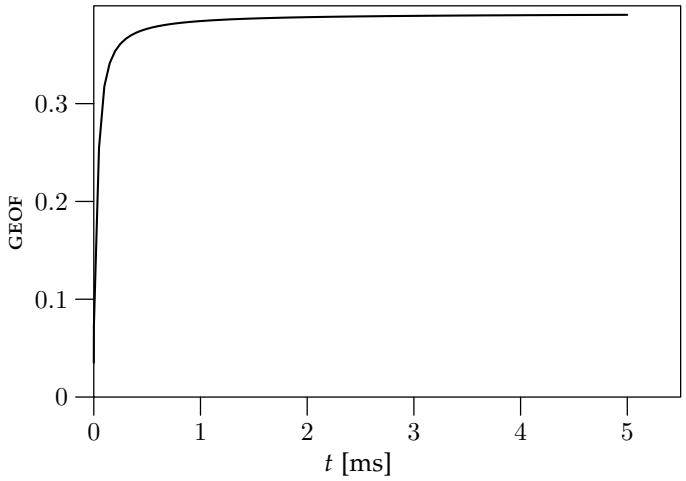

Figure 6.11: The GEOF for two gases polarized in opposite directions as considered in Fig. 6.8 where we estimated three B-field components by using six entangled gases. We have used the numerical values of Table 4.1.

Our setup with two entangled gases is quite equivalent to the one implemented in recent entanglement experiments [39] except that the atomic systems are under the additional influence of an initially unknown B-field. This slows down the initial rate of generation of entanglement, but as $\mathrm{Var}(B(t))$ approaches zero, the entanglement grows without limits as long as absorption and atomic decay can be neglected [55]. In the case of six gases which are probed in a non-symmetric way, some pairs show entanglement and some do

not. This can be understood by identification of operators that do not couple to the probe fields. The convergence of the entanglement between oppositely polarized gases toward a constant value is also observed without coupling to a B-field, and it is due to the incompleteness of the measurements on the pair by fields that also couple to other pairs of gases. In symmetric setups with multiple Gaussian variables, the theoretical maximum of pairwise entanglement between systems also has an upper limit, reflecting the impossibility for a quantum system to be maximally entangled with several other quantum systems at the same time [56, 57].

6.5 Conclusion

We have considered how to estimate a vector magnetic field using a Gaussian description of the variables describing the system. To estimate more than one B-field component it is fruitful to use pairwise entangled separate gases. In other applications, e.g. teleportation, shared entanglement over some distance is a useful resource too. We showed that entanglement can be a useful local resource to improve the accuracy in measurements and parameter estimation. We note that our protocol for the estimation of two B-field components using two optical probe beams and two entangled gases is experimentally very feasible. Essentially, it would require a combination of the magnetometry setup of Ref. [13] and the entanglement setup of Ref. [39].

Seven

Time-Dependent Magnetometry

We present a theoretical procedure of the ability to estimate a magnetic field that fluctuates according to an Ornstein-Uhlenbeck process. Our analysis is based on a Gaussian state description of the atoms and the probing field, and it presents the estimator of the field and a measure of its uncertainty which coincides in the appropriate limit with the achievements for a static field described in chapter 4. We show by simulations that the estimator for the current value of the B-field systematically lags behind the actual value of the field, and we suggest a more complete theory, where the measured values at any time are used to update and improve both the estimate of the current value and the estimate of earlier values of the B-field. This chapter is based on paper [IV].

7.1 Introduction

In this chapter we generalize our theory of estimating weak magnetic fields to time-dependent B-fields. Time dependent fields were recently studied experimentally [11], and we shall generalize that analysis and show that further improvements of the estimate of the field at a given time is possible by taking into account the detailed detection record at both earlier and later times. As discussed in chapter 3 Gaussian states are fully characterized by their mean value vector and covariance matrix, but so far we have only used the covariance matrix. When we investigate time-dependent B-fields it is necessary to look at the mean value vector too. We are able to give exact expressions for the probability distribution of the probed magnetic field, i.e., our result is neither too weak nor too strong (no procedure exists by which further information can be extracted from the available data, and the actual value must agree with our estimate within the probability distribution).

7.2 Gaussian State Formalism

7.2.1 Known Magnetic Field

In this section we shall assume a magnetic field $B(t)$ with an explicitly given time dependence. This analysis will be needed, when we proceed to simulate how an unknown field is estimated, since it is the actual realization of the field, that drives the atomic dynamics. The current section thus accounts for the "information available to the theorist", whereas the next section will deal with the "information available to the experimentalist" who only have access to the optical detection record and not to the actual value of the B-field.

We place a spin-polarized atomic gas in the B-field and probe it continuously by the polarized light beam like we did when we estimated a constant B-field. The Gaussian probability distribution (Wigner function) of the atomic variables and of the light pulse prior to the interaction evolves into a new Gaussian state, and the detection of the polarization rotation, which is a measurement of the field observable x_{ph} leads to an update of the atomic state, but it retains the Gaussian form [22]. This means that we can describe the atomic state by the mean values and by the covariance matrix which fully characterize a Gaussian state, and we shall now describe the time evolution of the mean values and the covariances of the atomic state due to interactions and measurements.

First we define a vector of variables (operators) $\mathbf{y} = (x_{\text{at}}, p_{\text{at}}, x_{\text{ph}}, p_{\text{ph}})^T$, with the corresponding vector of mean values $\mathbf{m} = \langle \mathbf{y} \rangle$ and with the covariance matrix γ where $\gamma_{ij} = 2\text{Re}\langle (y_i - \langle y_i \rangle)(y_j - \langle y_j \rangle) \rangle$. Because we assume that the B-field is known we do not include it in $\mathbf{y}$. Instead we include it explicitly in the update formulas. Our discussion of the Gaussian state description of a spin polarized sample and the linearly polarized light translates into the specification of the initial values

$$\mathbf{m} = 0, \tag{7.1}$$

$$\gamma = \mathbb{1}_{4\times 4}, \tag{7.2}$$

and the update formula due to interactions during a time interval τ

$$\mathbf{m} \mapsto \mathbf{S}\mathbf{m} + \mathbf{v}, \tag{7.3}$$

$$\gamma \mapsto \mathbf{S}\gamma\mathbf{S}^T, \tag{7.4}$$

where

$$\mathbf{S} = \begin{pmatrix} 1 & 0 & 0 & \kappa_\tau \\ 0 & 1 & 0 & 0 \\ 0 & \kappa_\tau & 1 & 0 \\ 0 & 0 & 0 & 1 \end{pmatrix} \tag{7.5}$$

and

$$\mathbf{v} = (0, -\mu_\tau B(t), 0, 0)^T. \tag{7.6}$$

When we perform a homodyne measurement we write

$$\gamma = \begin{pmatrix} \mathbf{A}_\gamma & \mathbf{C}_\gamma \\ \mathbf{C}_\gamma^T & \mathbf{B}_\gamma \end{pmatrix}, \tag{7.7}$$

$$\mathbf{m} = (\mathbf{m}_A, \mathbf{m}_B), \tag{7.8}$$

with $\mathbf{A}_\gamma$ the covariance matrix for the atomic variables, $\mathbf{y}_1 = (x_{\text{at}}, p_{\text{at}})^T$, $\mathbf{B}_\gamma$ the covariance matrix for the field variables, $\mathbf{y}_2 = (x_{\text{ph}}, p_{\text{ph}})^T$, and $\mathbf{C}_\gamma$ the correlation matrix between $\mathbf{y}_1$ and $\mathbf{y}_2^T$. When a measurement of the variable x_{ph} is performed, the outcome takes on a random value, given by the Gaussian probability distribution. For a short segment of light, the mean value of x_{ph} is $m_3 = \kappa_\tau m_2$, and the variance is $1/2$ (the incident field variance is only infinitesimally modified by the atoms). We let x_{meas} be the value we obtain

when we measure x_{ph}. The measurement of x_{ph} collapses the field state and transforms the atomic component according to

$$\mathbf{A}_\gamma \mapsto \mathbf{A}_\gamma - \mathbf{C}_\gamma(\pi\mathbf{B}_\gamma\pi)^-\mathbf{C}_\gamma^T, \tag{7.9}$$

$$\mathbf{m}_A \mapsto \mathbf{m}_A + \mathbf{C}_\gamma(\pi\mathbf{B}_\gamma\pi)^-((x_{\mathrm{meas}} - m_3), 0)^T, \tag{7.10}$$

$$\mathbf{B}_\gamma \mapsto \mathbb{1}_{2\times 2}, \tag{7.11}$$

$$\mathbf{C}_\gamma \mapsto 0, \tag{7.12}$$

$$\mathbf{m}_B \mapsto 0, \tag{7.13}$$

where $\pi = \mathrm{diag}(1, 0)$ and $(\dots)^-$ denotes the Moore-Penrose pseudo-inverse. To the lowest, relevant order, i.e., first order in τ, $(\pi\mathbf{B}_\gamma\pi)^- = \mathrm{diag}(1, 0)$. Equations (7.11), (7.12), and (7.13) "refresh" the atom and field variables corresponding to the subsequent light segment which has no correlations with the atoms prior to the interaction. Note that the quantity $(x_{\mathrm{meas}} - m_3)$ is a random variable with vanishing mean value and variance $1/2$, and since $\mathbf{C}_\gamma$ scales as $\sqrt{\tau}$, the measurement induced, random displacement of the mean values (7.10) can also be expressed in terms of a Wiener increment with zero mean value and variance τ, cf. [10, 11].

Before proceeding to the interaction between the atoms and an unknown magnetic field, we note that the dynamics is of quantum non-demolition type (QND), i.e., it permits a detection of the atomic variable p_{at} without changing this observable. Such a detection (carried out when the field variable x_{ph} is read out after the atom-light interaction), in effect leads to squeezing of the p_{at} component of the atomic spin around a random value, which is selected by the random outcome of the measurement process and by the deterministic Larmor rotation. Of course a single, infinitesimal time step as in Eq. (7.4) leads only to an infinitesimal squeezing, but as the evolution proceeds continuously in time it leads to a monotonic reduction of the variance of the atomic spin component.

7.2.2 Estimation of an Unknown Time Dependent Magnetic Field

As discussed in chapter 4, the B-field causes the Larmor precession (4.7). By probing the value of p_{at}, we acquire information about the magnetic field. In section 4.4, we found that a constant magnetic field is effectively probed with a time dependent variance on the estimate given by

$$\Delta B(t)^2 = \frac{\Delta B_0^2(1 + \kappa^2 t)}{1 + \kappa^2 t + \frac{2}{3}\kappa^2\mu^2(\Delta B_0)^2 t^3 + \frac{1}{6}\kappa^4\mu^2(\Delta B_0)^2 t^4}, \tag{7.14}$$

with ΔB_0^2 representing our prior knowledge of the field. In the limit of $\kappa^2 t \gg 1$, we have $\Delta B(t)^2 \simeq 6/(\kappa^2 \mu^2 t^3)$ which is independent of the prior knowledge of the B-field and which reflects a more rapid reduction with time of the variance than expected from a conventional statistical argument. This is due to the atomic squeezing, as it progressively makes the system more and more sensitive to the magnetic field perturbation.

In the following, we shall generalize the analysis to the case of time dependent B-fields. A convenient model for a random field is a damped diffusion (Ornstein-Uhlenbeck) process [58], governed by the stochastic differential equation

$$dB(t) = -\gamma_b B(t) dt + \sqrt{\sigma_b} dW_b, \tag{7.15}$$

where the Wiener increment dW_b has a Gaussian distribution with mean zero and variance dt. The bandwidth of the field is determined by the frequency γ_b alone. Our task is to expose atoms to a realization of this process and to use the polarization measurements to construct an estimate for the actual current value of the field.

The Ornstein-Uhlenbeck process can be simulated on a computer, but we can also make statistical predictions, e.g., the steady state mean vanishes and the variance is

$$\mathrm{Var}_{\mathrm{st}}(B) = \frac{\sigma_b}{2\gamma_b}. \tag{7.16}$$

If we estimate the field in the laboratory at time t_{L} to be $B_{t_{\mathrm{L}}}$ with a variance $V_{t_{\mathrm{L}}}$ on the estimate, then our best estimate for the value at a *future* time $t > t_{\mathrm{L}}$ takes the value

$$B(t) = B_{t_{\mathrm{L}}} \exp(-\gamma_b (t - t_{\mathrm{L}})) \tag{7.17}$$

with a variance

$$V_t = V_{t_{\mathrm{L}}} e^{-2\gamma_b (t - t_{\mathrm{L}})} + \mathrm{Var}_{\mathrm{st}}(B)(1 - e^{-2\gamma_b (t - t_{\mathrm{L}})}). \tag{7.18}$$

The Ornstein-Uhlenbeck process can be very slow, in which case the field retains its random value almost constantly over long times, and we then expect to recover the result in (7.14) for the estimation of a constant field, because the accumulated photodetection record over time carries information about the time dependent field, which is known to vary very little. If the Ornstein-Uhlenbeck process is very fast, the accumulated photodetection record until the present time t gives only little information about the present value. Note that by scaling γ_b and σ_b by the same factor, the variance (7.16) is unchanged, but the process changes from slow to rapid fluctuations.

Our theoretical description of the estimation process deals with a joint Gaussian distribution for the quantum variables and the classical magnetic field. As in chapter 4 we will formally treat the B-field as the first component in our vector of five Gaussian variables $\widetilde{\mathbf{y}} = (B, x_{\mathrm{at}}, p_{\mathrm{at}}, x_{\mathrm{ph}}, p_{\mathrm{ph}})$, where the tilde is used to distinguish these variables from those in the previous section describing the situation where the B-field is known. Again the Gaussian state is characterized by its mean value vector $\widetilde{\mathbf{m}} = \langle \widetilde{\mathbf{y}} \rangle$ and its covariance matrix $\widetilde{\gamma}$ where $\widetilde{\gamma}_{ij} = 2\mathrm{Re}\langle (\widetilde{y}_i - \langle \widetilde{y}_i \rangle)(\widetilde{y}_j - \langle \widetilde{y}_j \rangle) \rangle$.

Note that although, e.g., x_{at} is the same operator in this and the previous section, its Gaussian state mean value and variance are not the same, because the Gaussian state is the probability distribution assigned by the observer given his or her acquired knowledge about the system. In the previous section we determined this probability distribution conditioned on full knowledge of the time dependent B-field and the photodetection record, whereas in the current section, only "the experimentalist's" knowledge of the detection record is assumed.

We will now write down the update formulas for $\widetilde{\mathbf{m}}$ and $\widetilde{\gamma}$ due to the Larmor rotation, the atom-light interaction, the random outcomes of the probing process, and the Ornstein-Uhlenbeck process. We will then at any time obtain a mean value $\widetilde{m}_1$ and a variance $\widetilde{\gamma}_{11}/2$ for the B-field.

The initial values are

$$\widetilde{\mathbf{m}} = 0, \tag{7.19}$$

$$\gamma_0 = \mathrm{diag}(2\,\mathrm{Var}(B_0), 1, 1, 1, 1). \tag{7.20}$$

Due to the interaction between the B-field and the atoms and between the atoms and the photons we have

$$\widetilde{\mathbf{m}} \mapsto \mathbf{S}_1 \widetilde{\mathbf{m}}, \tag{7.21}$$

$$\widetilde{\gamma} \mapsto \mathbf{S}_1 \widetilde{\gamma} \mathbf{S}_1^T, \tag{7.22}$$

where

$$\mathbf{S}_1 = \begin{pmatrix} 1 & 0 & 0 & 0 & 0 \\ 0 & 1 & 0 & 0 & \kappa_\tau \\ -\mu_\tau & 0 & 1 & 0 & 0 \\ 0 & 0 & \kappa_\tau & 1 & 0 \\ 0 & 0 & 0 & 0 & 1 \end{pmatrix}. \tag{7.23}$$

In this section the B-field is one of the variables, and hence the equation (7.21) is linear unlike the affine transformation (7.3). The transformations due to the

Ornstein-Uhlenbeck process are

$$\widetilde{m}_1 \mapsto \widetilde{m}_1(1-\gamma_b\tau), \tag{7.24}$$
$$\widetilde{\gamma} \mapsto \mathbf{S}_2\widetilde{\gamma}\mathbf{S}_2 + \mathbf{L}, \tag{7.25}$$

where $\mathbf{S}_2 = \mathrm{diag}(1-\gamma_b\tau, 0, 0, 0, 0)$ and $\mathbf{L} = \mathrm{diag}(\sigma_b\tau, 0, 0, 0, 0)$.

To handle the measurement on $\widetilde{x}_{\mathrm{ph}}$ we write the covariance matrix and the mean value vector as

$$\widetilde{\gamma} = \begin{pmatrix} \widetilde{\mathbf{A}}_\gamma & \widetilde{\mathbf{C}}_\gamma \\ \widetilde{\mathbf{C}}_\gamma^T & \widetilde{\mathbf{B}}_\gamma \end{pmatrix}, \tag{7.26}$$
$$\widetilde{\mathbf{m}} = (\widetilde{\mathbf{m}}_A, \widetilde{\mathbf{m}}_B)^T, \tag{7.27}$$

where $\widetilde{\mathbf{A}}_\gamma$ is the covariance matrix for B-field and atoms, $\widetilde{\mathbf{y}}_1 = (B, \widetilde{x}_{\mathrm{at}}, \widetilde{p}_{\mathrm{at}})^T$, $\widetilde{\mathbf{B}}_\gamma$ the covariance matrix for the photons, $\widetilde{\mathbf{y}}_2 = (\widetilde{x}_{\mathrm{ph}}, \widetilde{p}_{\mathrm{ph}})^T$, and $\widetilde{\mathbf{C}}_\gamma$ the correlation matrix for $\widetilde{\mathbf{y}}_1$ and $\widetilde{\mathbf{y}}_2^T$. The measurement of $\widetilde{x}_{\mathrm{ph}}$ then transforms these matrices according to

$$\widetilde{\mathbf{A}}_\gamma \mapsto \widetilde{\mathbf{A}}_\gamma - \widetilde{\mathbf{C}}_\gamma(\pi\widetilde{\mathbf{B}}_\gamma\pi)^-\widetilde{\mathbf{C}}_\gamma^T, \tag{7.28}$$
$$\widetilde{\mathbf{B}}_\gamma \mapsto \mathbb{1}_{2\times 2}, \tag{7.29}$$
$$\widetilde{\mathbf{C}}_\gamma \mapsto 0, \tag{7.30}$$
$$\widetilde{\mathbf{m}}_A \mapsto \widetilde{\mathbf{m}}_A + \widetilde{\mathbf{C}}_\gamma(\pi\widetilde{\mathbf{B}}_\gamma\pi)^-(x_{\mathrm{meas}} - \widetilde{m}_4, 0)^T, \tag{7.31}$$
$$\widetilde{\mathbf{m}}_B \mapsto 0. \tag{7.32}$$

These equations fully describe the conditioned and the deterministic evolution of the multi-variable Gaussian distribution, and in particular we get access to the estimator for the B-field in the form of its mean and the corresponding covariance matrix element. The input to the estimation protocol is the constant parameters of the problem (κ, μ, γ_b, σ_b) and the outcome of the photodetection (x_{meas}), which will drive the mean values, and hence the estimator, to a non-trivial result, cf. Eq. (7.31). We note that whereas the estimator depends on the actual measurement outcome, the covariance matrix evolves in an entirely deterministic manner, and we can hence theoretically predict the magnitude of the error as it was also done in [11].

We want to simulate the protocol with a given realization of the noisy field, and to do this we have to combine the theories of this and the previous section.

- We simulate the B-field by using the Ornstein-Uhlenbeck process in Eq. (7.15).
- We can then simulate the measurements x_{meas} by using this B-field as input in the theory described in the previous section.
- Then we use the simulated measurements x_{meas} as input in the theory in this section, and in this way we can simulate the mean value of B.
- This mean value of B is our estimate of B and we can now compare it to the original B-field simulation.

In the simulation it is the actual field $B(t)$ that acts on the atoms and hence leads to the probability distribution for the photodetection record, and the measured quantum field variable x_{ph} has the mean value $m_3 = \kappa_\tau m_2$, given by the expressions of the previous section. Hence the measurement outcome can be written as $\kappa_\tau m_2 + \chi$ where χ is uncorrelated with its value at previous detection times, and it has a vanishing mean and a variance of $1/2$. We are thus effectively communicating the value of the simulated B-field through the use of the "theorist's" estimator of the atomic state in the simulation of measurement outcomes. Assuming a random measurement outcome with the statistics described, we update the mean value vector and covariance matrix of the previous subsection, and we use the same simulated measurement outcome in the update formula (7.31). The simulated measurement outcome may deviate from the value $\widetilde{m}_4$ currently expected by the "experimentalist" both because of the noisy contribution and because the mean is given by its true value and not his or her estimate. The latter is responsible for driving the B-field estimate towards the actual realization in our numerical simulations.

7.3 Results

We now have a complete theory which, given the detection record, provides the estimator for the time dependent B-field and its variance. In practice, the experiment should be run, and the analysis should be applied on the full detection record, either simultaneously with the experiment or afterwards. Some calculations are necessary since the B-field estimator at any time involves knowledge of the full vector of mean values and the covariance matrix. The covariance matrix, and in particular the variance of the B-field estimate, evolves deterministically with time. We can in fact solve the equations for the

covariance matrix analytically, and in the long time limit we find the steady state variance on our B-field estimate:

$$\mathrm{Var}(B) = \frac{1}{4\kappa^2\mu^2}\left(\sqrt{\gamma_b^2 + 2\mu\sqrt{\sigma_b}\kappa} - \gamma_b\right)^2\sqrt{\gamma_b^2 + 2\mu\sqrt{\sigma_b}\kappa}. \tag{7.33}$$

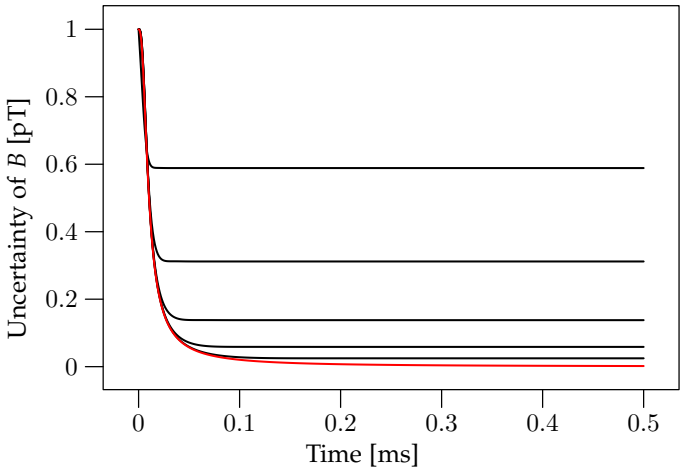

Figure 7.1: Uncertainty of the B-field as a function of time. We have used the numerical values of Table 4.1 in our calculations. The red line is the analytical result for a constant B-field. The black lines are for time-dependent B-fields with the following values (from above) $(\gamma_b, \sigma_b) = (10^5\,\mathrm{s}^{-1}, 2\times10^5\,\mathrm{pT}^2/\mathrm{s})$, $(\gamma_b, \sigma_b) = (10^4\,\mathrm{s}^{-1}, 2\times10^4\,\mathrm{pT}^2/\mathrm{s})$, $(\gamma_b, \sigma_b) = (10^3\,\mathrm{s}^{-1}, 2\times10^3\,\mathrm{pT}^2/\mathrm{s})$, $(\gamma_b, \sigma_b) = (10^2\,\mathrm{s}^{-1}, 2\times10^2\,\mathrm{pT}^2/\mathrm{s})$, and $(\gamma_b, \sigma_b) = (10^1\,\mathrm{s}^{-1}, 2\times10^1\,\mathrm{pT}^2/\mathrm{s})$. For small values of γ_B the black curves approach the constant B-field result as expected.

When the Ornstein-Uhlenbeck process is slow, early detection events and estimates provide already an estimate for future values of the field, cf. (7.18), which is further refined by the continued measurement record. It is also seen from (7.18), that if the rate γ_b is high, the estimates quickly loose their significance, and only probing for a short time before t is useful in the estimate of $B(t)$. In Fig. 7.1 we show how the variance of the B-field estimate starts with the prior steady state value (7.16) before any probing takes place and evolves to the steady state value given by (7.33). In the figure we assume the same steady state value for the B-field fluctuations in all curves, but with

different values of the rate of fluctuations γ_b. For comparison we also show the analytical result (7.14) for a constant, unknown field with the same prior uncertainty. This curve converges to zero, but it is clearly seen to follow the curves with finite γ_b on short time scales (determined by γ_b).

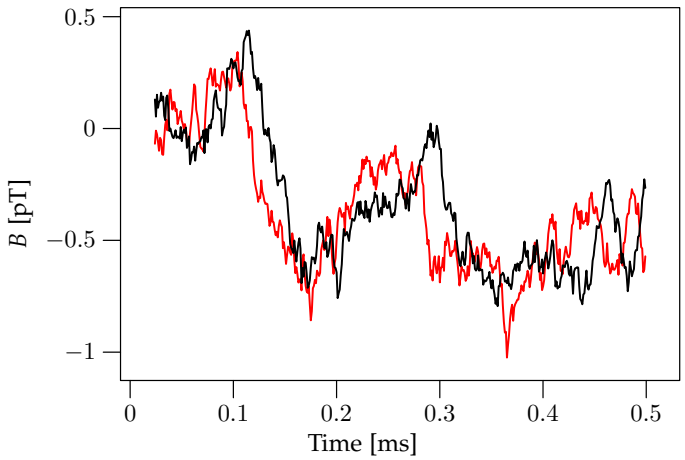

Figure 7.2: Time dependent value of the actual, simulated B-field (red line) and the estimate based on a simulated detection record (black line). The estimate is systematically lacking behind the actual B-field. The atomic parameters are given in Table 4.1, and the B-field is characterized by $\gamma_b = 10^3\,\mathrm{s}^{-1}$ and $\sigma_b = 2 \times 10^3\,\mathrm{pT}^2/\mathrm{s}$.

In Fig. 7.2 we show the result of a realization of the Ornstein-Uhlenbeck process. The figure shows the actual process as a red line and the estimator as a black line for a typical time window. We observe that the estimator tracks the gross structure of the dependence very well, but smaller transients are not reproduced. Taking a second look at the figure, we also observe that the estimate is systematically lacking behind the true realization of the field. This is not the least surprising, as the estimate makes explicit use of all past measurements to predict the current value. In particular, if no measurement results are provided, the estimate for the value is simply obtained from past values according to Eq. (7.15). This should, however, prompt attempts to make an even better estimate for the field using not only the detection record until the instant of interest, but also the later detection events. We recall that we are actually probing the atomic spin state, and the Larmor precession due

to the B-field may well be detected also after it took place. In the following sections we will discuss different methods to improve the estimate of the B-field.

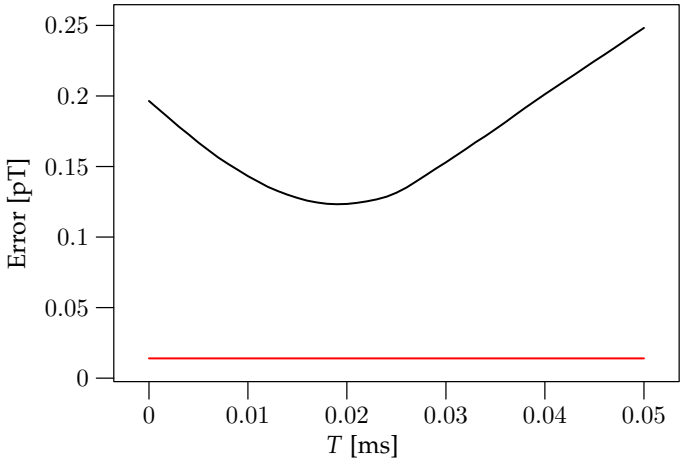

Figure 7.3: The black curve shows the error of the B-field estimate (7.34) as a function of a variable translation of the two curves in Fig. 7.2 with respect to each other. As it is seen the error has a minimum at around 0.02 ms. The horizontal red line shows the error obtained from a weighted average of delayed estimates, see text and Eq. (7.36). The atomic parameters are given in Table 4.1, and the B-field is characterized by $\gamma_b = 10^3\,\mathrm{s}^{-1}$ and $\sigma_b = 2 \times 10^3\,\mathrm{pT}^2/\mathrm{s}$.

7.3.1 Fixed Delay

As already noted the estimate of the B-field lacks systematically behind the simulated field. A simple way to improve the estimate is therefore to displace the estimate in time. To justify this increased effort, we have made a very simple transformation of the data, consisting in a temporal displacement of the two curves in Fig. 7.2, so that we compare the current estimator $\widetilde{m}_1(t)$ obtained by our theory with earlier values of the field $B(t-T)$. Figure 7.3 shows the numerically calculated error of the estimate, averaged over a long

detection record, plotted as a function of the delay T, and

$$\text{Error}^2(T) = \frac{1}{t_0}\int_T^{t_0+T} (\widetilde{m}_1(t) - B(t-T))^2 dt, \tag{7.34}$$

We indeed see, that for a range of values of T the error is smaller than if we do not shift the estimate. This means that we obtain a better estimate if we assign our estimate to the value of the B-field a little earlier. In Fig. 7.4 we have plotted the true realization of the B-field together with the estimated value displaced in time, such that the above Error is minimal.

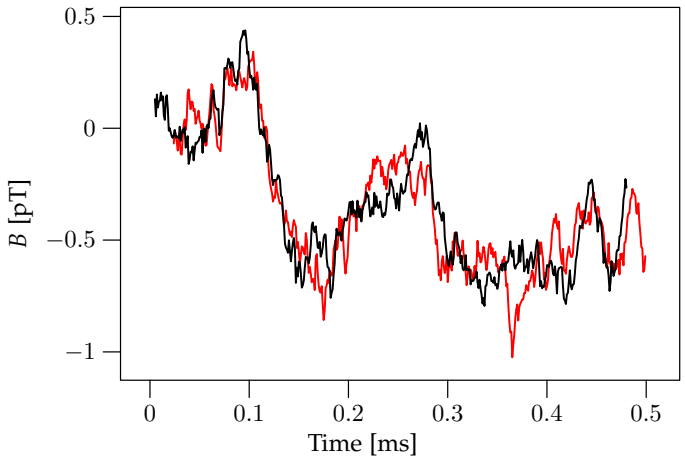

Figure 7.4: Time dependent value of the actual, simulated B-field from Fig. 7.2 (red line) and the estimate of B delayed in time with the optimal delay T obtained from Fig. 7.3 (black line). The atomic parameters are given in Table 4.1, and the B-field is characterized by $\gamma_b = 10^3\,\text{s}^{-1}$ and $\sigma_b = 2\times 10^3\,\text{pT}^2/\text{s}$.

7.3.2 Weighted Average of Delays

A slightly more elaborate procedure to improve the estimate obtained from the above procedure is obtained by assuming not just a simple delay but a temporal convolution of the estimators,

$$B^{\text{est}}_{\text{opt}}(t) = \int_{-\infty}^{\infty} a(t-t')\widetilde{m}_1(t')dt'. \tag{7.35}$$

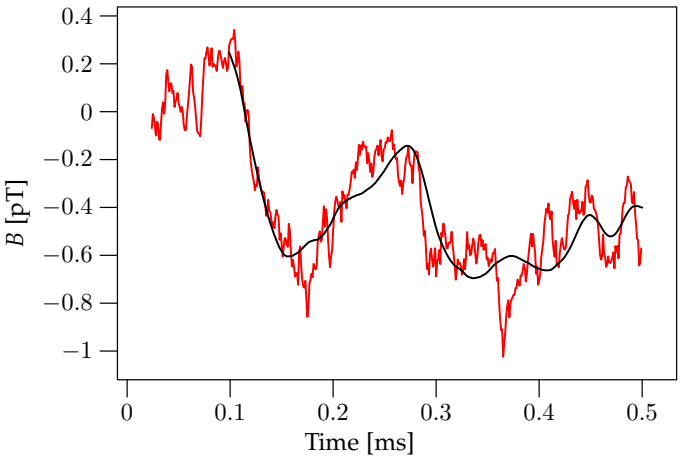

Figure 7.5: Time dependent value of the actual, simulated B-field from Fig. 7.2 (red line) and the estimate of B folded with Eq. (7.35) where the coefficients a_i are shown in Fig. 7.6 (black line). The atomic parameters are given in Table 4.1, and the B-field is characterized by $\gamma_b = 10^3\,\mathrm{s}^{-1}$ and $\sigma_b = 2 \times 10^3\,\mathrm{pT}^2/\mathrm{s}$.

Numerically, we have identified the optimum delay distribution by minimizing the (squared) error

$$\frac{1}{t_0}\int_T^{t_0+T}\Big(\sum_i a_i \widetilde{m}_1(t-i\tau) - B(t)\Big)^2 dt, \tag{7.36}$$

which turns out to be a linear algebra problem for the coefficients a_i. Running a series of simulations, we find the temporal variation of the delay distribution plotted in Fig. 7.6, peaking, as expected, around the optimum fixed delay found in the previous section in Fig. 7.3. The error obtained this way is smaller than by use of any fixed delay, as indicated by the horizontal red line in Fig. 7.3 which lies below the black line. In Fig. 7.5 we have plotted the true realization of the B-field together with the estimated value folded with the above function.

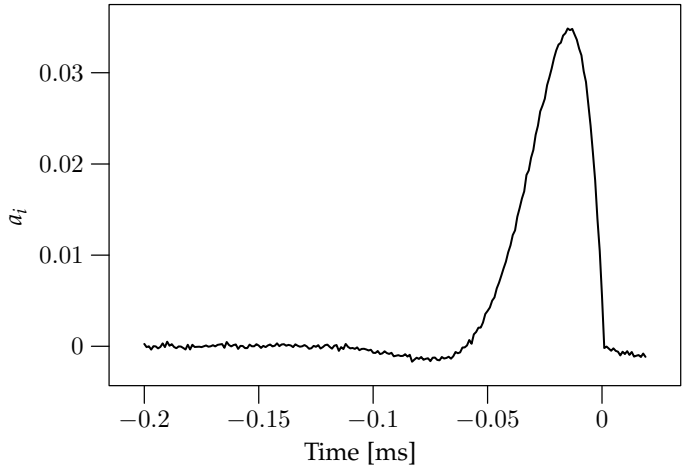

Figure 7.6: Time dependence of optimal weight factors a_i in Eq. (7.36), favoring contributions with a finite delay around 0.02 ms as suggested by Fig. 7.3. The atomic parameters are given in Table 4.1, and the B-field is characterized by $\gamma_b = 10^3\,\mathrm{s}^{-1}$ and $\sigma_b = 2 \times 10^3\,\mathrm{pT}^2/\mathrm{s}$.

7.3.3 Gaussian Theory of Hindsight

Both the fixed delay and the weighted average of delays bring promises for improved sensitivity of magnetometers, if one can wait for the estimate until (a short time) after the action of the field. Both procedures, however, suffer from their ad hoc character, and in particular from the fact that the optimum delay or delay distribution are not theoretically available, unless one accepts to use simulations as we did here as guideline. We shall now present the correct theory, which gives the optimum estimate without any ad hoc procedures and a tight bound on the error.

The current estimate of the B-field is given by a Gaussian probability distribution, and so is the estimate of the value of the B-field at all points in the past. As measurements on the atoms proceed, we may therefore keep improving also our past estimate. We hence treat not only the current value but also past values of the B-field as Gaussian variables together with the atom and field variables. To update the estimate at an instant T in the past, we need to keep track of the entire interval from $t - T$ to the present time t, and we extend our Gaussian state formalism by replacing $\widetilde{y}$ by a whole

vector of values, representing the unknown B-field at discrete times spanning an interval from $t - T$ until t: $\mathbf{y} = (B_N, B_{N-1}, \ldots, B_1, x_{\text{at}}, p_{\text{at}}, x_{\text{ph}}, p_{\text{ph}})^T$ where $B_i = B(t - (i-1)\tau)$. Since we are dealing with the values in the past, they are not evolving randomly due to the Ornstein-Uhlenbeck process, but inherit their value as time proceeds and the elements in the vector of mean values and the covariance matrix are simply "pushed towards the past". In each iteration we have to insert a new B-field and remove the oldest B-field. For $\mathbf{y}$ we do like this

$$\mathbf{y} \mapsto \left(\begin{array}{c} y_2 \\ \vdots \\ y_N \\ \hline y_N \\ \hline y_{N+1} \\ \vdots \\ y_{N+4} \end{array}\right) \tag{7.37}$$

and similarly for the mean value vector $\mathbf{m}$. The covariance matrix is updated like this

$$\gamma \mapsto \left(\begin{array}{ccc|c|ccc} \gamma_{2,2} & \cdots & \gamma_{2,N} & \gamma_{2,N} & \gamma_{2,N+1} & \cdots & \gamma_{2,N+4} \\ \vdots & \ddots & \vdots & \vdots & \vdots & \ddots & \vdots \\ \gamma_{N,2} & \cdots & \gamma_{N,N} & \gamma_{N,N} & \gamma_{N,N+1} & \cdots & \gamma_{N,N+4} \\ \hline \gamma_{N,2} & \cdots & \gamma_{N,N} & \gamma_{N,N} & \gamma_{N,N+1} & \cdots & \gamma_{N,N+4} \\ \hline \gamma_{N+1,2} & \cdots & \gamma_{N+1,N} & \gamma_{N+1,N} & \gamma_{N+1,N+1} & \cdots & \gamma_{N+1,N+4} \\ \vdots & \ddots & \vdots & \vdots & \vdots & \ddots & \vdots \\ \gamma_{N+4,2} & \cdots & \gamma_{N+4,N} & \gamma_{N+4,N} & \gamma_{N+4,N+1} & \cdots & \gamma_{N+4,N+4} \end{array}\right). \tag{7.38}$$

Only the current value of $B(t)$ is given by the stochastic process. The transformation matrix due to the Larmor and Faraday rotation, $\mathbf{S}_1$, and the matrices due to the Ornstein-Uhlenbeck process, $\mathbf{S}_2$ and $\mathbf{L}$, should be extended

$$\mathbf{S}_{1,\text{new}} = \begin{pmatrix} \mathbb{1}_{N-1\times N-1} & 0 \\ 0 & \mathbf{S}_1 \end{pmatrix}, \tag{7.39}$$

where $\mathbf{S}_1$ is the matrix from Eq. (7.23). $\mathbf{S}_2$ and $\mathbf{L}$ should be updated the same way, except that for $\mathbf{L}$ the identity matrix should be replaced by zeros. The

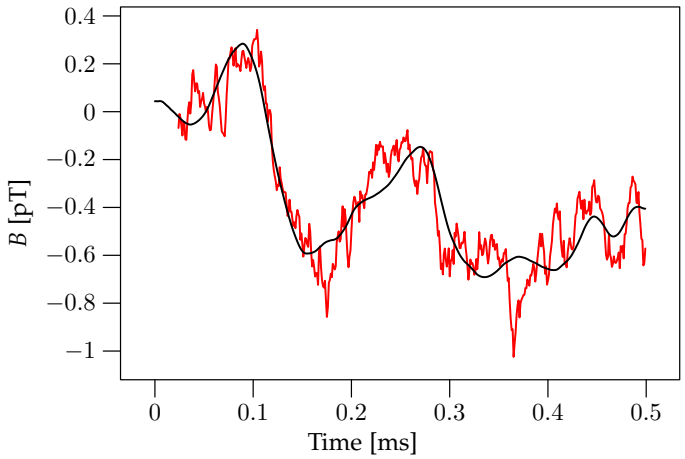

Figure 7.7: Time dependent value of the actual, simulated B-field (red line) and the estimate based on a simulated detection record available 0.1 ms after the action of the field (black line). The atomic parameters are given in Table 4.1, and the B-field is characterized by $\gamma_b = 10^3\,\mathrm{s}^{-1}$ and $\sigma_b = 2 \times 10^3\,\mathrm{pT}^2/\mathrm{s}$.

atomic system is correlated with both the current and the previous values of the field as witnessed by non-vanishing elements in the extended covariance matrix, and hence the updating due to measurements on the atoms also influence the variance of the B-field estimate in the past, c.f. the appropriate generalization of Eq. (7.31). We still measure on x_{ph} but now it is not the 4^{th} entry but instead the $(N+3)^{\mathrm{th}}$ entry. Now, there is nothing ad hoc about the procedure. At any time, we have an estimator for the value of the field over a finite interval looking backwards in time. We also have the variance of these values, which is a decreasing function of the time difference, approaching a constant, for values so long time ago, that their action on the atoms is no longer discernible, and hence no further updating takes place due to Eq. (7.31).

Figure 7.7 shows a comparison of the actual, simulated field with our Gaussian estimator, available 0.1 ms after the action of the B-field on the atoms. So at a given time we both get an estimate of the current value of the B-field *and* improve the estimate of the B-field values for the previous 0.1 ms.

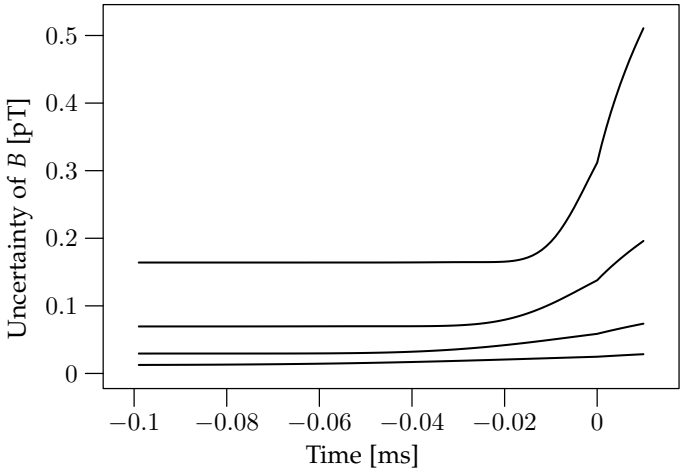

Figure 7.8: Time dependence of the variance of our estimate of the time dependent field B-field around the current time t_L in the laboratory. The atomic parameters are given in Table 4.1, and the B-field is characterized by these different values (from above) $(\gamma_b, \sigma_b) = (10^4\,\mathrm{s}^{-1}, 2\times10^4\,\mathrm{pT}^2/\mathrm{s})$, $(\gamma_b, \sigma_b) = (10^3\,\mathrm{s}^{-1}, 2\times10^3\,\mathrm{pT}^2/\mathrm{s})$, $(\gamma_b, \sigma_b) = (10^2\,\mathrm{s}^{-1}, 2\times10^2\,\mathrm{pT}^2/\mathrm{s})$, and $(\gamma_b, \sigma_b) = (10^1\,\mathrm{s}^{-1}, 2\times10^1\,\mathrm{pT}^2/\mathrm{s})$. For later times we have to guess the value from the properties of the Ornstein-Uhlenbeck process (7.18), at the current time we have the value (7.33), and for earlier times we get the improvement given by the solution of the extended Gaussian state updating.

In Fig. 7.8 the variance of the estimate of the $B(t)$-field is plotted at a given time t_L in the laboratory after a long measurement time, so transients in the atomic dynamics have died out. Results are shown for different values of γ_b but a constant ratio between γ_b and σ_b. The estimate for B at the laboratory time t_L is based on measurements that have registered the action of the field at all previous times and takes the value given by (7.33). For future times $t > t_L$, we have to use the current estimate and extend it by our knowledge of the Ornstein-Uhlenbeck process, i.e. we use the variance V_{t_L} from Eq. (7.18) in Fig. 7.8. The curves show that it is easier to guess the present value than future ones, and that future values are particularly hard to guess for a rapidly fluctuating process. Finally, the curves also explore the range of $t < t_L$, where we estimate past values of the field, and we observe the benefit of hindsight.

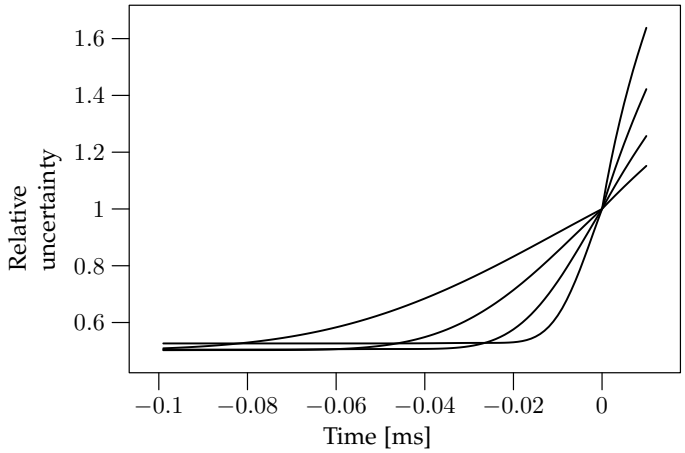

Figure 7.9: The figure shows the variance of estimates for earlier times normalized to the variance at $t = t_L = 4\,\mathrm{ms}$, see text. The atomic parameters are given in Table 4.1, and the B-field is characterized by these different values (from below for $t < 0$) $(\gamma_b, \sigma_b) = (10^4\,\mathrm{s}^{-1}, 2\times10^4\,\mathrm{pT}^2/\mathrm{s})$, $(\gamma_b, \sigma_b) = (10^3\,\mathrm{s}^{-1}, 2\times10^3\,\mathrm{pT}^2/\mathrm{s})$, $(\gamma_b, \sigma_b) = (10^2\,\mathrm{s}^{-1}, 2\times10^2\,\mathrm{pT}^2/\mathrm{s})$, and $(\gamma_b, \sigma_b) = (10^1\,\mathrm{s}^{-1}, 2\times10^1\,\mathrm{pT}^2/\mathrm{s})$.

We see in figure 7.9, where the variance is plotted relative to its value at $t = t_L$, that quite independently of the time constant of the fluctuations, if we can only wait long enough, we find a significant improvement on the variance compared to the equal time estimate, considered in previous theories [11]. This improvement is a function of the physical coupling parameters, and the present study suggests a careful analysis of the optimum probing strategy, including the possibility of time dependent field strengths and detunings and taking into account also atomic decay processes.

7.4 Conclusion

We have presented a formalism that provides the correct estimate of a time dependent B-field which is known to fluctuate randomly according to an Ornstein-Uhlenbeck process. The estimate exhausts the measurement data and makes the tightest possible conclusions from the photodetection record. It is "correct" in the sense that any better estimate necessarily requires further

information, which could either be in the form of prior information about the field or the results of further measurements on the system. Our ability at time t to estimate $B(t)$ connects in a natural manner to previous results for the estimation of static fields, and it is comparable with the results of the analysis of time dependent fields in [11]. Simulations show that this theory actually provides a better estimate of the value in the recent past (or, instrumentally, if you need to estimate the field at time t, you should use the formally obtained estimate at time $t + T$ for some suitable T). Our formalism naturally generalizes to describe also a scenario, where previous estimates are updated by current measurements, and this provides an essential improvement for magnetometers as documented in this chapter.

Eight

Conclusion and Outlook

In this last chapter, the main results of the thesis will be summarized and perspectives for extension of this work will be given.

8.1 Summary and Perspectives

In **chapter 2 and 3** we have considered squeezed light generated in an optical parametric oscillator. By using a Gaussian state description we have described squeezing of light inside the cavity both with and without homodyne measurements of the output field. We have also described the squeezing of the output field and shown that the output field is only squeezed if we look for long enough times. Furthermore, in **chapter 5** we have used the squeezed light as probe beams to improve an atomic magnetometer.

The method described in this thesis is fully general, and further studies can be carried out in a similar way on other proposals involving squeezed light. The theory is readily generalized to incorporate more atomic systems, more field modes, and non-degenerate OPOs. Moreover we showed that finite detection bandwidth can be modeled by the addition of auxiliary modes. Finite bandwidth of the light sources and of the detection system may also play non-trivial roles in conjunction with atomic decay and decoherence which set an upper limit to the degree of entanglement obtained in gases [55].

We also note that squeezed light has been proposed as an ingredient in various quantum information protocols, such as teleportation [59], as a source of heralded single photons [60, 61], and as a resource in continuous variable quantum computing and error correction [62]. In many of these protocols, an elementary analysis is given in terms of single mode fields. However, a full time and frequency dependent analysis would be more appropriate. The Gaussian theory which we have used works for Gaussian states, but some protocols like heralded single photons [60, 61], generation of Schrödinger Cats states, and some quantum information protocols such as distillation of entangled states [21, 22, 63] involves non-Gaussian states. It is therefore important to be able to include non-Gaussian states in the theory too. If only the last step includes non-Gaussian states, then one could use the Gaussian theory until the last step and then "drop" the Gaussian theory.

In **chapter 4** we used the Gaussian theory to estimate magnetic fields, and for constant B-fields we got below the shotnoise limit. The fact that the Gaussian state is fully characterized in terms of its expectation value vector and covariance matrix means that the theory is easy to formulate and to evaluate. It is an outstanding advantage of the Gaussian state description that explicit update formulas exist for, e.g., the interactions in a system, homodyne detection, and noise due to stimulated emission of the atoms and photon absorption.

Another kind of noise process is if the atomic gas is optically thick such

that the probability for photon absorption is larger than, say, a few percent. In this case we get an inhomogeneous light-atom coupling. As shown in Ref. [23] it is possible to reformulate the theory presented in this thesis by slicing the atomic gas into pieces, each having only a small photon absorption probability. This is important in, e.g., quantum memory for light experiments where different protocols rely on multiple passes of the light beam through the atomic sample [53, 64–67]. Due to absorption the photon flux is smaller if the beam has passed through the gas earlier and this can be accounted for in the Gaussian theory.

In **chapter 6** we have shown that if we want to estimate two or three components of a B-field, it is most efficient to use pairwise entangled separate gases. Pairwise entangled gassed are used in other applications like teleportation. It could be very interesting to describe teleportation using the Gaussian description. In a broader perspective, the work presented in this thesis brings out the virtues of the Gaussian state formalism and this is useful both in the detailed characterization of entanglement (see, e.g., Refs. [19–22] and references therein), and in the practical description of quantum systems [8, 23, 53].

Finally, in **chapter 7** we analyzed fluctuating B-fields and showed that we obtain a better estimate if the measurement results at any time are used to improve the estimates at earlier times.

We have not made a complete survey of the optimal performance of the magnetometer as a function of all physical parameters. At this stage, it seems futile to vary all parameters without inclusion, in particular, of the atomic decay, which will either restrict the magnetometers to finite time analyses or which will have to be compensated by a continuous optical re-pumping of the atoms. As pointed out in [11], the field estimation can be made robust to imprecise information about some of the physical parameters, in particular the number of atoms which enters the atom-light interaction strength. Instead of just calculating the field, one can apply, in a feedback setup, a compensating field which should freeze the Larmor precession, independently of the number of atoms, and the field estimate is now given by this compensating field [68, 69]. It is also possible to include a time dependent feedback field in our equations, and hence to simulate the performance of any feedback strategy and its robustness against fluctuations in physical parameters. Another possible important extension of the theory deals with the assumption of the Ornstein-Uhlenbeck process with given parameters. The parameters enter explicitly in our estimation procedure, and if these parameters are not known, or if they are functions of time, e.g., as in the case of cardiography on

a beating heart, more refined theory will be needed. At this point, we recall, that the Ornstein-Uhlenbeck model represents our prior knowledge about the field fluctuations. A conservative high estimate on the noise fluctuations will hence give a similar conservative estimate on the field, which might be improved if better limits were known. A theoretical investigation of this problem could for example simulate the estimation of a noisy field, assuming a different value of the parameters than those applied in the synthesis of the field, and then investigate numerically the difference between the variance on the estimate obtained from the theory and the actual statistical agreement between the estimate and the field.

A

Analytical Result

In chapter 5 we showed how to use squeezed light to improve an atomic magnetometer. In the case where we used squeezed light generated in an OPO the analytical result is very lengthy, so we present the result in this appendix (the result is continued on the next page).

$$
\begin{aligned}
\operatorname{Var} B = & \left\{ \left[\kappa^2\Gamma(\Gamma+4g)^2(\Gamma-4g)t + \Gamma(\Gamma-4g)^3 - 16\kappa^2 g\Gamma(3\Gamma+4g) \right] \right. \\
& + 64\kappa^2 g\Gamma(\Gamma+4g)e^{(-\Gamma/2+2g)t} \\
& + \left[-4\kappa^2 g(\Gamma+4g)^2(\Gamma-4g)t \right. \\
& \quad \left. \left. - 4g(\Gamma-4g)^3 - 16\kappa^2\Gamma g(\Gamma+12g) \right] e^{(-\Gamma+4g)t} \right\} \\
& \times 6\Delta B_0^2(\Gamma-4g)^4 \Big/ \\
& \left\{ \left[\Delta B_0^2\mu^2\kappa^4\Gamma(\Gamma+4g)^4(\Gamma-4g)^3t^4 \right. \right. \\
& + 4\Delta B_0^2\mu^2\kappa^2\Gamma(\Gamma-4g)^2(\Gamma+4g)^2\Big((\Gamma-4g)^3 - 16\kappa^2 g(3\Gamma-4g)\Big)t^3 \\
& + 192\Delta B_0^2\mu^2\kappa^2 g\Gamma(\Gamma-4g)(\Gamma+4g) \\
& \quad \times \Big(2\kappa^2(\Gamma^2+24\Gamma g+16g^2) - (\Gamma-4g)^3\Big)t^2 \\
& + 6\kappa^2\Gamma\Big((\Gamma-4g)^5(\Gamma+4g)^2 + 128\Delta B_0^2\mu^2 g \\
& \quad \times \Big(\kappa^2(\Gamma^3 - 12\Gamma^2 g - 208\Gamma g^2 - 64g^3) + 4g(\Gamma-4g)^3\Big)\Big)t \\
& + 6\Gamma\Big((\Gamma-4g)^7 - 16\kappa^2 g(\Gamma-4g)^4(3\Gamma+4g) \\
& \qquad \left. + 128\Delta B_0^2\mu^2\kappa^2 g(\Gamma-4g)^3 - 8192\Delta B_0^2\mu^2\kappa^4 g^2\Gamma\Big)\right] \\
& + \left[-128\Delta B_0^2\mu^2\kappa^4 g\Gamma(\Gamma-4g)^2(\Gamma+4g)^3t^3 \right. \\
& \quad - 768\Delta B_0^2\mu^2\kappa^4 g\Gamma(\Gamma-4g)^2(\Gamma+4g)^2t^2 \\
& \quad + 49152\Delta B_0^2\mu^2\kappa^4 g^2\Gamma^2(\Gamma+4g)t \\
& \quad \left. + 384\kappa^2 g\Gamma\Big(256\Delta B_0^2\mu^2\kappa^2\gamma\Gamma + (\Gamma-4g)^4(\Gamma+4g)\Big)\right] \\
& \quad \times e^{(-\Gamma/2+2g)t}
\end{aligned}
\tag{A.1}
$$

$$
\begin{aligned}
&+\Big[-4\Delta B_0^2\mu^2\kappa^4 g(\Gamma-4g)^3(\Gamma+4g)^4t^4\\
&\quad+16\Delta B_0^2\mu^2\kappa^2 g(\Gamma-4g)^2(\Gamma+4g)^2\\
&\qquad\times\Big(-4\kappa^2\Gamma(\Gamma+12g)-(\Gamma-4g)^3\Big)t^3\\
&\quad+192\Delta B_0^2\mu^2\kappa^2 g\Gamma(\Gamma-4g)(\Gamma+4g)\\
&\qquad\times\Big(-2\kappa^2(\Gamma^2+24\Gamma g+16g^2)-(\Gamma-4g)^3\Big)t^2\\
&\quad+24\kappa^2 g\Big(-32\Delta B_0^2\mu^2\kappa^2\Gamma(\Gamma^3+52\Gamma^2 g+48\Gamma g^2-64g^3)\\
&\qquad\qquad-32\Delta B_0^2\mu^2\Gamma^2(\Gamma-4g)^3-(\Gamma-4g)^5(\Gamma+4g)^2\Big)t\\
&\quad+24g\Big(-32\Delta B_0^2\mu^2\kappa^2\Gamma(\Gamma-4g)^3-2048\Delta B_0^2\mu^2\kappa^4 g\Gamma^2\\
&\qquad\qquad-4\kappa^2\Gamma(\Gamma-4g)^4(\Gamma+12g)-(\Gamma-4g)^7\Big)\Big]\\
&\quad\times e^{(-\Gamma+4g)t}\Big\}
\end{aligned}
$$

Bibliography

[1] M. O. Scully and M. S. Zubairy, *Quantum Optics* (Cambridge University Press, 1997).

[2] E. S. Polzik, J. Carri, and H. J. Kimble, *Spectroscopy with squeezed light*, Phys. Rev. Lett. **68**, 3020 (1992).

[3] E. S. Polzik, J. Carri, and H. J. Kimble, *Atomic spectroscopy with squeezed light for sensitivity beyound the vacuum-state limit*, Appl. Phys. B **55**, 279 (1992).

[4] I. K. Kominis, T. W. Kornack, J. C. Allred, and M. V. Romalis, *A subfemtotesla multichannel atomic magnetometer*, Nature **422**, 596 (2003).

[5] D. Budker, W. Gawlik, D. F. Kimball, S. M. Rochester, V. V. Yashchuk, and A. Weis, *Resonant nonlinear magneto-optical effects in atoms*, Rev. Mod. Phys. **74**, 1153 (2002).

[6] M. Auzinsh, D. Budger, D. F. Kimball, S. M. Rochester, J. E. Stalnaker, A. O. Sushkov, and V. V. Yashchuk, *Can a quantum nondemolition measurement improve the sensitivity of an atomic magnetometer?*, physics/0403097 (2004).

[7] C. Kim and H. Lee, *Optical pumping magnetic resonance in cs atoms for use in precise low-field magnetometry*, Rev. Sci. Instrum. **74**, 1153 (1998).

[8] K. Mølmer and L. B. Madsen, *Estimation of a classical parameter with gaussian probes: Magnetometry with collective atomic spins*, Phys. Rev. A **70**, 052102 (2004).

[9] H. Carmichael, *An Open Systems Approach to Quantum Optics* (Springer-Verlag, Berlin Heidelberg, 1993).

[10] J. M. Geremia, J. K. Stockton, A. C. Doherty, and H. Mabuchi, *Quantum kalman filtering and the heisenberg limit in atomic magnetometry*, Phys. Rev. Lett. **91**, 250801 (2003).

[11] J. K. Stockton, J. M. Geremia, A. C. Doherty, and H. Mabuchi, *Robust quantum parameter estimation: Coherent magnetometry with feedback*, Phys. Rev. A **69**, 032109 (2004).

[12] V. P. Belavkin, *Measurement, filtering and control in quantum open dynamical systems*, Rep. on Math. Phys. **43**, 405 (1999).

[13] J. M. Geremia, J. K. Stockton, and H. Mabuchi, *Suppression of spin projection noise in broadband atomic magnetometry*, Phys. Rev. Lett. **94**, 203002 (2005).

[14] Y. S. Greenberg, *Application of superconducting quantum interference devices to nuclear magnetic resonance*, Rev. Mod. Phys. **70**, 175 (1998).

[15] E. Rodriguez, N. George, J.-P. Lachaux, J. Martinerie, B. Renault, and F. J. Varela, *Perception's shadow: long-distance synchronization of human brain activity*, Nature **397**, 430 (1999), February.

[16] G. M. Harry, I. Jin, H. J. Paik, T. R. Stevenson, and F. C. Wellstood, *Two-stage superconducting-quantum-interference-device amplifier in a high-q gravitational wave transducer*, Appl. Phys. Lett. **76**, 1446 (2000).

[17] G. Bison, R. Wynands, and A. Weis, *Dynamical mapping of the human cardiomagnetic field with a room-temperature, laser-optical sensor*, Opt. Express **11**, 904 (2003).

[18] G. Bison, R. Wynards, and A. Weis, *A laser-pumped magnetometer for the mapping of human cardiomagnetic fields*, Appl. Phys. B **76**, 325 (2003).

[19] G. Giedke, J. Eisert, J. I. Cirac, and M. B. Plenio, *Entanglement transformations of pure gaussian states*, Quantum Inform. Compu. **3**, 211 (2003).

[20] G. Giedke and J. I. Cirac, *Characterization of gaussian operations and distillation of gaussian states*, Phys. Rev. A **66**, 032316 (2002).

[21] J. Fiurášek, *Gaussian transformations and distillation of entangled gaussian states*, Phys. Rev. Lett. **89**, 137904 (2002).

[22] J. Eisert and M. B. Plenio, *Introduction to the basics of entanglement theory in continuous-variable systems*, Int. J. Quant. Inf. **1**, 479 (2003).

[23] L. B. Madsen and K. Mølmer, *Spin squeezing and precision probing with light and samples of atoms in the gaussian approximation*, Phys. Rev. A **70**, 052324 (2004).

[24] L. B. Madsen and K. Mølmer, *Entanglement between remote continuous variable quantum systems: effects of transmission loss*, quant-ph/0603265 (2006).

[25] A. Silberfarb and I. H. Deutsch, *Continuous measurement with traveling-wave probes*, Phys. Rev. A **68**, 013817 (2003).

[26] G. A. Smith, S. Chaudhury, and P. S. Jessen, *Faraday spectroscopy in an optical lattice: a continuous probe of atom dynamics*, J. Opt. B: Quantum Semiclassical Opt. **5**, 323 (2003).

[27] M. J. Collett and C. W. Gardiner, *Squeezing of intracavity and traveling-wave light fields produced in parametric amplification*, Phys. Rev. A **30**, 1386 (1984).

[28] C. W. Gardiner and M. J. Collett, *Input and output in damped quantum systems: Quantum stochastic differential equations and the master equation*, Phys. Rev. A **31**, 3761 (1985).

[29] M. Kitagawa and M. Ueda, *Squeezed spin states*, Phys. Rev. A **47**, 5138 (1993).

[30] A. Einstein, B. Podolsky, and N. Rosen, *Can quantum-mechanical description of physical reality be considered complete?*, Phys. Rev. **47**, 777 (1935).

[31] C. W. Gardiner, *Quantum Noise* (Springer, Berlin, Heidelberg, 1991).

[32] D. F. Walls and G. J. Milburn, *Quantum Optics* (Springer-Verlag, 1994).

[33] H. P. Yuen and V. W. S. Chan, *Noise in homodyne and heterodyne-detection*, Opt. Lett. **8**, 177 (1983).

[34] N. G. Walker and J. E. Carrol, *Multiport homodyne detection near the quantum noise limit*, Opt. Quantum Electron. **18**, 355 (1986).

[35] H. M. Wiseman and G. J. Milburn, *Quantum theory of field-quadrature measurements*, Phys. Rev. A **47**, 642 (1993).

[36] P. S. Maybeck, *Stochastic Models, Estimation and Control*, volume 1 of *Mathematics in Science and Engineering, Volume 141* (Academic Press, New York, 1979).

[37] R. A. Horn and C. R. Johnson, *Matrix Analysis* (Cambridge University Press, Cambridge, 1985).

[38] J. L. Sørensen, *Private communication*.

[39] B. Julsgaard, A. Kozhekin, and E. S. Polzik, *Experimental long-lived entanglement of two macroscopic objects*, Nature **413**, 400 (2001).

[40] A. Kuzmich, N. P. Bigelow, and L. Mandel, *Atomic quantum nondemolition measurements and squeezing*, Europhys. Lett. **42**, 481 (1998).

[41] L.-M. Duan, J. I. Cirac, P. Zoller, and E. S. Polzik, *Quantum communication between atomic ensembles using coherent light*, Phys. Rev. Lett. **85**, 5643 (2000).

[42] Y. Takahashi, K. Honda, N. Tanaka, K. Toyoda, K. Ishikawa, and T. Yabuzaki, *Quantum nondemolition measurement of spin via the paramagnetic faraday rotation*, Phys. Rev. A **60**, 4974 (1999).

[43] A. Kuzmich, L. Mandel, J. Janis, Y. E. Young, R. Ejnisman, and N. P. Bigelow, *Quantum nondemolition measurements of collective atomic spin*, Phys. Rev. A **60**, 2346 (1999).

[44] J. F. Sherson and K. Mølmer, *Polarization squeezing by optical faraday rotation*, quant-ph/0606076 (2006).

[45] J. Sherson, B. Julsgaard, and E. S. Polzik, *Deterministic atom-light quantum interface*, quant-ph/0601186 (2006).

[46] B. Julsgaard, J. Sherson, J. I. Cirac, J. Fiurášek, and E. Polzik, *Experimental demonstration of quantum memory for light*, Nature **432**, 482 (2004).

[47] W. A. Shurcliff, *Polarized Light* (Harvard University Press, Cambridge, 1962).

[48] B. H. Bransden and C. J. Joachain, *Physics of Atoms and Molecules* (Longman, Essex, 1983).

[49] B. Julsgaard, *Entanglement and Quantum Interactions with Macroscopic Gas Samples*, Ph.D. thesis, Department of Physics and Astronomy, University of Aarhus, Denmark (2003).

[50] K. Hammerer, E. S. Polzik, and J. I. Cirac, *Teleportation and spin squeezing utilizing multimode entanglement of light with atoms*, Phys. Rev. A **72**, 052313 (2005).

[51] S. A. Tretter, *Estimating the frequency of a noisy sinusoid by linear regression*, IEEE Transactions on Information Theory **31**, 832 (1985).

[52] S. Groeger, G. Bison, P. Knowles, and A. Weis, *A sound card based multichannel frequency measurement system*, Eur. Phys. J. Appl. Phys. **33**, 221 (2006).

[53] K. Hammerer, K. Mølmer, E. S. Polzik, and J. I. Cirac, *Light-matter quantum interface*, Phys. Rev. A **70**, 044304 (2004).

[54] G. Giedke, M. M. Wolf, O. Krüger, R. F. Werner, and J. I. Cirac, *Entanglement of formation for symmetric gaussian states*, Phys. Rev. Lett. **91**, 107901 (2003).

[55] J. Sherson and K. Mølmer, *Entanglement of large atomic samples: A gaussian-state analysis*, Phys. Rev. A **71**, 033813 (2005).

[56] M. M. Wolf, F. Verstraete, and J. I. Cirac, *Entanglement frustration for gaussian states on symmetric graphs*, Phys. Rev. Lett. **92**, 087903 (2004).

[57] M. B. Plenio, J. Eisert, J. Dreißig, and M. Cramer, *Entropy, entanglement, and area: Analytical results for harmonic lattice systems*, Phys. Rev. Lett. **94**, 060503 (2005).

[58] C. W. Gardiner, *Handbook of Stochastic Methods* (Springer, New York, 1985), 2 edition.

[59] A. Furusawa, J. L. Sørensen, S. L. Braunstein, C. A. Fuchs, H. J. Kimble, and E. S. Polzik, *Unconditional quantum teleportation*, Science **282**, 706 (1998).

[60] C. K. Hong and L. Mandel, *Experimental realization of a localized one-photon state*, Phys. Rev. Lett. **56**, 58 (1986).

[61] C. R. Myers, M. Ericsson, and R. Laflamme, *A single photon source with linear optics and squeezed states*, quant-ph/0408194 (2004).

[62] S. L. Braunstein, *Error correction for continuous quantum variables*, Phys. Rev. Lett. **80**, 4084 (1998).

[63] D. E. Browne, J. Eisert, S. Scheel, and M. B. Plenio, *Driving non-gaussian to gaussian states with linear optics*, Phys. Rev. A **67**, 062320 (2003).

[64] C. A. Muschik, K. Hammerer, E. S. Polzik, and J. I. Cirac, *Efficient quantum memory and entanglement between light and an atomic ensemble using magnetic fields*, quant-ph/0512226 (2006).

[65] B. Kraus, K. Hammerer, G. Giedke, and J. I. Cirac, *Entanglement generation and hamiltonian simulation in continuous-variable systems*, Phys. Rev. A **67**, 042314 (2003).

[66] J. Sherson, A. S. Soerensen, J. Fiurášek, K. Mølmer, and E. Polzik, *Light qubit storage and retrieval using macroscopic atomic ensembles*, quant-ph/0505170 (2005).

[67] J. Fiurášek, J. Sherson, T. Opatrný, and E. S. Polzik, *Single-passage readout of atomic quantum memory*, Phys. Rev. A **73**, 022331 (2006).

[68] J. M. Geremia, J. K. Stockton, and H. Mabuchi, *Closed-loop quantum parameter estimation: Spins in a magnetic field*, quant-ph/0309034 (2003).

[69] J. M. Geremia, J. K. Stockton, and H. Mabuchi, *Real-time quantum feedback control of atomic spin-squeezing*, Science **304**, 270 (2004).